Development of Sulfur-Tolerant Components for Second-Generation Molten Carbonate Fuel Cells

EM-1114
Research Project 1085-2

Interim Report, July 1979

Prepared by

INSTITUTE OF GAS TECHNOLOGY
IIT Center
3424 South State Street
Chicago, Illinois 60616

Principal Investigators
T. D. Claar
L. G. Marianowski
A. F. Sammells

Prepared for

Electric Power Research Institute
3412 Hillview Avenue
Palo Alto, California 94304

EPRI Project Manager
A. John Appleby
Fossil Fuel and Advanced Systems Division

ORDERING INFORMATION

Requests for copies of this report should be directed to Research Reports Center (RRC), Box 10090, Palo Alto, CA 94303, (415) 961-9043. There is no charge for reports requested by EPRI member utilities and affiliates, contributing nonmembers, U.S. utility associations, U.S. government agencies (federal, state, and local), media, and foreign organizations with which EPRI has an information exchange agreement. On request, RRC will send a catalog of EPRI reports.

NOTICE

This report was prepared by the organization(s) named below as an account of work sponsored by the Electric Power Research Institute, Inc. (EPRI). Neither EPRI, members of EPRI, the organization(s) named below, nor any person acting on their behalf: (a) makes any warranty or representation, express or implied, with respect to the accuracy, completeness, or usefulness of the information contained in this report, or that the use of any information, apparatus, method, or process disclosed in this report may not infringe privately owned rights; or (b) assumes any liabilities with respect to the use of, or for damages resulting from the use of, any information, apparatus, method, or process disclosed in this report.

Prepared by
Institute of Gas Technology
Chicago, Illinois

ABSTRACT

Future large-scale fuel cell power plant applications will require the use of hydrocarbon feeds such as coal, heavy oils, and distillates containing sulfur. As a result, depending on the fuel conversion and cleanup processes used, varying amounts of sulfur will appear in the fuel cell feed. Because both the cost and complexity of the total plant increase as the removal levels increase, it is essential to identify the gas purity requirements of molten carbonate fuel cells. In addition, these power plants may operate above atmospheric pressures to increase system performance. Therefore, the objectives of EPRI RP 1085-2 are —

- To establish the performance and endurance characteristics of molten carbonate fuel cells as a function of sulfur contaminants in both fuel and oxidant feed gases,
- To identify the sulfur tolerance of cell materials, and
- To establish cell performance as a function of gas composition at 5 and 10-atm pressure.

Cell tests using a variety of sulfur concentrations indicated that the sulfur tolerance of present molten carbonate fuel cells is below 10 ppm in the incoming feed gases. Both cell performance losses and endurance limitations were observed at these levels and they were shown to occur primarily on the anode side of the cell. The performance losses are due to a combination of structural changes in the anode and reduced mass transfer characteristics of the carbonate melt caused by interactions between the carbonate melt and the sulfur species. The endurance limitations are due to corrosion of the current collector and other metallic components that were shown to be more severely corroded in the presence of the sulfur-containing gases. Potentially more sulfur-tolerant materials were identified in supplementary screening tests; however, their performance characteristics need to be demonstrated in operating cells.

Cell testing at 5 and 10-atm pressure showed that the Energy Conversion Alternative Study (ECAS) performance projections are realistic. However, a number of system

control problems and cell component problems, primarily with the electrolyte tile, were identified and need further development before long-term endurance testing can be accomplished at elevated pressure.

EPRI PERSPECTIVE

PROJECT DESCRIPTION

This interim report of Research Project 1085-2, entitled Development of Sulfur-Tolerant Components of Molten Carbonate Fuel Cells, addresses a subject that has emerged as a key factor in the future technological importance of the molten carbonate fuel cell. This generating device is very attractive because of its use of comparatively inexpensive materials and lack of noble-metal catalysts, its higher voltage performance than the phosphoric acid fuel cell, and above all its high-quality waste heat, which allows direct integration with a coal gasifier and bottoming cycle. Based on reference level cell performance (currently attainable in test cells), an overall heat-rate of 6800 Btu/kWh (50.2% efficiency coal-pile to ac) may be predicted in certain configurations using current-technology turbines and compressors. The degree of sulfur cleanup necessary must be quantified to define the system design and overall efficiency. This report, which describes the results of an initial series of tests on sulfur tolerance, will be followed by a further final report in 1981. The latter will refine the long-term sulfur tolerance levels and report further work on advanced molten carbonate technologies.

PROJECT OBJECTIVES

This report describes the effects of sulfur-containing anode and cathode gases on molten carbonate fuel cell components and performance at levels down to 10 ppm. One major objective was to determine the tolerance of present components to sulfur, and to develop more tolerant materials. The report shows that it is improbable that functional cells can be made to work even at the 10 ppm level. Later work will define a lower level representing the upper limit of continuous sulfur tolerance, and will determine other parameters that have been identified as milestones in cell development. In particular, these will be melt performance optimization and the determination of carbonate loss mechanisms under pressure conditions. The latter is particularly important for definition of carbonate inventory aspects of cell design.

PROJECT RESULTS

This study shows that carbonate fuel cells posses very poor sulfur tolerance. Even at the 10 ppm level, nickel anodes and stainless steel current collectors are unstable. The former produce a molten nickel--nickel sulfide eutectic, and the latter show deformation, corrosion, and cracking. Cobalt is better from this viewpoint, but is prohibitively expensive for practical applications. Only one potential anode material that shows reasonably high sulfur tolerance has been identified--magnesium-doped lanthanum chromite. However, this ceramic will certainly be costly, fragile, and difficult to manufacture. It will also be unusable in certain new cell concepts in which manufacturability and fail-safe operation are to be assured by the use of a metallic anode as support for the paste/ceramic cell structure and as the seal area.

In any case, scrubbing of sulfur by the carbonate itself, a quantitative chemical reaction at the cathode, is likely to result in an electrolyte composition changing with time. This has increased polarization and corrosion implications. A sulfur-tolerant anode material does not solve the problems inherent in the current collector, nor does it solve a further difficulty that this report identifies at 10 ppm sulfur concentration--that of increased cell polarization in all cases. This is particularly marked with the ceramic anode material. With nickel or cobalt, an increased polarization at the anode of 60 mV is observed, equivalent to about a 3-percentage-point loss in overall system efficiency. Research Project 239 (Fluor) has shown that complete sulfur removal from the gas before introduction to the cell will involve only a slight efficiency loss and a capital cost increase of less than 5%. It would therefore appear that complete sulfur removal is the preferred choice. Hence, sulfur tolerance limits will only be of importance in the future in the case of abnormal cell operation.

A. John Appleby, Project Manager
Fossil Fuel and Advanced Systems Division

ACKNOWLEDGMENTS

The effort reported herein was carried out by a number of personnel at the Institute of Gas Technology. P. Ang was in charge of the electrochemical testing performed in Tasks 1 and 2; R. Donado was in charge of the cell testing with sulfur-containing gases; E. Ong was in charge of the sulfur-equilibration and $LiAlO_2$ stability studies; E. Camara was in charge of the pressure testing, and D. Vasil, K. Hahn, and T. Tang performed the gas analysis and pressure testing.

CONTENTS

CONTENTS, Cont.

ILLUSTRATIONS

TABLES

INTRODUCTION AND SUMMARY

BACKGROUND

A molten carbonate fuel cell consists of an electrolyte containing alkali metal carbonates supported in a lithium aluminate matrix, a porous sintered nickel anode, and a porous nickel oxide cathode. Generally, the anode is stabilized to prevent sintering, and the cathode is oxidized in situ during cell operation to nickel oxide. To date, these fuel cell components have shown good electrochemical performance and corrosion stability under cell operating conditions for over 13,000 hours in the absence of sulfur-containing species in the fuel and oxidant. However, commercialization of this system for electric utility power plants dictates that the fuel cell operate on distillate and residual fuel oils in the short term and on the products of coal gasification in the longer term. There will, therefore, be significant quantities of sulfur (primarily as H_2S and COS) in the fuel cell feed gas. In addition, because the CO_2 requirements of the cathode are supplied by recycling the spent anode effluent to the cathode, the sulfur in the anode effluent will appear as SO_2 in the cathode inlet gas. Thus, both electrodes will be exposed to sulfur-containing gases. Furthermore, the molten carbonate electrolyte is expected to react with these sulfur-containing gases to form alkali sulfates at the cathode and a mixture of alkali sulfates and sulfides at the anode. As a result, all cell components will be exposed to a combination of sulfur species. Therefore, not only the performance of the molten carbonate fuel cell can be affected by the sulfur-containing feed gases, but the endurance may also be affected because of —

- Electrode corrosion,
- Current collector corrosion,
- Wet-seal corrosion,
- Separator plate corrosion,
- Carbonate loss, and
- Lithium aluminate changes.

Two general approaches can be followed towards solution of the sulfur problem in the molten carbonate fuel cell. The first approach is to completely remove the sulfur species before the fuel cell anode. The second approach is to identify the sulfur tolerance of the fuel cell components that are currently used, and, if degradation in performance and materials stability becomes evident, develop sulfur-tolerant components that show acceptable long-term electrochemical performance and/or corrosion stability. The second of these two approaches has been evaluated in this work.

Previous information in the literature on gas-phase catalysis indicated that nickel is poisoned by H_2S chemisorption, possibly with the formation of nickel sulfide(1). Therefore, H_2S (above a certain threshold concentration) in contact with nickel at the normal operating temperature of the molten carbonate fuel cell (around 650°C) would be expected to cause a loss of structural integrity in this porous electrode and possibly also affect the electrocatalytic activity of the anode. Other evidence suggests catalytic poisoning of the nickel anode might occur at H_2S concentrations considerably below that necessary for the formation of metal sulfide(2,3). Little work has been reported on the corrosion of nickel by sulfide or sulfate while in the presence of molten carbonate. Most of the work reported to date has focused on nickel in contact with various sulfur-containing gases. For example, the corrosion rate of nickel either in pure SO_2 or in SO_2/O_2 mixtures has shown parabolic gravimetric kinetics(4), resulting in the growth of external NiO and internal Ni_3S_2 scales. At temperatures above 645°C, Ni_3S_2 in contact with nickel forms a molten eutectic phase.

The carbonate/sulfate/sulfide equilibria on the anode side of the electrolyte tile in the presence of sulfur-containing gases is determined by —

$$M_2SO_4 + CO_2 + 4H_2 \rightleftarrows M_2CO_3 + H_2S + 3H_2O \qquad (S\text{-}1)$$

$$M_2S + CO_2 + H_2O \rightleftarrows M_2CO_3 + H_2S \qquad (S\text{-}2)$$

In addition, it can be anticipated that the concentration of sulfur species at the anode may be affected by the electrochemical transport of sulfur species from the sulfur-contaminated cathode.

Molten carbonate fuel cells require transfer of CO_2 from the anode outlet and the cathode inlet for CO_2 management. This requirement will introduce sulfur to the

cathode, which under the oxidizing conditions present there will occur as SO_2. SO_2 can be expected to readily absorb into the molten carbonate mixture present both at the porous nickel oxide cathode and within the tile by the equilibrium reaction —

$$M_2CO_3 + SO_2 + 1/2\ O_2 \rightarrow M_2SO_4 + CO_2 \qquad (S\text{-}3)$$

Very limited data appears in the literature regarding the stability of NiO in the presence of SO_2. The concentration of SO_2 required to form $NiSO_4$ has been indicated to be around 120 ppm(5). It must be remembered, however, that in the ideal case the porous NiO electrode is covered with a thin-film of molten carbonate, a factor which makes it difficult to readily predict electrode material stability by direct extrapolation from Ellingham-type plots(6).

Fuel cell performance models have projected that the performance could be significantly increased by operating at higher pressures. While such extrapolations are relatively straightforward, extensive testing at high pressure had not previously been conducted to confirm the models and, more importantly, to determine other characteristics of high-pressure operation, such as changes in gas compositions and endurance. The characterizations of high-pressure operation were conducted in 100 cm^2 cells at pressures of 1, 5, and 10 atmospheres.

The efforts conducted under EPRI Project RP 1085-2 during the period August 11,1977, to October 15, 1978, are reported in the following four sections, which are organized to correspond to the five tasks:

- Section 1 - Evaluate and Develop Sulfur-Tolerant Anodes; Evaluate and Develop Sulfur-Tolerant Anode Current Collectors and Structural Materials (Tasks 1 and 2)
- Section 2 - Assess Anode and Cathode Materials Limitations (Task 3)
- Section 3 - Evaluate Electrolyte Tile Stability (Task 4)
- Section 4 - Evaluate Cell Performance at 5 and 10-atm Pressure (Task 5)

SUMMARY OF FINDINGS

The majority of fuel cell performance and endurance data obtained to date has been with clean gases. Because future fuel cell power plants will most likely use

hydrocarbon fuels containing some sulfur, it is essential to determine the effect of these contaminants on fuel cell operation. This report describes the results of such a program. Molten carbonate fuel cells were operated at 650°C using sulfur-containing feed gases to identify their endurance, performance, and sulfur tolerance. Electrochemical half-cell measurements were made to identify the mechanism of sulfur poisoning. Cells were also operated at 5 and 10-atm pressure to verify performance gains and to determine cell operating characteristics.

The major conclusions of this work are —

- Current molten carbonate fuel cells show large performance losses, 60 mV at 160 mA/cm^2, when exposed to feed gases containing sulfur concentrations as low as 10 ppm.

- In addition to the initial 60 mV loss with 10 ppm sulfur, cells using nickel anodes show a continuous further decay. However, similar tests using cobalt anodes showed more stable performance. Screening tests showed that magnesium-doped lanthanum chromite can tolerate much higher concentrations of sulfur (up to 1000 ppm).

- The majority of the performance loss is due to higher anode polarization even when sulfur is introduced into the cathode.

- Half-cell electrochemical tests have shown the kinetics of anode reaction to be unaffected by H_2S in the anode feed gases up to a sulfur level of 50 ppm. Therefore, the cause of the higher anode polarization observed in cell tests may be related to changes in mass transfer characteristics of the S-contaminated melts, and/or to structural changes in the electrode.

- Only small changes in cathode polarization are observed using SO_2-containing cathode feed gases.

- Sulfur species are transported from the cathode to the anode when SO_2-containing feed gases are used. This transport, coupled with the equilibrium existing between the carbonate and the feed gases at each electrode, results in a sharp concentration gradient of sulfur species in the electrolyte tile between the cathode and the anode. The average, or bulk, concentration of sulfur species in the tile is low -- less than 10^{-2} mole fraction.

- Corrosion of type 316 stainless steel anode current collectors used in cells operating with low (~10 ppm) S-containing gases is high and, as a result, presents an endurance limitation. Three more corrosion-resistant current collector materials were identified in laboratory screening tests.

- Pressure testing showed that ECAS performance projections are realistic, better electrolyte tile structures are necessary, and some inlet hydrogen is consumed to form methane and therefore is unavailable to react electrochemically, thus resulting in a lower cell performance.

PERFORMANCE AND ENDURANCE

For the purpose of identifying the sulfur tolerance levels, standard molten carbonate fuel cell components were used to assemble laboratory-size cells, which have a capability of using reference electrodes to identify individual anode and cathode performance changes. Fuel gases containing 10 ppm H_2S + COS and oxidant gases containing 10 to 50 ppm SO_2* were individually fed to these cells operating at 650°C and 1 atm pressure. Cells were operated for varying periods of time up to 2616 hours, the cell performance changes were measured, and detailed post-test examination of all components were made to identify mechanistic decay modes.

The most sensitive or critical cell component appears to be the stabilized porous nickel anode electrode, which was shown to be unsatisfactory even at contaminant concentrations as low as 10 ppm in either the fuel or the oxidant. The initial performance penalties, 60 mV at 160 mA/cm^2, are not acceptable, and continuous long-term decay was observed. Similar stabilized cobalt anodes showed only an initial performance loss, and moderate cell stability was obtained thereafter for the duration of the tests.

Part of the anode problem is caused by sulfidation and the resultant morphological changes caused by sulfide formation. This sulfidation is a function of the material used (nickel or cobalt) and the concentration (H_2S/H_2 ratio) of the sulfur species. The results of this program showed that a) cobalt is more sulfur-tolerant than nickel; that is, cobalt can both tolerate higher concentrations of H_2S prior to sulfidation than nickel and its sulfide is solid at 650°C, whereas the nickel sulfide/nickel eutectic is liquid at 650°C and causes additional severe morphological changes; and b) when using sulfur-containing feed gases, the cell performance losses due to anode polarization increase as the concentration of H_2 is decreased from 60% H_2 (high-Btu reformed methane) to 21% H_2 (low-Btu air-blown coal gas). This increase in cell performance losses is more than that caused by H_2 concentration changes alone. Figure S-1 shows the endurance of nickel and cobalt anodes using a low-Btu fuel containing 10 ppm H_2S + COS. As shown in Figure S-2, the anode open-circuit potential was virtually unaffected in all cases by the sulfur and the losses observed were due primarily to additional polarization effects as the current density increased.

---

*Because the anode effluent must be recycled to the cathode to supply its CO_2 requirements, sulfur will also appear, as SO_2, in the cathode feed gas if it is initially present in the anode feed gases.

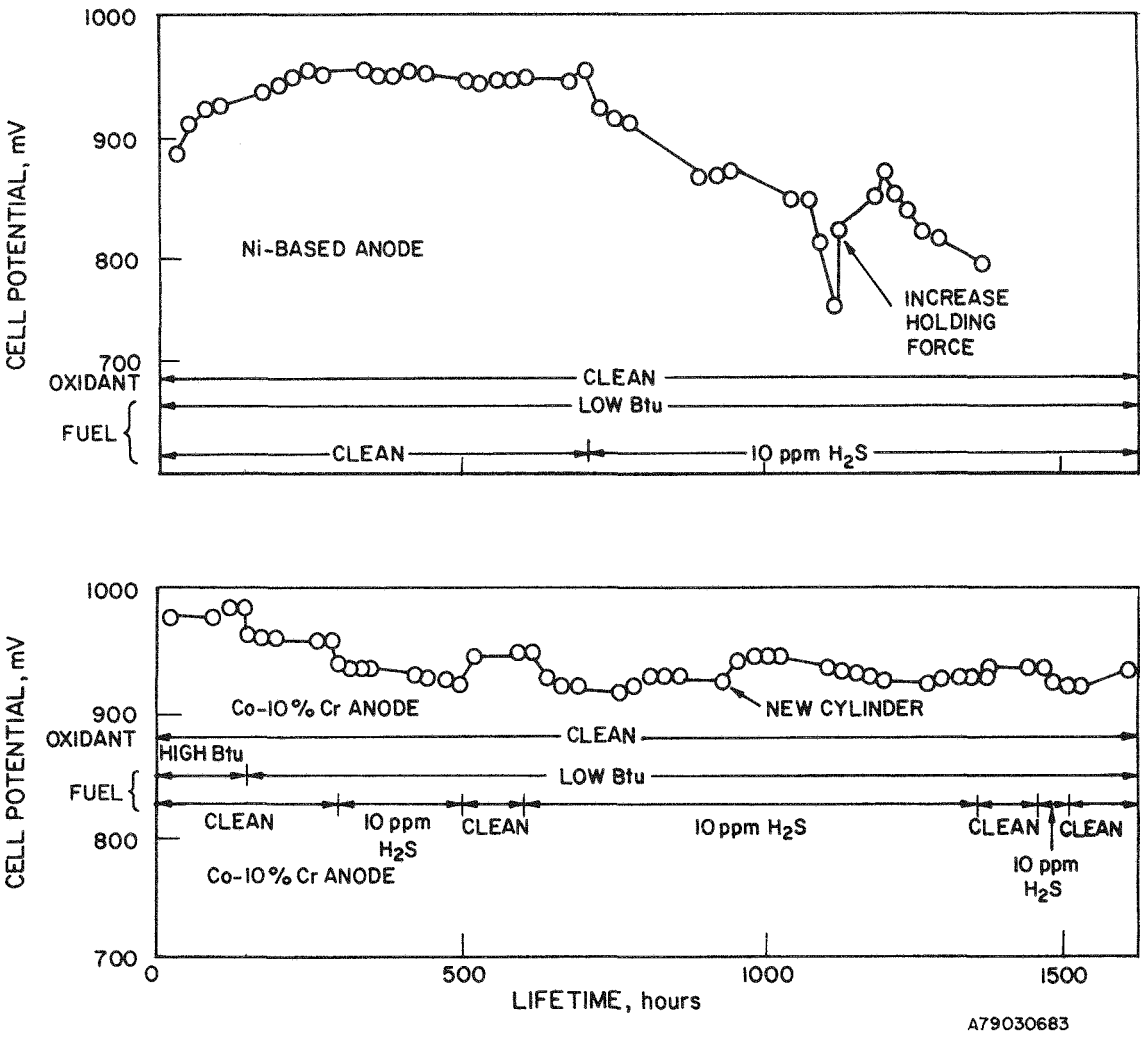

Figure S-1. Comparative Endurance of Molten Carbonate Fuel Cells Using Cobalt and Nickel Anodes and Low-Btu Fuel Gases Containing 10 ppm H_2S at 650°C

On the other hand, when sulfur-containing gases were fed to the cathode (using clean anode gases), the cathode open-circuit potential and its polarization did not change significantly in tests using between 10 and 50 ppm SO_2. However, because sulfur migrates in a manner similar to carbonate ions from the cathode to the anode, the anode open-circuit potential and its polarization are affected, as shown in Figure S-3. No tests were made simultaneously feeding H_2S to the anode and SO_2 to the cathode. However, it is expected that losses observed individually may be cumulative. This supposition will be verified in the follow-on effort.

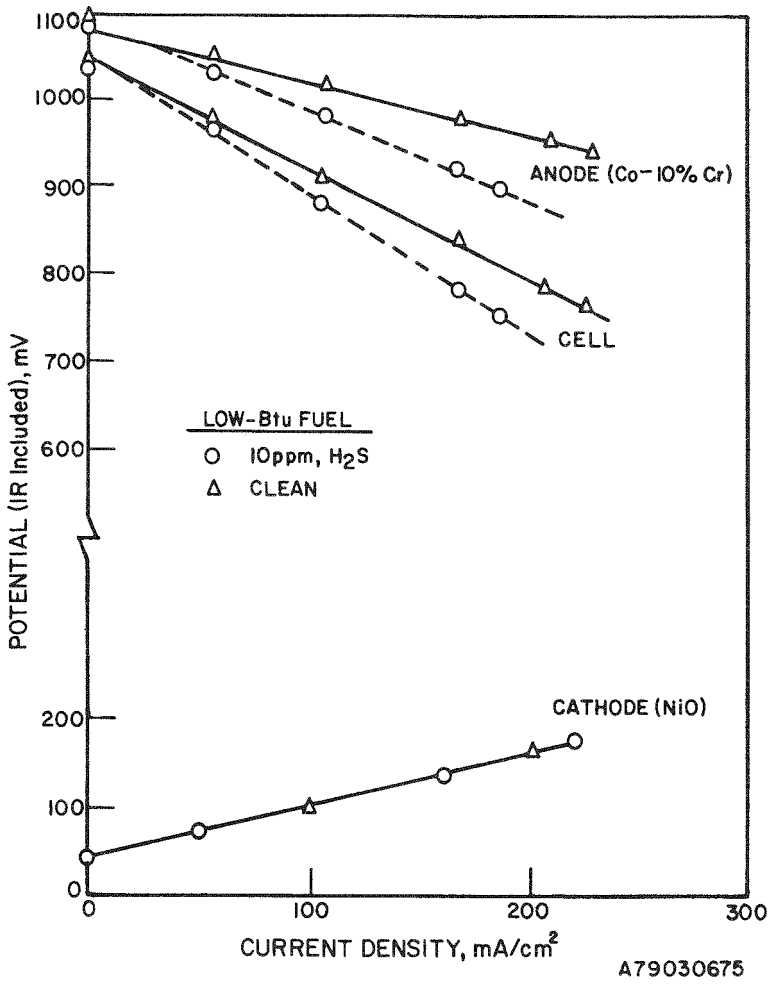

Figure S-2. Effect of Sulfur Species in Fuel Gases on Anode and Cathode Polarizations

SULFUR TOLERANCE OF CELL MATERIALS

The objectives of this portion of the program were to a) quantify the material limitations of standard cell components, b) identify mechanisms of performance and endurance losses, and c) identify potentially more sulfur-tolerant anode and anode current collector materials.

The material limitations of current standard cell components were obtained using a combination of laboratory cell testing, electrochemical half-cell measurements, and corrosion pot testing. The absorption/desorption of sulfur species between the gas phase and the carbonate electrolyte were monitored by both gas-phase analysis of outlet gases and post-test analysis of the electrolyte phase.

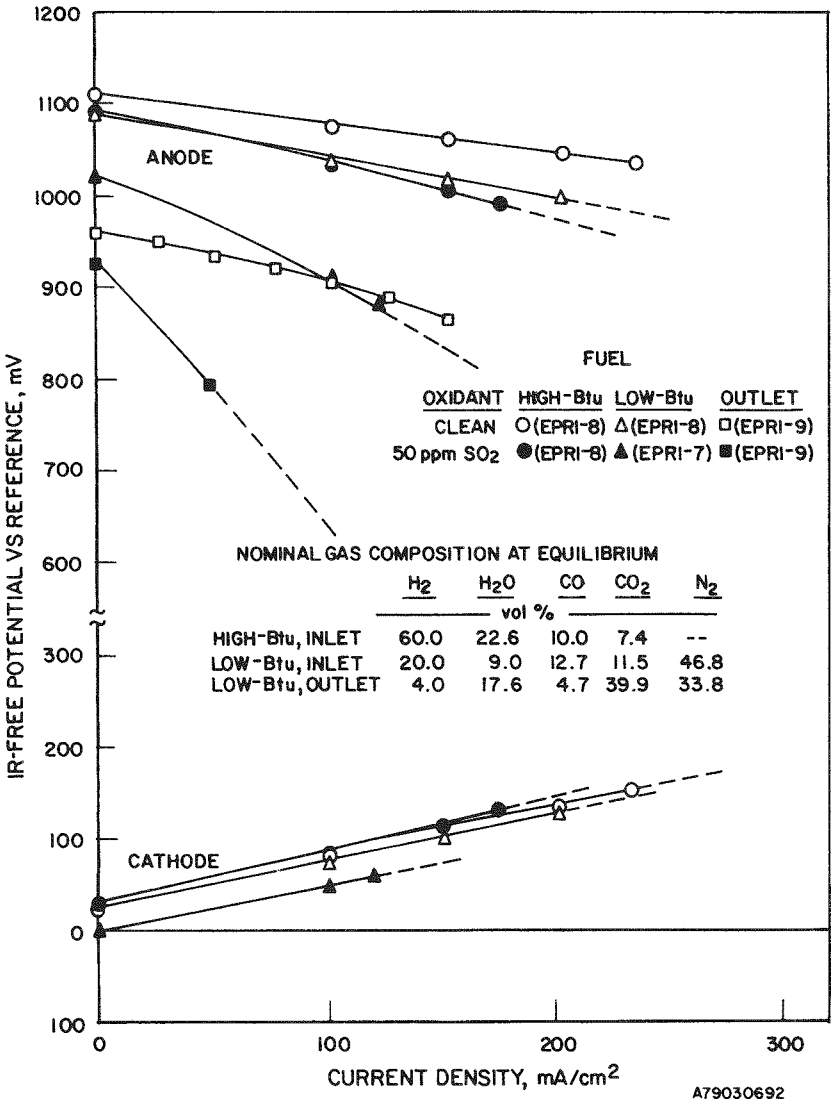

Figure S-3. Anode and Cathode Polarizations Observed Under Different Fuel and Oxidant Conditions (Stabilized Ni Anode, Ni Cathode)

As expected from thermodynamic calculations, cobalt was experimentally shown to be more sulfur tolerant than nickel. At 650°C the H_2S/H_2 ratio required for incipient sulfide formation is 5.0×10^{-3} for cobalt and 1.8×10^{-3} for nickel. For a low-Btu fuel gas (21.1% H_2), these ratios translate to 1055 ppm and 380 ppm required for sulfidation of cobalt and nickel, respectively. However, because of the complex reaction equilibrium existing in a carbonate-film-covered porous electrode, these values should be used only as approximate relative values. In general, the porous nickel anode sulfides at much lower values, and both nickel and cobalt exhibited high electrode polarization under conditions where only chemisorption of sulfur should

have occurred. Because the Ni-S system forms a liquid eutectic at 650°C, severe morphological changes such as those shown in Figures S-4 and S-5 occurred in tests using nickel electrodes. Not only is more sulfur required to sulfide cobalt, but the Co-S system does not form liquid eutectics at 650°C. Visual post-test examination indicated the superior sulfur tolerance of cobalt over nickel.

Concurrently with the above program, an effort to screen and test more sulfur-tolerant anode material candidates was begun. Candidate materials were selected from materials currently used as methanation and hydrodesulfurization catalysts for sulfur-bearing feeds, as well as materials used in high-temperature metal/metal sulfide batteries and high-temperature solid oxide fuel cells. Candidates were first screened in corrosion pot tests. Those showing good stability, $Mg_{0.05}La_{0.95}CrO_3$, TiC, cobalt, nickel, and several other potential anode candidates, passed on to electrochemical testing as wire electrodes. Of the materials tested, magnesium-doped lanthanum chromite ($Mg_{0.05}La_{0.95}CrO_3$) showed the greatest sulfur tolerance. Although its polarization characteristics are somewhat inferior to nickel (Figure S-6), no evidence of sulfidation was evidenced even at very high, 1000 ppm, concentrations of H_2S. As a result, depending on the evaluation of sulfur-scrubbing cost studies, it may be desirable to pursue further studies using this promising higher-cost anode candidate using porous electrodes in laboratory cells.

The stability of the nickel oxide cathode in SO_2-containing gas was determined primarily by post-test examination of terminated laboratory cells because little appropriate literature data was found. Paralleling the observed small performance effects when SO_2-containing gases were used, only minimal changes in the cathode microstructure were observed.

Examination of the Type 316 stainless steel current collectors used in laboratory cell tests showed, again, that the majority of the problems introduced by sulfur-containing gases occur at the anode. The data in Table S-1 shows that the corrosion of the cathode current collector is virtually unaffected by cathode gases containing SO_2. On the other hand, because of the transport of sulfur through the tile, the corrosion of the anode increases by 66% when these same SO_2 cathode gases are used in conjunction with clean anode fuels. When clean cathode gases are used with sulfur-containing fuel gases, the corrosion of the anode current collector as shown in Figure S-7 is even more severe, and the cathode current collector is virtually unaffected.

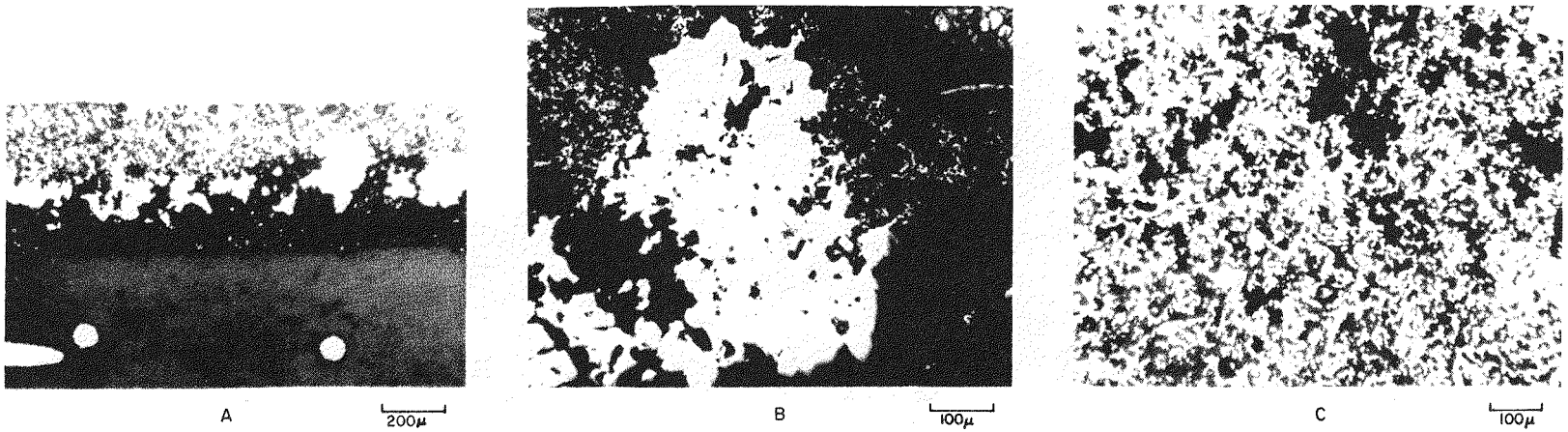

Figure S-4. Structural changes in nickel-based anode of cell EPRI-7 (50 ppm SO_2 in oxidant) are shown in parts A and B. Part C shows a similar electrode used with clean gases.

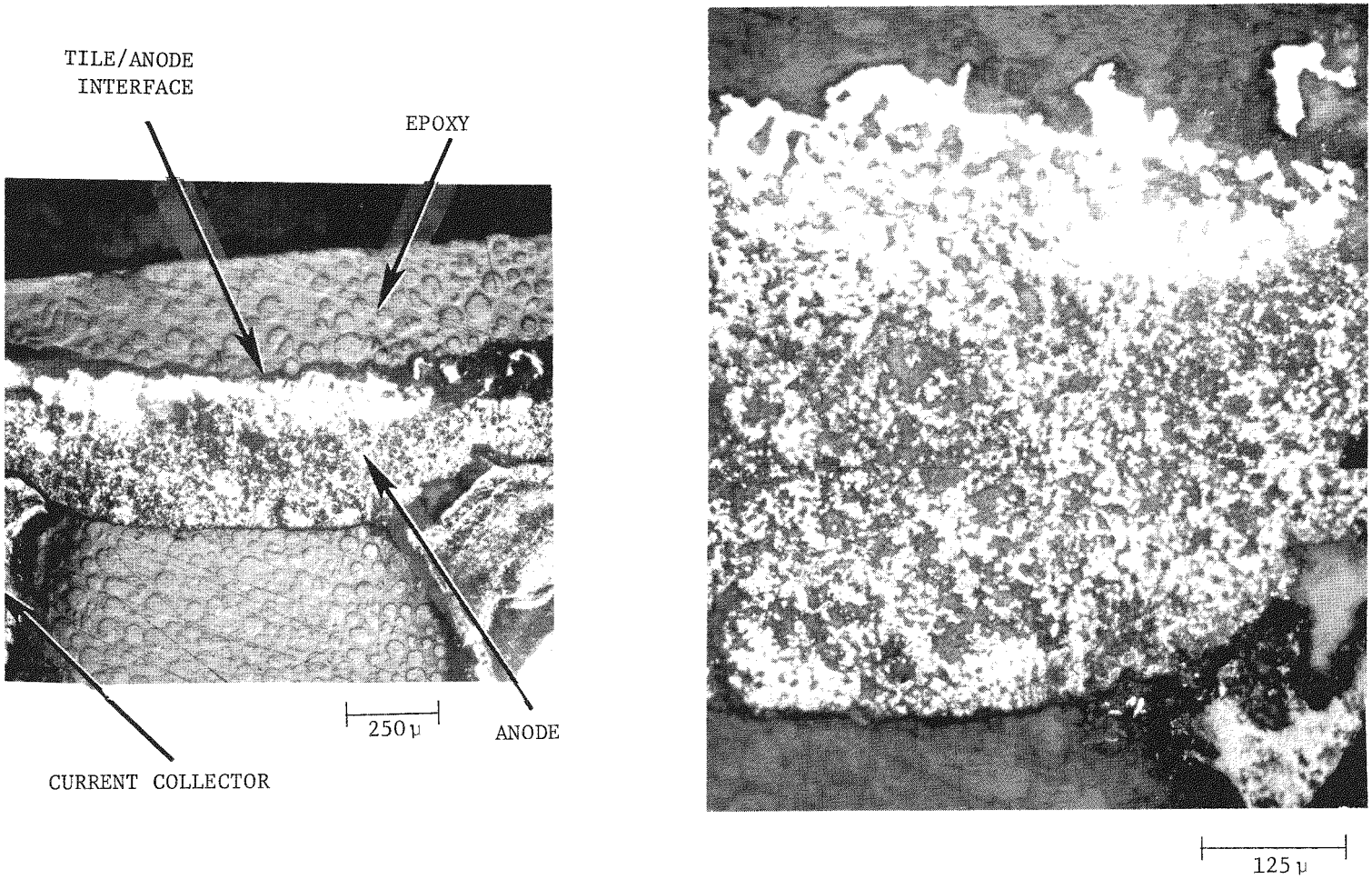

Figure S-5. Microstructure of Sulfur-Affected Stabilized Nickel Anode from Cell EPRI-8

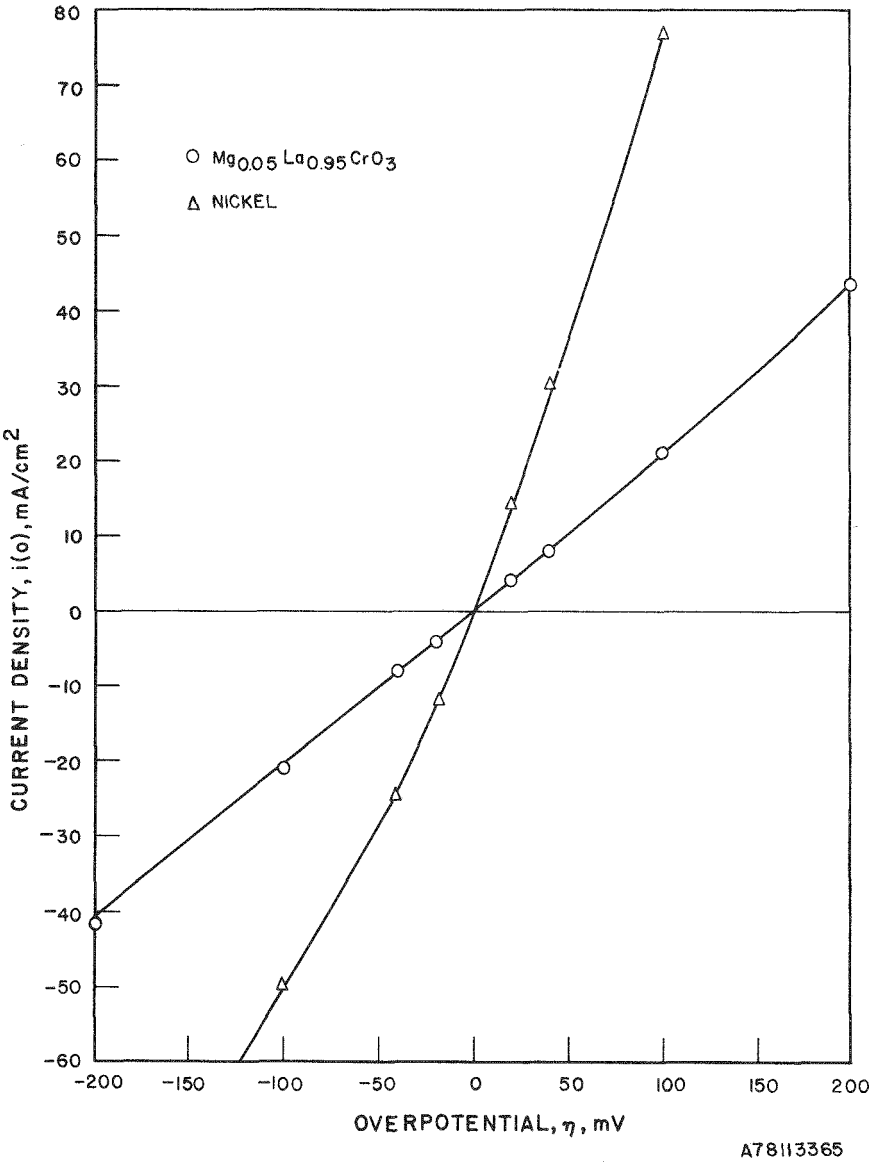

Figure S-6. Activation Polarization Plot Comparison Between Nickel and $Mg_{0.05}La_{0.95}CrO_3$ Using Potential Step Data at 650°C (Low-Btu Fuel With 50 ppm H_2S)

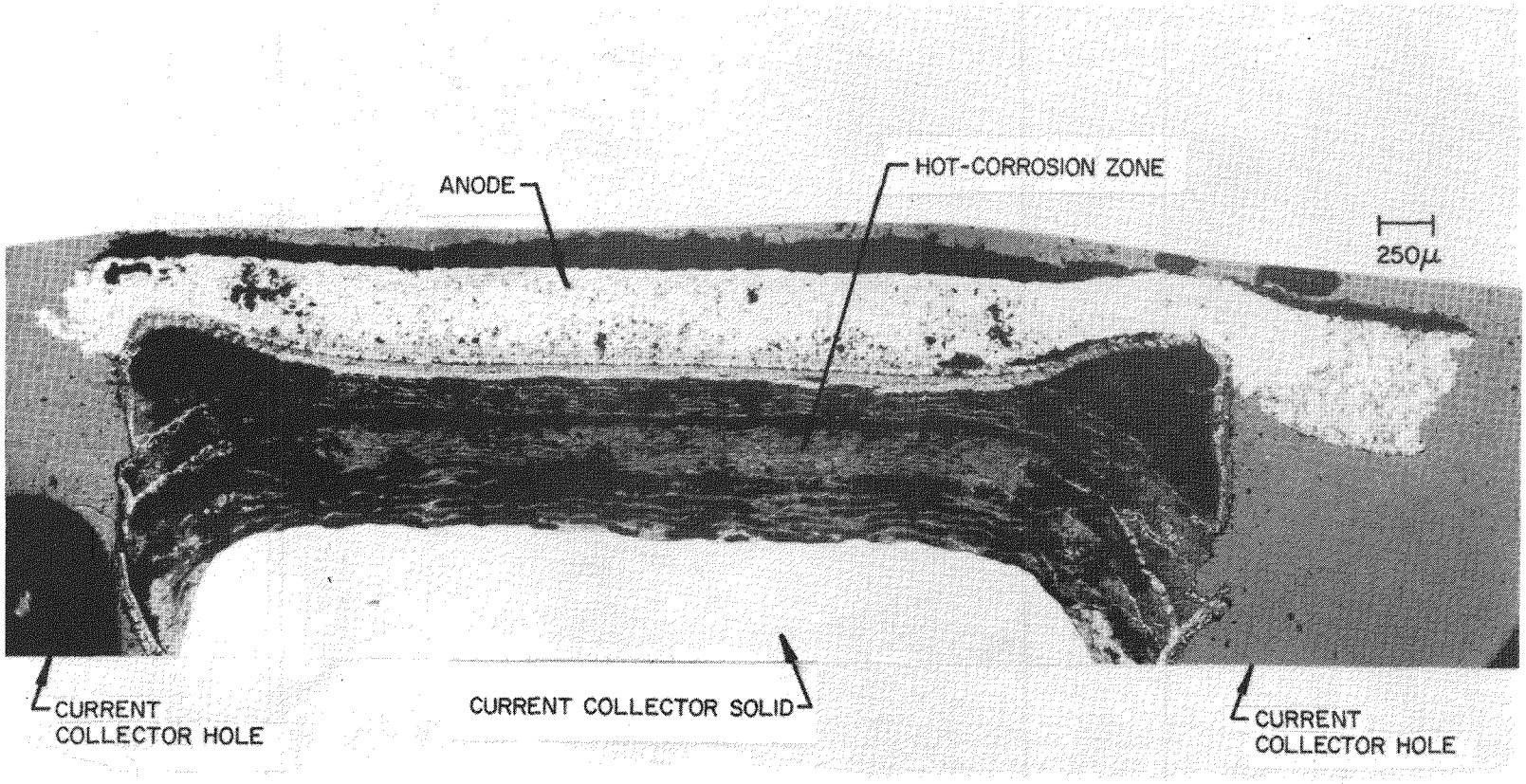

Figure S-7. Composite Cross Section of Stabilized Nickel Anode and Anode Current Collector From Cell EPRI-13, Exposed to 10 ppm H_2S (as polished)

Table S-1

THICKNESS OF OXIDE SCALES ON TYPE 316 SS CURRENT COLLECTOR MATERIALS AT 650°C

Cell No.	Anode				Cathode		
	Gas Side	Electrode Side	Total	μ	Gas Side	Electrode Side	Total
EPRI-3*	5	30	35		5	10	15
EPRI-7**	28	30	58		10	10	20

*Cell operated 1562 hours under sulfur-free gases with reformed natural gas fuel.

**Cell operated 1104 hours total, 620 hours with a 50 ppm SO_2 oxidant flowing (Low-Btu fuel was used for 240 hours, high-Btu for 380 hours).

Parallel screening studies, similar to those conducted with anode electrode materials, showed that Types 446, 410, and 310 stainless steels showed better initial corrosion resistance than the standard Type 316 stainless steel used in all cell testing. Longer term testing of these materials in laboratory cells must be conducted to verify these initial trends.

Because precise thermodynamic data on the alkali sulfate/sulfide/carbonate system are not available, the relative stabilities of these species in sulfur-containing gases were experimentally determined from laboratory cells and equilibration pot tests. Our results confirmed the calculations that showed that almost quantitative absorption of SO_2 occurs at the cathode to form sulfates. These species will migrate toward the anode via a combination of the chemical/electrochemical driving forces. Depending on the rate of transport and the rate of regeneration/reduction at the anode, significant concentrations of sulfur species could accumulate in the electrolyte tile -- that is, the carbonate could be converted to sulfates/sulfides. The available literature data (thermodynamic, as well as experimental results from sulfur-scrubbing studies) indicate that substantial reduction/regeneration would occur at the anode. Therefore, the concentration of sulfur species in the tile will be dependent, at least partially, on the rate of transport from the cathode to the anode through the tile. Experimentally, we found that this rate of transport

(and subsequent reduction/regeneration at the anode) was a function of the current density, shown in Figure S-8. In addition, because our calculations, which are summarized in Table S-2, showed that low concentrations of sulfur species should exist at the anode interface, we concluded that the molten carbonate electrolyte would have an overall low concentration of sulfur species present, as shown schematically in Figure S-9. The concurrent analyses summarized in Table S-3 of terminated laboratory cells operating with sulfur-containing feed gases verified these trends. Parallel equilibration pot test studies, starting with various concentrations of sulfur species in carbonate melts, showed the carbonate phase to be by far the most stable phase in a variety of anode gas compositions. (See Figure S-10.) The agreement of these results with those predicted from thermodynamic data is shown in Figure S-11. Again, fair agreement was obtained showing that low concentrations of sulfur species should be present on the anode side of the cell with a variety of hydrogen-containing fuel gases.

Post-test analysis of cells using sulfur-containing feed gases (compared with analysis of tests using clean gases) showed that the lithium aluminate support may be affected when sulfur gases are used. This trend is not perfectly clear because the anode gas composition was changed from high- to low-Btu gases in the sulfur tests. Because the clean gas composition has been shown to affect the $LiAlO_2$ stability, additional testing is required to quantify this point.

CELL OPERATION AT 5 AND 10-ATM PRESSURE

The objectives of this portion of the program were to a) verify the performance gains expected with pressurized operation, b) identify the carbon-deposition potential due to pressurized operation, and c) identify the methane formation potential due to pressurized operation.

Twelve bench-scale 4 x 4 in. cells were operated to verify the performance gains expected with pressurized cell operation. A combination of test stand control problems and loss of tile integrity precluded the achievement of long-term cell operations. However, the approximate gains shown in Reference 1 were obtained for short periods of time.

Calculations (verified in cell tests) showed that low-Btu product gas from a gasifier will deposit carbon as it is cooled to the 1200°F operating temperature of the fuel cell. Anode recycle or additional H_2O can eliminate this problem.

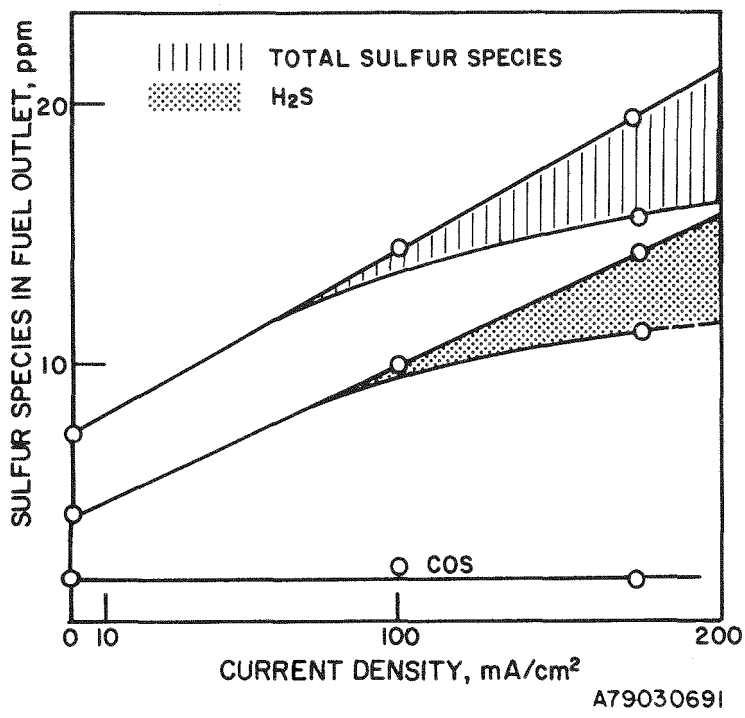

Figure S-8. Changes in Concentration of Sulfur Species in the Effluent Fuel With Current Density in Cell EPRI-8

Table S-2

RESULTS OF THERMODYNAMIC ANALYSIS OF CARBONATE/SULFIDE/SULFATE EQUILIBRIA UNDER VARYING ANODE GAS CONDITIONS AT 650°C

	Gas	Composition (mol fraction)						Activity Ratios for M=Na		
		H_2	H_2O	CO	CO_2	N_2	H_2S	$\frac{[M_2SO_4]}{[M_2CO_3]}$	$\frac{[M_2S]}{[M_2CO_3]}$	$\frac{[M_2S]}{[M_2SO_4]}$
1.	Reformed Methane Inlet	0.60	0.23	0.09	0.08	--	5×10^{-5}	8.2×10^{-10}	2.0×10^{-3}	2.3×10^{6}
2.	Low-Btu Inlet	0.211	0.056	0.178	0.092	0.463	5×10^{-5}	6.7×10^{-9}	7.0×10^{-3}	1.0×10^{6}
3.	Low-Btu Outlet, 75% Util.	0.040	0.176	0.047	0.399	0.338	5×10^{-5}	3.7×10^{-6}	5.1×10^{-4}	1.3×10^{2}
4.	Low-Btu Outlet, 90% Util.	0.015	0.190	0.018	0.455	0.322	5×10^{-5}	2.1×10^{-4}	4.1×10^{-4}	1.9

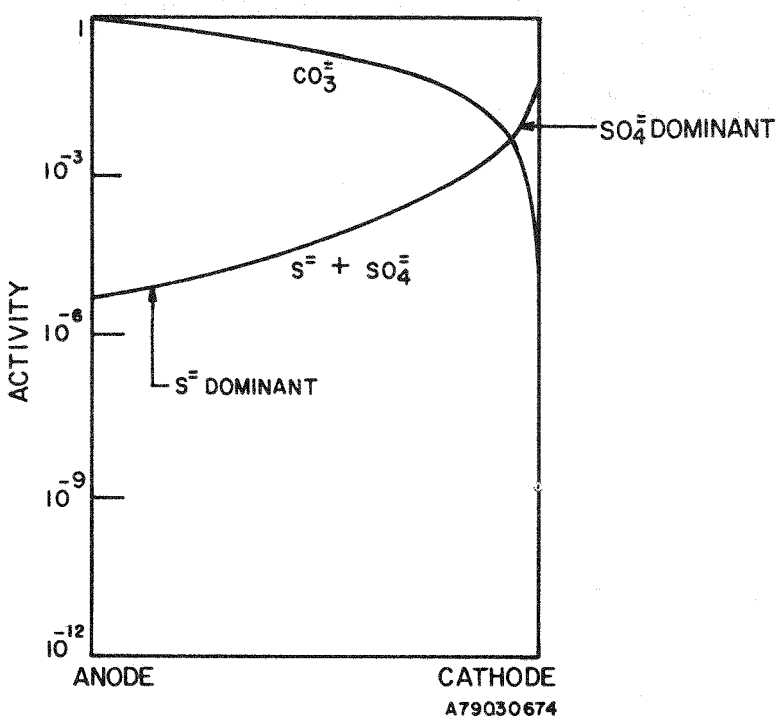

Figure S-9. Schematic Ionic Activity Profiles in Electrolyte Tile Under Low-Btu Inlet Conditions

Table S-3

SULFUR ANALYSES OF TILES FROM CELLS EPRI-7 AND EPRI-8 (mole fraction)

	Cell EPRI-7	Cell EPRI-8	Cell EPRI-10	Cell EPRI-13
S as $S^=$	1.0×10^{-2}	$<9 \times 10^{-5}$	3.8×10^{-3}	5.6×10^{-3}
S as $SO_4^=$	$<1.5 \times 10^{-3}$	4×10^{-5}	3.2×10^{-3}	3.6×10^{-3}

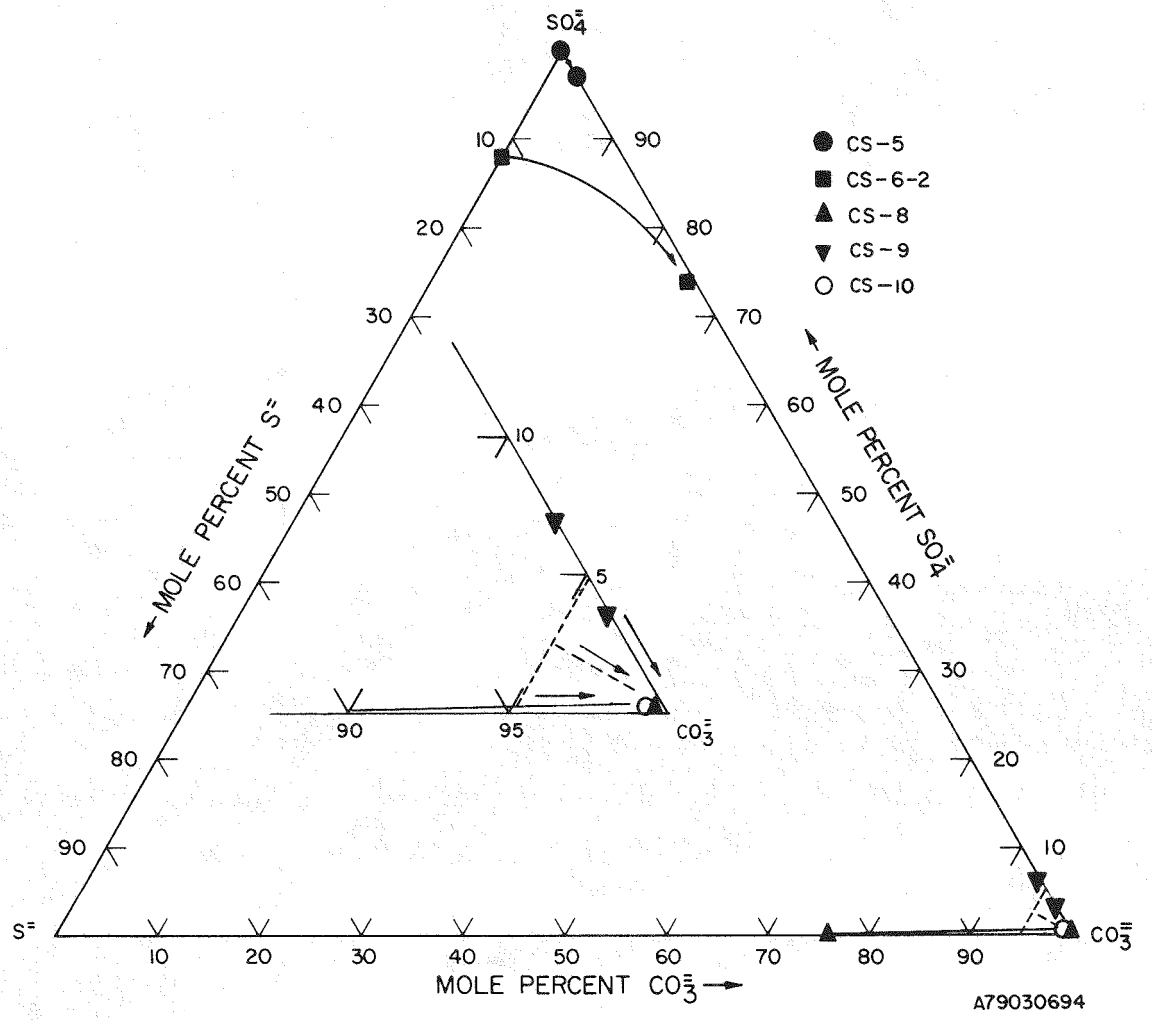

Figure S-10. Conversion Paths for Various Test Melts Exposed to 75% Utilized Low-Btu Fuel Containing 50 ppm H_2S

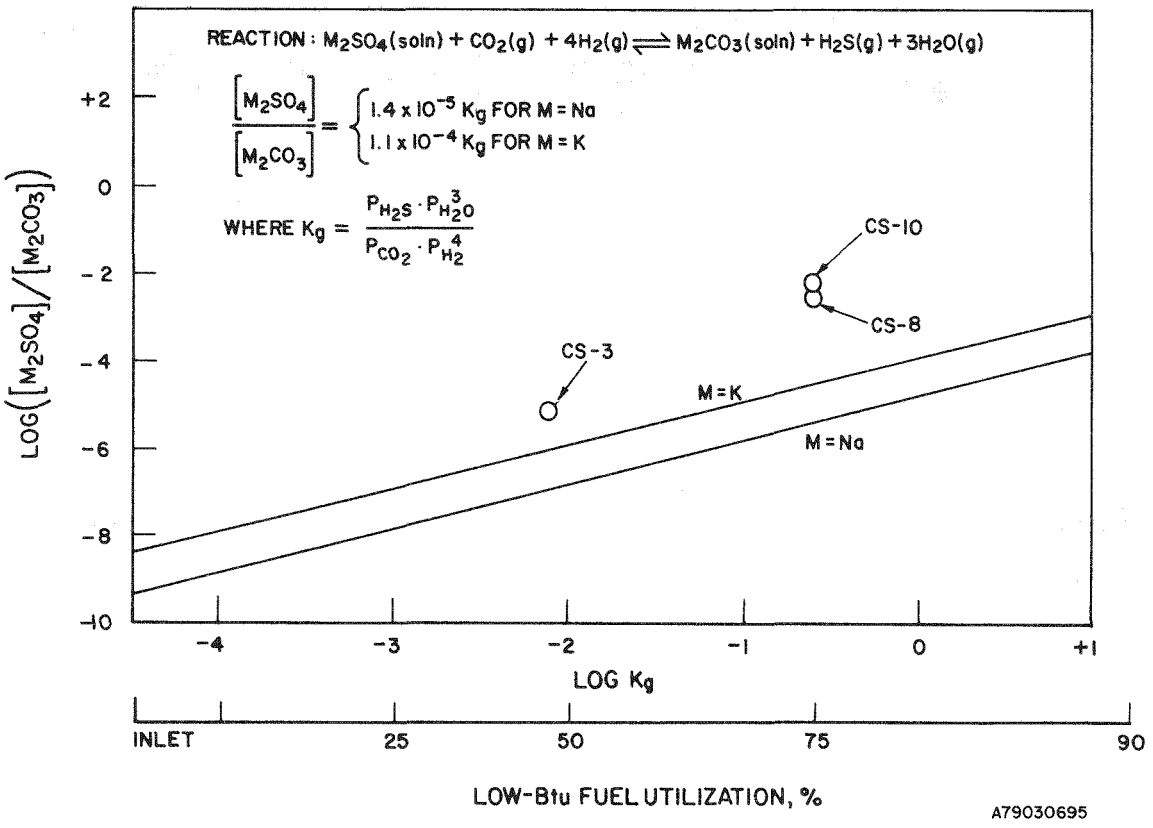

Figure S-11. Variation of $[M_2SO_4]/[M_2CO_3]$ Activity Ratio With Thermodynamic Conditions at the Anode

Formation of methane in the inlet fuel gases is thermodynamically favored as the cell pressure is increased from 1 to 10 atm. As the H_2 is consumed at the anode, however, thermodynamic equilibrium predicts that the methane should be reformed. Previous results showed measurable amounts of methane in the anode outlet gases(1). That is, only a small fraction of the methane present in the inlet gases is reformed in the cell. The results of this work also showed methane in the outlet gases. Although we were not able to operate for extended periods of time, tentative verification was achieved. The impact of methane formation on the calculated overall cell efficiency was shown to be significant. Therefore, quantitative verification of the methane stability in the anode environment is essential. In addition, the fact that methanation is taking place on the carbonate-covered anode and not on other structural components must be confirmed.

REFERENCES

1. E. A. Gulbransen and S. A. Jansson. "General Concepts on Oxidation and Sulfidation Reactions, A Thermochemical Approach." In High Temperature Metallic Corrosion of Sulfur and Its Compounds, edited by Z. A. Foroulis, pp. 3-51. New York: The Electrochemical Society, 1970.

2. J. R. Rostrup-Nielson. "Chemisorption of Hydrogen Sulfide on a Supported Nickel Catalyst." Journal of Catalysis, Vol. 11, 1968, pp. 220-227.

3. R. B. Pannell, K. S. Chung, and C. H. Bartholmew. "The Stoichiometry and Poisoning by Sulfur of Hydrogen, Oxygen, and Carbon Monoxide Chemisorption on Unsupported Nickel." Journal of Catalysis, Vol. 46, 1977, pp. 340-347.

4. K. Luthra and W. Worrel. "Corrosion of Nickel in SO_2-O_2-SO_3 Atmospheres at 603°C." In Properties of High Temperature Alloys, edited by Z. Foroulis and F. Pettit, pp. 318-330. New York: The Electrochemical Society, 1976.

5. H. H. Kellogg. "A Critical Review of Sulfation Equilibria." In Transactions of the Metallurgical Society of AIME, Vol. 230, 1964, p. 1622.

6. C. Alcock, M. Hocking, and S. Zadar. "Corrosion of Nickel in Oxygen Plus Sulfur Dioxide Atmospheres in the Temperature Range 500-700°." Corrosion Science, Vol. 9 (2), 1969, pp. 111-122.

Section 1

TASK 1. EVALUATE AND DEVELOP SULFUR-TOLERANT ANODES; TASK 2. EVALUATE AND DEVELOP SULFUR-TOLERANT ANODE CURRENT COLLECTORS

SUMMARY

The objectives of this portion of the program were to determine the causes of anodic performance losses when sulfur-containing fuel gases are used with porous nickel anodes and to test potentially more sulfur-tolerant anode and anode current collector candidates. The initial selection of candidate sulfur-tolerant components included consideration of materials previously used for methanation catalysts, high-temperature batteries, and solid-oxide fuel cells. These materials were initially subjected to preliminary corrosion testing under those chemical conditions expected in the anode environment of the system. Materials evaluated as sulfur-tolerant anodes in the electrochemical half-cell included nickel, cobalt, CoMo, CoW, WC, TiC, $Mg_{0.05}La_{0.95}CrO_3$, Cr_2O_3 (doped with TiO_2), and NbN. Materials for the anode current collector included Hastelloys, Kanthal, 400 and 300 stainless steels, and iron-aluminum-manganese and iron-aluminum-molybdenum alloys. The relative stabilities of these materials at the anode and anode current collectors for the molten carbonate fuel cell and a comparison of the electrocatalytic behavior of the candidate anodes selected will be discussed in detail in Task 1 and Task 2, respectively.

Under conditions where bulk sulfidation of nickel is not expected to occur, (~50 ppm H_2S) the kinetics of hydrogen oxidation was found to be relatively unaffected by the presence of H_2S for the most promising materials tested (Ni, Co, and $Mg_{0.05}La_{0.95}CrO_3$). The exchange current densities measured were all high (8 to 20 mA/cm^2), indicating rapid hydrogen oxidation kinetics in the presence and absence of sulfur. Therefore, as in the case with clean gases, the performance of porous (diffusion) electrodes containing these materials is expected to be mass transfer controlled. Because porous electrodes tested in 3-cm^2 cells using cobalt or nickel showed increased electrode polarization in the presence of H_2S (in addition, nickel electrodes showed rapid decay thereafter due to structure changes), it appears that the presence of sulfur species retard the mass transfer properties of the electrolyte melt. (See Task 3.) Therefore, although the kinetics of the hydrogen oxidation

reaction is rapid on the materials tested, the mass transfer characteristics of the sulfur-containing carbonate melt are lower than for similar clean melts and, as a result, are one of the primary causes of the lower cell performance observed with sulfur-containing gases. Another major cause of the lower cell performance, discussed under Task 3, are morphological changes of the porous anode structure caused by sulfidation. $Mg_{0.05}La_{0.95}CrO_3$ did not show signs of sulfidation even at H_2S concentrations as high as 1000 ppm, thus indicating stable porous electrodes operating in even higher H_2S concentrations are possible. However, the same mass transfer limitations of the sulfur-containing carbonate melts are still expected. Therefore, although some improvement over nickel is expected, attainment of clean gas performance levels is unlikely.

Anode current collectors were screened and tested using procedures similar to those used for the anode electrode materials. However, the minimization of corrosion/oxide formation was used as the prime criterion for selection. Of the materials evaluated, the highest initial corrosion resistances were found for 446, 410, and 310 stainless steels and Uniloy. Because Type 316 stainless steel was found unacceptable in longer term tests (Task 3), testing of the above materials for longer periods of time in cell tests must be done for quantitative comparison purposes.

TASK 1. EVALUATE AND DEVELOP A SULFUR-TOLERANT ANODE

Materials Selection

Candidate sulfur-tolerant anode materials were selected from materials currently used as methanation and hydrodesulfurization catalysts and materials for the anode and cathode current collectors used in high-temperature batteries, such as the lithium/metal sulfide and sodium/sulfur systems. Materials used for the interconnect in the high-temperature solid oxide fuel cell were also considered because these materials have shown very good stability to both oxidizing and reducing conditions at 1000°C in fuel cells and high-temperature water electrolyzers.

Selected materials were subjected to preliminary corrosion evaluation by being partially submerged in the lithium/potassium carbonate melt at 650°C with fuel of composition 53.86% H_2, 9.36% CO_2, 27.33% H_2O, and 9.43% CO containing 174 ppm H_2S. The materials subjected to this testing are listed in Table 1-1. Those candidate anode materials that showed the highest corrosion stability were $Mg_{0.05}La_{0.95}CrO_3$, TiC, TiO_2 doped with either Ta or Nb, $CoAs_2$, nickel, and cobalt. These materials and other candidates were later subjected to steady-state potentiostatic measurements

to identify their stability under an applied anodic and cathodic potential. Materials selected for the anode and anode current collectors are shown respectively in Tables 1-1 and 1-2.

Experimental Testing

Materials for the anode and anode current collectors were obtained from commercial sources (Materials Research Corporation, Orangeburg, New York, and CERAC, Inc., Milwaukee, Wisconsin). All electrochemical measurements were performed in the half-cell system shown in Figure 1-1. The working electrodes were attached to an alumina-sheathed current collector (lead wire), which usually was a 316 stainless steel wire. For nickel and cobalt, the current collectors were nickel and cobalt, respectively. A gold wire bubbled with 33.3% O_2-66.7% CO_2 inside an alumina tube served as a reference electrode. The wire communicated with the melt through a small hole (0.015-inch diameter) at the bottom of the tube. The electrolyte was prepared from a mixture of 62 mole % Li_2CO_3-38 mole % K_2CO_3 (Mallinckrodt, Analytical Reagent). A piece of round gold or Palau (80% gold, 20% palladium) foil was used as the counterelectrode.

The potential of the working electrode was controlled by a Wenking Model 66TSI potentiostat. Steady-state currents were recorded on a Hewlett-Packard 7046A X-Y recorder. To eliminate errors caused by mass transfer effects, the transient potentiostatic technique was used(1). For such experiments, a Wenking ST72 potentiostat, which has a risetime of about 7 μs when a step voltage is applied, was used. A Tacussel Type GSTP2B pulse-sweep generator was used to control this potentiostat. The output voltage of the Tacussel generator was monitored with a digital voltmeter (Fluke, Type 8020A). Signals from the transient techniques were displayed and photographed on a Tektronix Type 547 oscilloscope. The recordings were performed with appropriate IR compensation using a feedback circuit.

A furnace with a Lindberg Hevi-Duty BPC Type 59344 temperature control was used to heat the half-cell to 650°C. The temperature of the melt was monitored with an alumina-sheathed chromel/alumel thermocouple. In the corrosion experiments, samples were placed in miniature alumina crucibles containing the melt, and the test gas was equilibrated over the melt. The inlet gas was humidified by passing through a column of water in a large test tube. Premixed fuel gases and H_2S were purchased from Matheson Gas Products.

Table 1-1

CORROSION RESULTS FOR CANDIDATE ANODE MATERIALS

Composition (%)	Total Exposure to Low-Btu Fuel (hr)	Period in H_2S (274 ppm) (hr)	Total Weight Change (%)	Comments
WC-10; CO-90	1588	1301	- 3.3	
TaC	1122	1122	--	Completely corroded
TiB_2	432	432	--	Completely corroded
ZrC	168	none	--	Completely corroded
TiC	1506	1051	- 1.0	
VC	355	187	-24.7	
NbN	1506	1051	+10.1	
$Mg_{0.05}La_{0.95}CrO_3$	1506	1051	+ 0.1	
TiO_2 (Ta-doped)	1343	1080	+ 0.7	
TiO_2 (Nb-doped)	1343	1080	- 1.1	
Mo-90; Ti-10	1080	1080	-32.4	
Co-64.8; Mo-35.2	1554	1554	-27.8	
Co-38.1; Mo-61.9	432	432	-53.2	
Nickel	1554	1554	- 0.9	
Fe-90.0 Cr-9.0; Mo-1.0	432	432	-48.5	
Cr-30.6; Co-69.4	648	648	--	Completely corroded
Co-49; 51-W	648	648	--	Completely corroded
Co-24.3; 75.7-W	648	648	--	Completely corroded
Co-63.0; Cr-30; Mo-7.0	1122	1122	--	Completely corroded
Co-22.1; Cr-77.9	1122	1122	+13.7	
Cobalt	1122	1122	+ 0.3	
Cr_2O_3(1 mole % TiO_2)	1122	1122	+ 7.0	Sample broken
Tungsten	1122	1122	-44.7	
Molybdenum	1122	1122	--	Completely corroded
FeB	474	474	--	Completely corroded
Ni-50; Co-50	474	474	+ 3.5	
CoPS	474	474	--	Completely corroded
WS_2	474	474	--	Completely corroded
CoP_3	474	474	--	Completely corroded
Ni-50; Al-50	474	474	+25.9	
$CoAs_2$	474	474	+ 0.9	
MoS_2	474	474	--	Completely corroded
Cr_3Co_2	474	474	--	Completely corroded
WC	648	648	--	Completely corroded
MnS	648	648	-27.0	Sample broken

With the electrochemical conditions present in the half-cell, the rate of the overall electrochemical reaction was found to be dependent not only on the fuel bubbling rate, but also on the voltage sweep rate used. Such observations indicated diffusion or mixed control. To assess the impact of introducing sulfur species into the electrolyte from the fuel, it was of interest to compare the electrode kinetics

Table 1-2

POTENTIOSTATIC EVALUATION OF ANODE MATERIALS USING LOW-BTU FUEL GAS IN BINARY CARBONATE MELT AT 650°C

Composition (%)	Clean Fuel		Fuel with 50 ppm H_2S		Comments
	Open Circuit Potential (mV)	Current, i, at 50 mV From Rest Potential (mA/cm^2)	Open Circuit Potential (mV)	Current, i, at 50 mV From Rest Potential (mA/cm^2)	
Cr_2O_3-99; TiO_2-1	-1032	0.122			Electrode badly cracked.
Nickel-50; Cobalt-50	-1138	0.383	-1102	0.202	Trace of current very noisy.
Tungsten Carbide	-1368	2.918	-1305	1.134	Indicates corrosion; not run cathodically.
Tungsten Cobalt	-1402	2.299			Electrode corroded; not run in H_2S.
Titanium Carbide	-1142*	0.166*	-1135	0.167	
$Mg_{0.05}La_{0.95}CrO_3$	-1130	0.040	-1132	0.041	
Ni-50; Al-50	-1160	0.918			Electrode corroded; not run in H_2S.
TiO_2 (Ta doped)			-1106**	0.157**	
TiO_2 (Nb doped)	-1097	0.114	-1134**	0.105**	Very large cathodic current.
Nickel	-1154	0.250	-1141	0.193	
Nickel			-1185**	17.51 **	Indicates corrosion.
Cobalt	-1158	0.304	-1163	0.304	
Cobalt			-1201**	8.47 **	
Niobium Nitride	-1104	0.493			Indicates corrosion; not run in H_2S.
Chromium-77.0; Cobalt-22.1	-1290	0.0			No anodic current.
$CoAs_2$	-1136	0.32			

* High-Btu fuel

** -1000 ppm H_2S

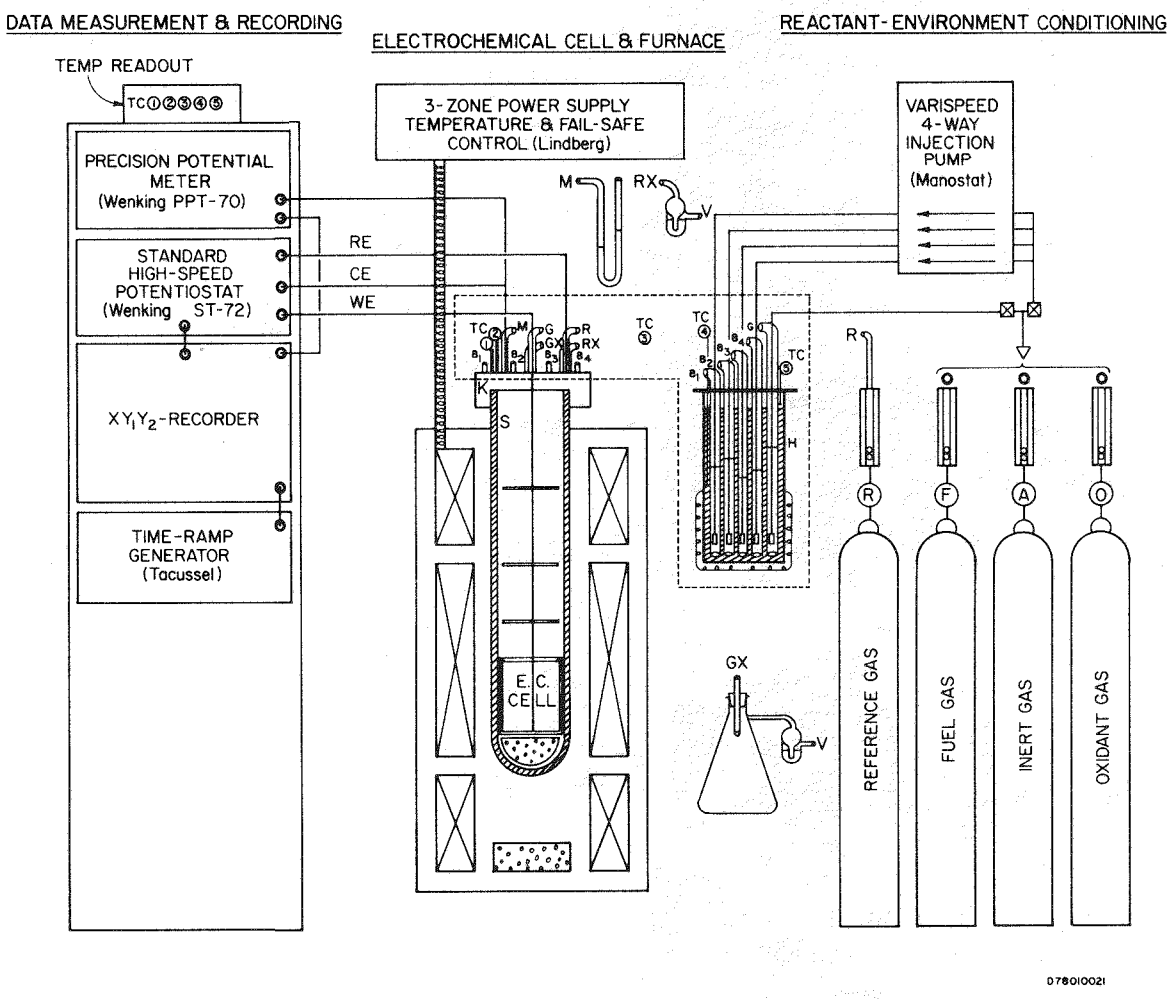

Figure 1-1. Electrochemical Half-cell Used in Anode and Anode Current Collector Evaluation

for both nickel and cobalt with clean and sulfur-containing fuels to determine if any electrocatalytic poisoning effects occurred by the introduction of such sulfur impurities. Transient potentiostatic measurements(1,2) were performed for the separation of kinetic data under the probable mixed control conditions present in the half-cell. This technique involved applying a voltage step to the nickel or cobalt working electrode and recording the current as a function of time. Under such conditions of mixed or diffusion control, the assumption was made that at time zero only activation control will be present -- that is, sufficient supply of electroactive species will be present, together with minimal reaction products, so that any mass transfer effects will be minimized. Figure 1-2 shows typical oscilograms for nickel with and without 50 ppm H_2S in low-Btu fuel. The kinetic current, i(0), was obtained by extrapolating currents between 0.8 and 1.2 ms to time zero. The exchange current density calculated from the i(0) value was found to be around 25 mA/cm^2 in both cases, indicating that such low levels of sulfur (50 ppm H_2S) appear to have little effect upon the electrode kinetics for fuel oxidation. A series of progressively more anodic and more cathodic potential steps were applied to both nickel and cobalt in fuel both with and without 50 ppm H_2S at 650°C. The respective activation polarization curves for these two anodes are shown in Figures 1-3 and 1-4, where they are compared with data obtained using clean fuel.

Experimental Results

To gain some preliminary insight into the impact of sulfur-containing fuels on the electrochemical performance of nickel and cobalt anodes, both steady-state and potential step measurements were performed using clean and sulfur-containing fuels in an electrochemical half-cell. All measurements were performed in electrolyte of composition 62 mol % Li_2CO_3-38 mol % K_2CO_3 at 650°C. The counterelectrode used in this work consisted of Palau of nominal composition 80% Au-20% Pd, which proved to have a higher sulfur tolerance than a pure gold counterelectrode, the usual material used with clean fuels in electrochemical half-cell work. Fuels with a predetermined high sulfur content or pure H_2S were mixed into the primary fuel after the humidification step at the rate required to achieve the desired sulfur content. Preliminary observations in this work indicated some apparent sensitivity of the open-circuit potential obtained at both nickel and cobalt electrodes to the presence of H_2S introduced into the fuel gas. At concentrations of 50 ppm and below, such variation in the open-circuit potential was found to be somewhat erratic and not completely reproducible, indicating that H_2S had little permanent effect on the open-circuit potential. Apart from some variations in the open-circuit potential,

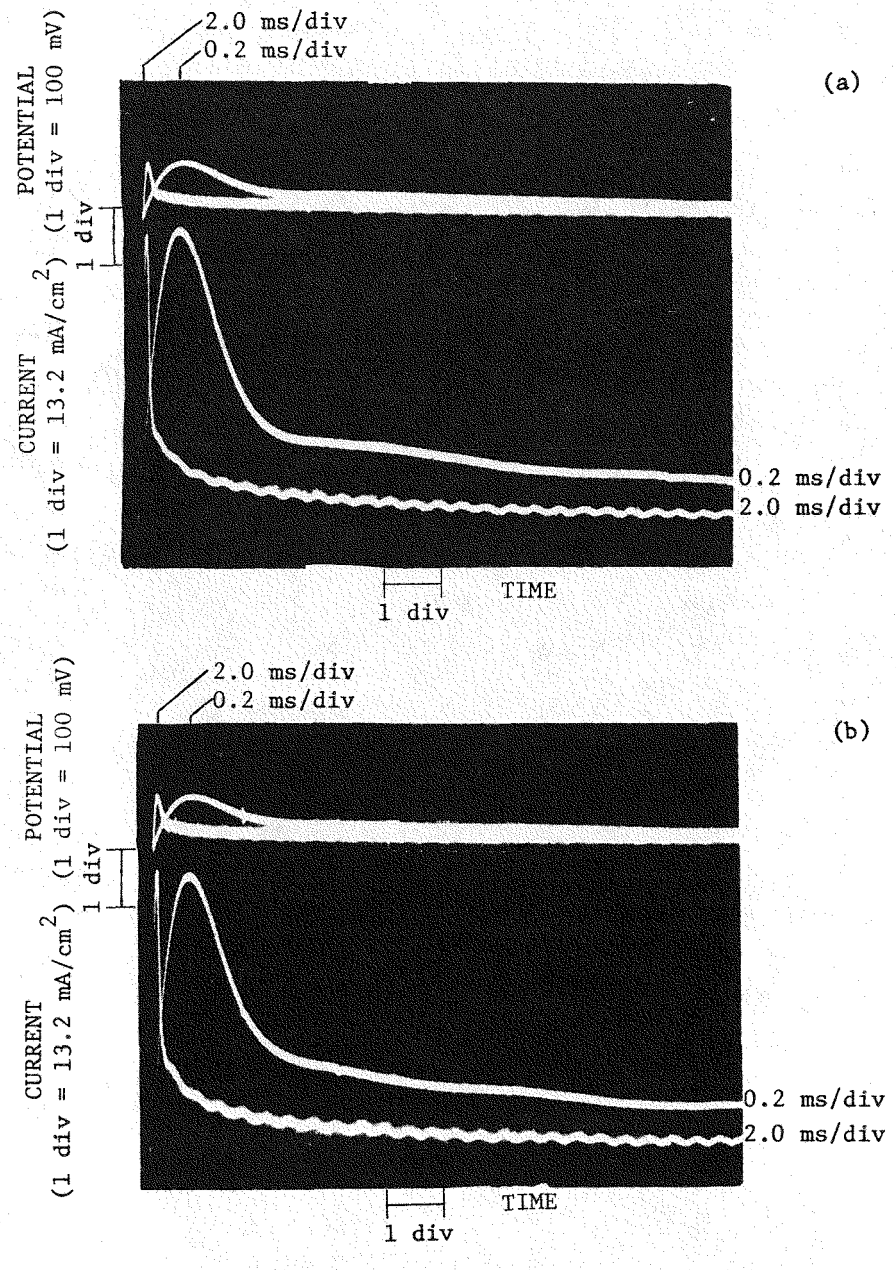

Figure 1-2. Transient Potentiostatic Measurements on Nickel in Lithium-Potassium Melt at 650°C (Low-Btu Fuel Used Both With (a) and Without (b) 50 ppm H_2S Introduced With Fuel)

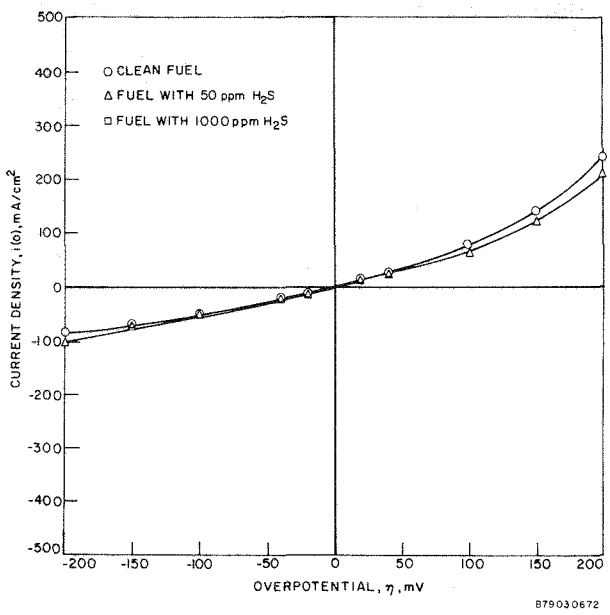

Figure 1-3. Comparison of Activation Polarization Curves for Nickel in Low-Btu Fuel That Is Clean, With 50 ppm H_2S Added, and With 1000 ppm H_2S Added (Li/K Electrolyte, 650°C)

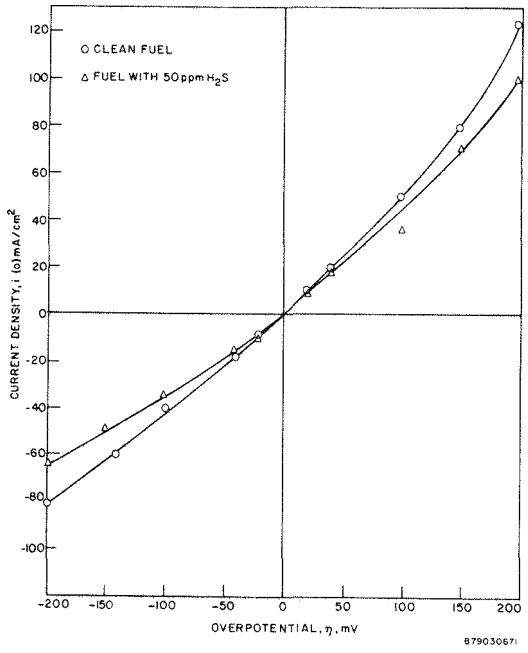

Figure 1-4. Comparison of Activation Polarization Curves for Cobalt in Low-Btu Fuel That Is Clean, With 50 ppm H_2S, and With 1000 ppm H_2S Added

steady-state polarization curves for clean fuel and fuel containing 50 ppm H_2S were of almost identical slope, indicating little evidence of electrode poisoning. Examination of the nickel and cobalt electrodes did not indicate any evidence of sulfidation. Polarization data was performed in both low- and high-Btu fuels corresponding to the respective compositions 22.4% H_2, 17.7% CO, 9.2% CO_2, 11% CH_4, 5.6% H_2O, and 68.1% H_2, 23.4% CO, 3.39% CO_2, and 5.03% H_2O. Emphasis in this work was placed, however, on the low-Btu fuels corresponding to coal gasification. Figures 1-5 and 1-6 compare steady-state polarization curves for nickel and cobalt anodes in low-Btu fuel with and without 50 ppm H_2S. In both cases, introduction of the sulfur into the fuel was observed to very slightly perturb the open-circuit potential.

In the case of nickel (Figure 1-5), the shift was 15 mV positive of the initial -1154 mV open-circuit potential, whereas in the case of cobalt (Figure 1-6), the shift was very slightly in the cathodic direction by around 7 mV. Other than these minor shifts in the open-circuit potential, the current voltage characteristics are very similar in each case.

In the molten carbonate fuel cell, sulfur enters the cathode (oxidant) electrode (via transfer of CO_2 from the anode exhaust, as SO_2) where it forms sulfate species. The sulfate species then migrate (transport) to the anode, where they are reduced to sulfide species. As a result, it may well be that H_2S introduced into the electrochemical half-cell may not be representative of these total sulfide concentrations that may build up near the anode from SO_2 introduced into the cathode. To identify what impact high concentrations of sulfide would have on the open-circuit potential of both nickel and cobalt anodes, up to 1000 ppm H_2S were introduced into low-Btu fuel. For both nickel and cobalt electrodes, the open-circuit potential was observed to shift to more negative values (versus the $O_2/2CO_2$ Au reference electrode). For nickel at 650°C in low-Btu fuel, the open-circuit potential was shifted from -1154 to -1185 mV and for cobalt the shift was -1160 to -1200 mV. The anodic currents at such high concentrations of H_2S were found to be substantially higher at both nickel and cobalt electrodes, and upon removal from the half-cell, evidence of extensive sulfidation (Figure 1-7) on each of these electrode materials became evident. Clearly, neither of these two anode materials can be expected to be stable at such high sulfur levels. As was indicated earlier, 50 ppm H_2S does not appear to drastically poison the electrode kinetics as measured using the potential step method for either the anodic or the cathodic processes, although some small lowering in electrode activity does become apparent at higher applied overpotentials. Upon introduction of 50 ppm H_2S, the exchange current density obtained

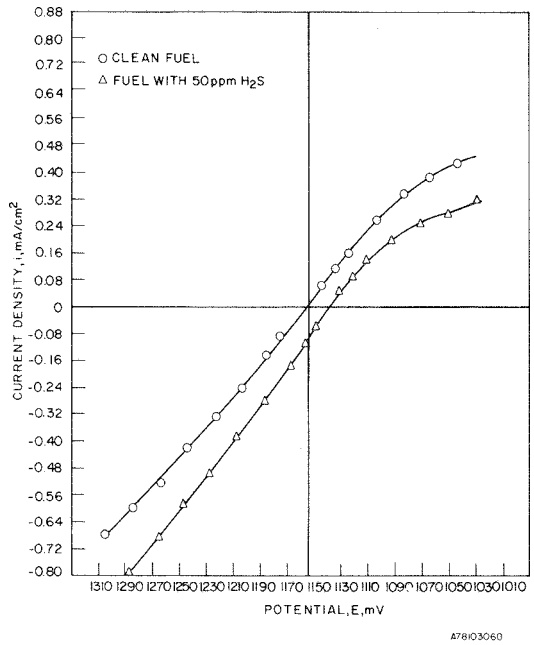

Figure 1-5. Steady-State Polarization Curves for Nickel Using Low-Btu Fuel With and Without 50 ppm H_2S Added (Li/K Electrolyte, 650°C)[2]

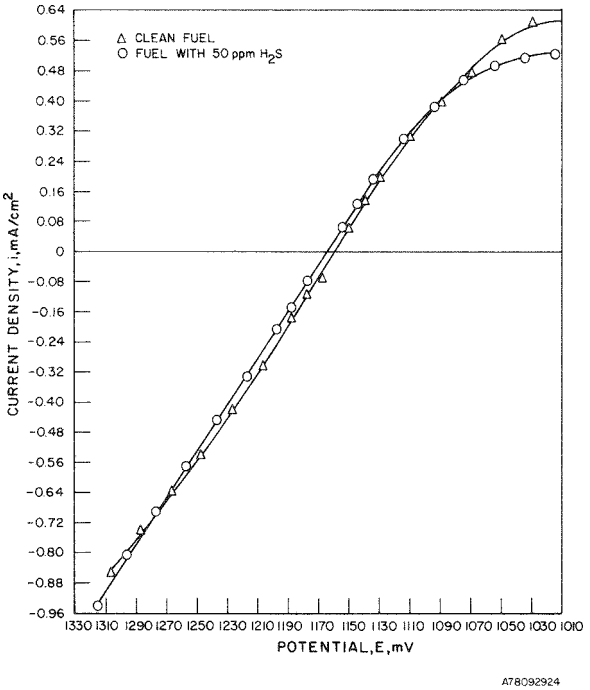

Figure 1-6. Steady-State Polarization Curves for Cobalt Using Low-Btu Fuel With and Without 50 ppm H_2S Added (Li/K Electrolyte, 650°C)[2]

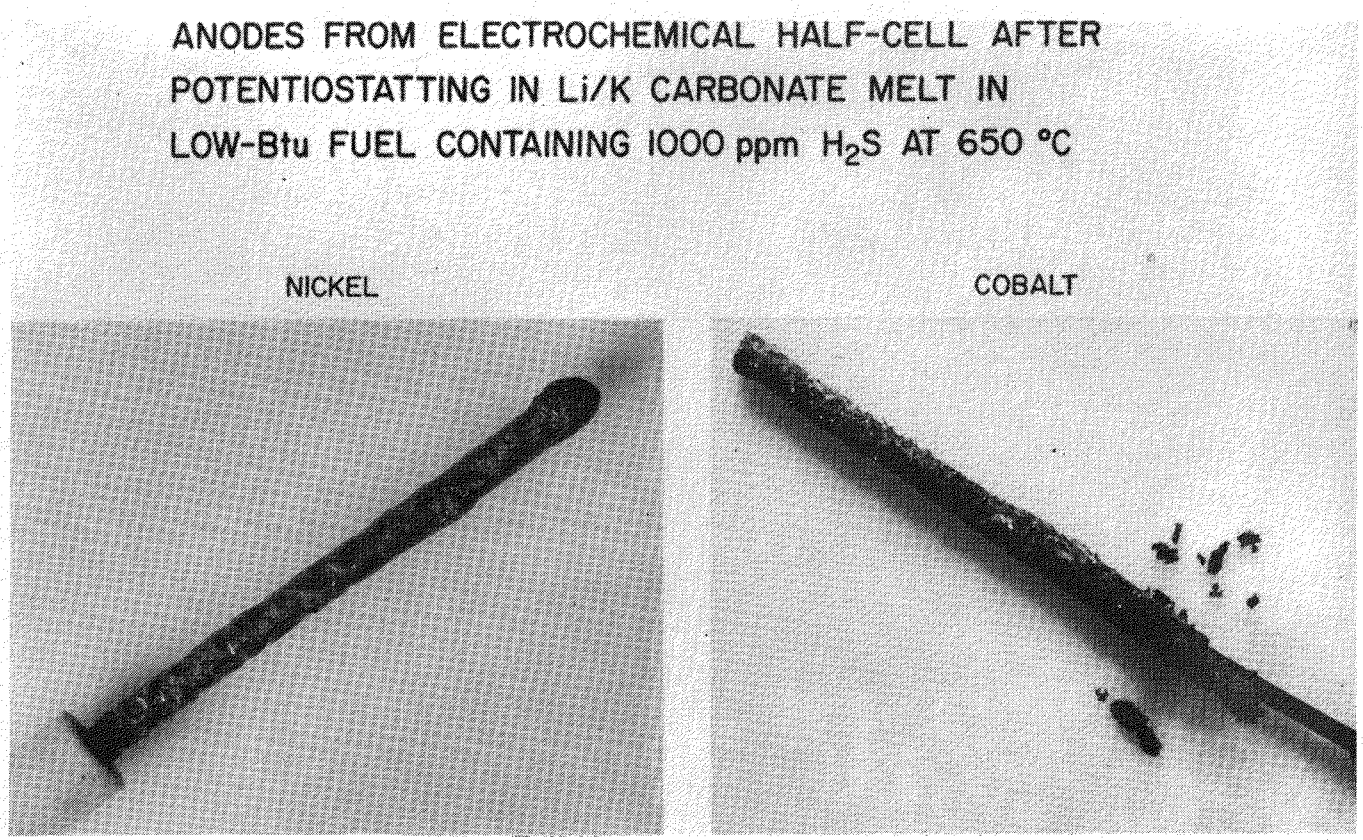

Figure 1-7. Anodes From Electrochemical Half-Cell After Potentiostatting in Li/K Carbonate Melt in Low-Btu Fuel Containing 1000 ppm H_2S at 650°C

from the activation polarization plots shown in Figures 1-3 and 1-4 were observed to become very slightly lower, reducing from 26 to 25 mA/cm^2, and from 19.5 to 18.5 mA/cm^2, respectively, for nickel and cobalt, although such small variations in kinetic data can be considered to be well within the experimental error of this work. As discussed earlier, introduction of 1000 ppm H_2S shifts the open-circuit potential to negative values in low-Btu fuel; very high apparent anodic and cathodic kinetic currents were observed. This may indicate formation of a metal sulfide on the surface of both the nickel and cobalt electrodes. The large cathodic current suggests reduction of the surface metal sulfide species, somewhat similar to the cathode reaction at the positive electrode of the lithium/metal sulfide battery.

It very well may be that when high sulfide concentrations build up in the proximity of the anode, neither nickel nor cobalt would be viable anode materials, particularly if the sulfur is introduced as SO_2 at the cathode. There is, therefore, considerable incentive to identify potentially sulfur-tolerant anode materials for this fuel cell system.

As discussed earlier, the selected candidates (potentially more sulfur-tolerant than cobalt or nickel) were initially screened in a simple corrosion test before being subjected to steady-state potentiostatic polarization evaluation in the electrochemical half-cell. These results are summarized in Table 1-2 where open-circuit potentials and anodic currents at 50 mV overpotential are compared. Apart from nickel and cobalt anodes, which have already been discussed, the highest stabilities were found for $Mg_{0.05}La_{0.95}CrO_3$ and TiC. Figure 1-8 compares steady-state polarization data on $Mg_{0.05}La_{0.95}CrO_3$ in low-Btu fuel with and without 50 ppm H_2S. No shift in the open-circuit potential was observed, and current voltage characteristics were very similar in both cases, particularly in the anodic region. Introduction of fuel containing 1000 ppm H_2S did not shift the open-circuit potential to negative values as observed with nickel and cobalt anodes, and examination of this material afterwards indicated no surface corrosion (Figure 1-9) even after prolonged anodic potentiostatting.

Figure 1-10 compares activation data performed on this material using the potential step technique with that obtained for nickel. For $Mg_{0.05}La_{0.95}CrO_3$, exchange current densities of around 8 mA/cm^2 were obtained in low-Btu fuel. Although considerably faster kinetics can be observed with the nickel anode, the exchange current density at the $Mg_{0.05}La_{0.95}CrO_3$ electrode is still rapid and the rate of the fuel oxidation process at a diffusion electrode will probably still be mass transfer controlled.

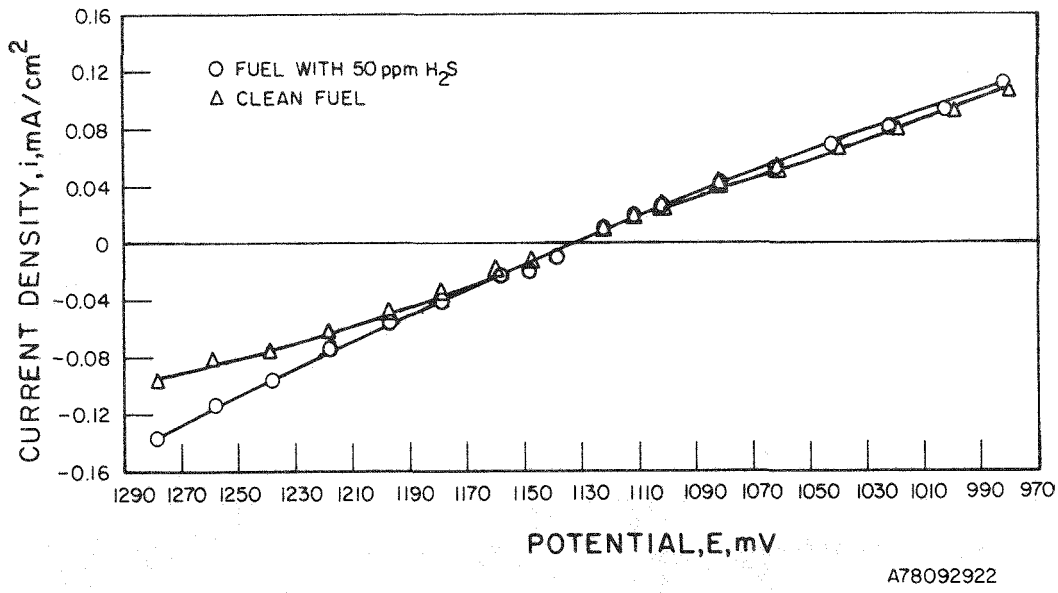

Figure 1-8. Steady-State Polarization Curve for $Mg_{0.05}La_{0.95}CrO_3$ Using Low-Btu Fuel With and Without 50 ppm H_2S Added (Li/K Electrolyte, 650°C)

Consequently, from the kinetic data and high apparent sulfur tolerance of $Mg_{0.05}$-$La_{0.95}CrO_3$, this material is an interesting candidate for a sulfur-tolerant anode. However, in comparing steady-state potentiostatic data obtained with $Mg_{0.05}La_{0.95}$-CrO_3 and nickel in clean electrolyte, lower currents were observed for the chromite. Because both electrodes exhibited rapid electrode kinetics, the smaller currents observed with $Mg_{0.05}La_{0.95}CrO_3$ in comparison with nickel may be due either to more local hinderance by the diffusion of reaction products away from the electrode surface or to differences in electrolyte stirring rates in the two experiments.

Steady-state polarization measurements have been performed on TiC, Cr_2O_3 (1 mol % of TiO_2), WC (75.7% W-24.3% Co), nichrome (80% Ni-20% Cr) and NiAl all in the lithium-potassium carbonate electrolyte at 650°C in low-Btu fuel. Examination of all of these materials showed evidence of surface corrosion.

Figure 1-11 compares the steady-state polarization data for WC in low-Btu fuel both with and without 50 ppm H_2S. The unusually negative open-circuit voltage of WC probably represents a corrosion potential under these experimental conditions. Introduction of 50 ppm was observed to shift this potential to positive values. Surface corrosion was evident when the WC was removed from the melt.

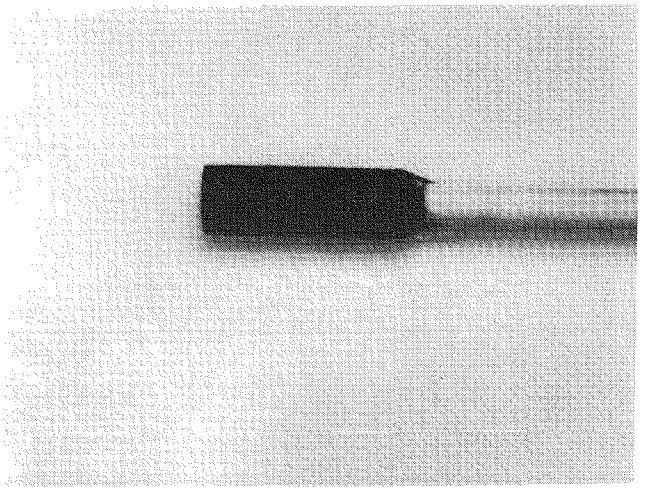

Before

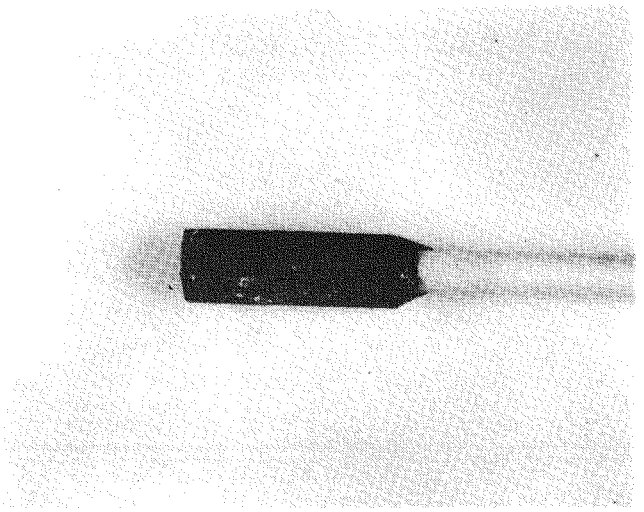

After

Figure 1-9. $Mg_{0.05}La_{0.95}CrO_3$ Electrode Before and After Exposure to Fuel Containing 1000 ppm H_2S (Li/K Electrolyte Used)

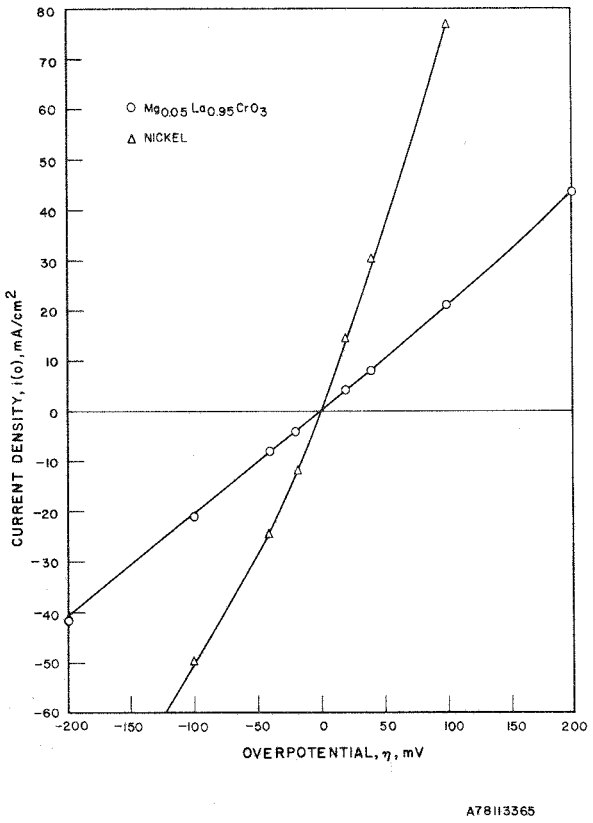

Figure 1-10. Activation Polarization Curve for $Mg_{0.05}La_{0.95}CrO_3$ and Nickel Using Low-Btu Fuel (Li/K Carbonate Electrolyte, 650°C)

TASK 2. EVALUATE AND DEVELOP SULFUR-TOLERANT ANODE CURRENT COLLECTOR

Candidate anode current collector materials were subjected to a similar corrosion test as were the anodes. The materials selected and the corrosion results are shown in Table 1-3. Of the materials evaluated, the highest corrosion stabilities were found for 446 and 310 stainless steels and Uniloy.

Some of these materials were also subjected to steady-state potentiostatic evaluation.

Figure 1-12 shows a steady-state polarization curve for 446 stainless steel; the results for all materials evaluated are summarized in Table 1-4. The more promising materials were anodically potentiostatted at 75 mV in low-Btu fuel with and without H_2S and the currents were recorded as a function of time. A decay in

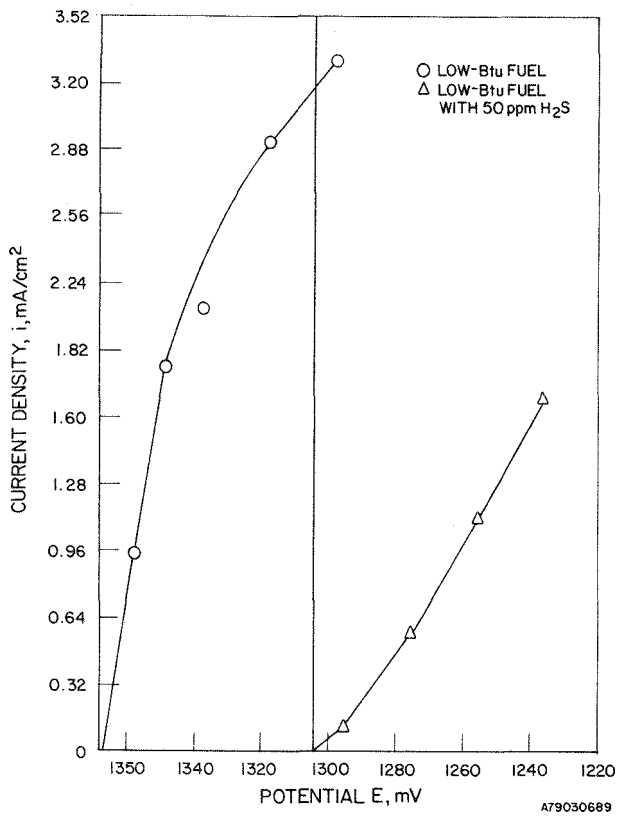

Figure 1-11. Steady-State Polarization Curve for WC in Li/K Carbonate Electrolyte at 650°C (Low-Btu Fuel Used With and Without 50 ppm H_2S)

current with time was taken as indicative of passivation due to surface oxide formation, as shown in Figure 1-13 for 446 stainless steel. This was confirmed later by visual examination.

Other materials subjected to steady-state polarization were the alloys Fe 70, Al 10, Mo 20, and Hastalloy X, together with 410, 316, and 310 stainless steels in low-Btu fuel with and without 50 ppm H_2S. Of the candidate anode current collector materials evaluated, the initial open-circuit potentials were observed to shift in the positive direction when in contact with 50 ppm H_2S. The open-circuit potentials observed may well be dictated by mixed potential effects caused by the fuel oxidation potential and the corrosion potential of the current collector.

Of these materials evaluated, the highest stabilities were found for 410 and 310 stainless steels. This does not suggest, however, that these materials will provide acceptable long-term stability at either the anode or the cathode for the molten carbonate fuel cell.

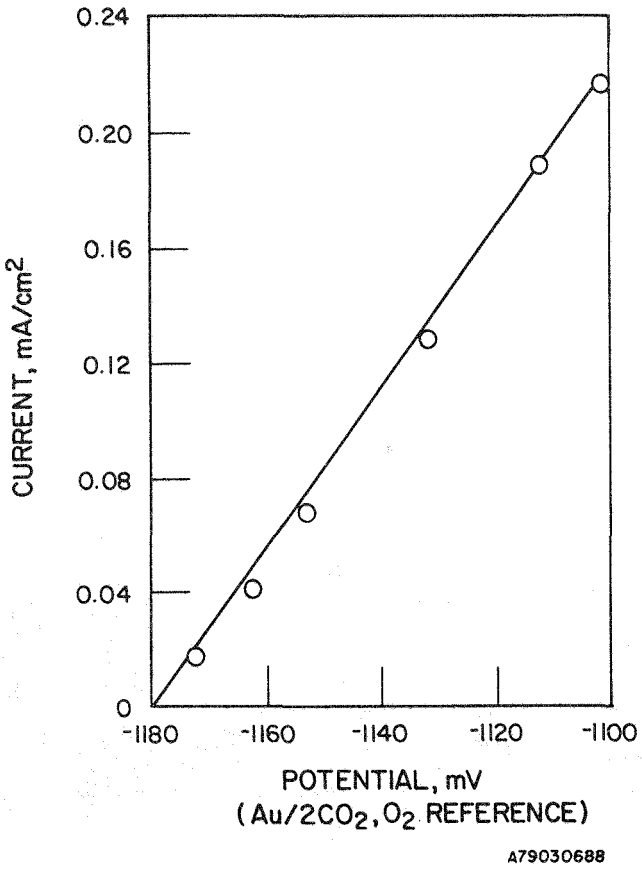

Figure 1-12. Steady-State Polarization Curve for 446 Stainless Steel in Low-Btu Fuel at 650°C

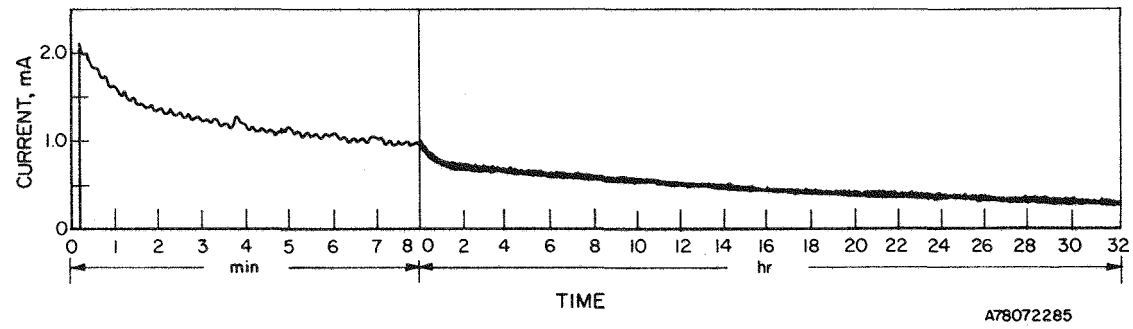

Figure 13. Variation of Current With Time at an Applied Anodic Overpotential of 75 mV for 446 Stainless Steel (Low-Btu Fuel Used)

Table 1-3

CORROSION RESULTS FOR CANDIDATE ANODE CURRENT COLLECTOR MATERIALS

Composition (%)	Total Exposure to Low-Btu Fuel (hr)	Period in 274 ppm H_2S (hr)	Total Weight Change (%)	Comments
C-0.25; Mn-2.0; Si-1.5; Cr-25.0; Ni-20; Fe-51.25 (SS-310)	1588	1301	+ 0.2	
Cr-50.0; Ni-49.0; Ti-1.0 (UNILOY)	1588	1301	+ 0.5	
Co-50.0; Cr-28.0; Fe-16.5; W-5.5	355	187	-20.3	
Fe-81.8; Al-15; Mo-3.2 (VE-441)	648	648	+82.9	
Cr-21.0; Mn-9.0; Ni-6.0; Fe-64	1588	1301	+ 0.5	
Fe-70; Al-10; Mn-20 (EX-20)	648	648	+26.7	
C-0.2; Cr-25.0; Ni-0.5; Fe-74.3 (SS-446)	1588	1301	+ 0.6	
Cr-22.0; Co-0.5; Al-5.0; Fe-73.5 (KANTHAL)	258	258	--	Completely corroded
C-0.15; Mn-2.0; Si-1.0; P-0.2; S-0.15; Cr-18.0; Ni-9.0; Mo-0.6; Fe-Bal. (SS-303)	1554	1554	- 5.3	
C-0.08; Cr-17.0; Ni-12; Mo-3.0; Fe-Bal. (SS-316)	1554	1554	+ 2.2	

Table 1-4

POTENTIOSTATIC EVALUATION OF ANODE CURRENT COLLECTOR MATERIALS USING LOW-Btu FUEL GAS IN BINARY CARBONATE MELT AT 650°C

Composition (%)	Clean Fuel		Fuel with 50 ppm H_2S		Comments
	Open Circuit Potential (mV)	Current, i, at 50 mV From Rest Potential (mA/cm^2)	Open Circuit Potential (mV)	Current, i, at 50 mV From Rest Potential (mA/cm^2)	
C-0.2; Cr-25.0; Ni-0.5; Fe-74.3 (SS 446)	-1182	0.128	-1137	0.147	
C-0.25; Mn-2.0; Si-1.5; Cr-25.0; Ni-20; Fe-51.25 (SS 310)	-1186	0.063	-1145	0.089	Black coating after test.
C-0.08; Cr-17.0; Ni-120; Mo-3.0; FeBal (SS 316)	-1173	0.156	-1164	0.197	Black coating after test.
C-0.15; Mn-1.0; Si-1.0; Cr-12.5; FeBal (SS 410)	-1173	0.184	-1148	0.157	
C-0.15; Mn-1.0; Si-1.0; Ni-45.45; Fe-18.5; Cr-21.8; Co-2.5; Mo-9.0; W-0.6 (Hastalloy X)	-1167	0.236	-1147	0.207	
Ni-80.0; Cr-20.0 (nichrome)	-1257	3.508			Corroded.
Cr-22.0; Co-0.5; Al-5.0; Fe-73.5 (Kanthal)	-1330	0.0			Corroded.
Fe-70; Al-10; Mn-20 (Ex 20)	-1347	0.218	-1222	0.911	
Fe-81.8; Al-15.0; Mo-3.2 (VE 441)	-1382	0.413			Crusted with thick black oxide.

REFERENCES

1. H. F. Gerischer. "Methods of Investigating the Kinetics of Electrode Processes." Zeitschrift fuer Elektrochemie, Vol. 51, 1955, pp. 604-612.

2. H. F. Gerischer and W. F. Vielstich. "Electrolysis at Constant Electrode Potential. I. Current-time Slope at Inhibited Discharge With Subsequent Delivery by Diffusion, and Conclusion About the Kinetics." Zeitschrift fuer Physikalische Chemie, Vol. 3, 1955, pp. 16-33.

Section 2

TASK 3. ASSESS ANODE AND CATHODE MATERIALS LIMITATIONS

SUMMARY

The original objective of this task was to evaluate the cathode materials limitations associated with utilization of SO_2-containing oxidants. Such a situation will occur in a real fuel cell stack when spent sulfur-containing fuels are combusted with excess air and recycled to the cathode to provide the CO_2 required in the oxidant. Experimental data obtained early in the program indicated that the most significant performance losses were occurring at the anode as a result of transport of sulfur species from cathode to anode through the electrolyte tile. Thus, the task was expanded to include determination of the tolerance of nickel- and cobalt-based anodes both to SO_2 in the oxidant stream and to H_2S/COS in the fuel. Emphasis was also shifted from performance with high-Btu fuels to low-Btu fuels because detrimental sulfur effects were found to be more severe under the latter conditions.

The most significant results of this portion of the program are -

- Present molten carbonate fuel cells show large performance losses, 60 mV at 160 mA/cm^2, when exposed to feed gases containing sulfur concentrations as low as 10 ppm.
- In addition to the initial 60 mV loss with 10 ppm sulfur, cells using nickel anodes show a continuous further decay. However, similar tests using cobalt anodes showed more stable performance.
- The majority of the performance loss is caused by the higher anode polarization even when sulfur is introduced into the cathode.
- The degree of anode stability and electrochemical performance losses are generally proportional to the H_2S/H_2 ratio. That is, for a fixed concentration of sulfur, larger degradations are observed with low concentration of H_2. As a result, the most severe problems occur at the anode outlet under higher conversion conditions.
- Anode materials stability and electrochemical performance are significantly affected by:

  1) Transport of S species through the tile from the cathode
  2) Incoming S species in the anode feed gas.

- SO_2 is scrubbed from the cathode gases almost quantitatively. This absorption results in conversion of alkali carbonates to alkali sulfates at the cathode interface. (Details will be discussed in Task 4.)

- Cathode materials stability and electrochemical performance are not significantly affected by SO_2-containing feed gases.

- Sulfur species are transported from the cathode to the anode when SO_2-containing feed gases are used. This transport, coupled with the equilibrium existing between the carbonate and the feed gases at each electrode, results in a sharp concentration gradient of sulfur species in the electrolyte tile between the cathode and the anode. The average, or bulk, concentration of sulfur species in the tile is low -- less than 10^{-2} mole fraction. (Details will be discussed in Task 4.)

CONCENTRATION OF SO_2 IN OXIDANT GASES

Calculations of the concentration of SO_2 entering the cathode were performed, assuming that spent fuel at 75% utilization would be combusted and the resulting gases (with necessary excess oxygen) would be fed to the cathode to supply its CO_2 and O_2 requirements. The calculated SO_2 concentrations for three values of oxygen utilization of cathode gas are shown in Table 2-1. Details of these calculations are presented in the Appendix.

Table 2-1

ESTIMATED SO_2 CONCENTRATION IN OXIDANT GAS ENTERING THE CATHODE

Process	H_2S in Anode Outlet At 75% H_2 Util.	SO_2 Concentration Entering Cathode		
		25% O_2 Util.	50% O_2 Util.	75% O_2 Util.
	ppm			
Steam-Reformed Naphtha	200	50	84	108
Low-Btu Coal Gasification, Air-Blown	200	79	128	162

STABILITY OF CATHODE MATERIALS

A literature survey was conducted regarding the effect of SO_2 on the catalytic activity of NiO and Co_3O_4 electrode materials, but no experimental information could be found. Likewise, no information could be found on the effect of SO_3, which could be present via the reaction:

$$SO_2 + 1/2\ O_2 \rightleftarrows SO_3 \qquad (2\text{-}1)$$

Using an oxidant containing 40 to 160 ppm SO_2 and 0.15 atm O_2, the equilibrium concentration of SO_3 was calculated to be 6 and 24 ppm, respectively, at 650°C. However, because it is known that the reaction is slow and requires an active catalyst such as bright platinum, it is doubtful that such concentrations of SO_3 would be present in the oxidant stream. As a result, we did not consider the effect of SO_3 on the activity of the cathode.

On the basis of the above discussion, the conversion of NiO or Co_3O_4 to sulfates and their possible dissolution in the carbonate electrolyte was considered on the basis of the reaction with SO_2, as follows:

$$NiO + SO_2 + 1/2\ O_2 \rightleftarrows NiSO_4 \qquad (2\text{-}2)$$

and

$$1/3\ Co_3O_4 + SO_2 + 1/3\ O_2 \rightleftarrows CoSO_4 \qquad (2\text{-}3)$$

Using the data of Kellogg(1), we calculated that the concentrations of SO_2 required to form $NiSO_4$ and $CoSO_4$ of unit activities are 119 ppm SO_2 and 156 ppm SO_2, respectively. These values fall in the range of SO_2 concentrations expected for typical cathode gases. (See Table 2-1.) Thus, some dissolution of both cathodic materials (NiO or Co_3O_4) may be expected under these conditions. However, as with anodic gases, cobalt is expected to be more stable than nickel with respect to sulfur compound formation.

Our literature survey identified nine studies made on the oxidation of metals in gases containing SO_2 that could be applicable to the selection of cathode current collectors. Most of the reported work dealt with much higher concentrations of SO_2 than can be expected in the cathodic gases. However, even at these more severe conditions, the series 300 stainless steels showed adequate corrosion resistance in

some studies below 650°C. Apparently, the stability of the Cr_2O_3 protective films formed on the metals studied are sufficiently impervious to the SO_2-containing gases. Rahmel rationalized and generalized his observations of protective scale growth as follows: When diffusion control in the scale results in parabolic kinetics, then the scale equilibrates with the reacting gas mixture at the scale/gas interface to exclude any influence of a less reactive second oxidant (SO_2)(2).

EXPERIMENTAL TESTING

Experimental Arrangement

Cell performance data with both clean and sulfur-contaminated gas mixtures were obtained in 3-cm^2 laboratory-scale cells. As shown in the schematic diagram in Figure 2-1, the porous electrodes, electrolyte tile, and Type 316 stainless steel current collectors were assembled into a high-purity alumina, cylindrical housing. Electrode potentials were measured with respect to duplicate $2CO_2$, O_2/Au reference electrodes. Fuel and oxidant gas flow patterns were established by means of a dual concentric alumina tube arrangement on either side of the cell. Alumina sampling tubes were provided to determine the concentration of sulfur species leaving the cell in the fuel and oxidant streams. Both stabilized nickel- and cobalt-based anode materials were investigated. The cathode in all tests was porous nickel that was oxidized in situ to NiO. All electrolyte tiles were hot-pressed from a state-of-the-art electrolyte batch containing 39.5 wt % $LiAlO_2$ and 60.5 wt % carbonate of composition 64.4 mol % Li_2CO_3/35.6 mol % K_2CO_3.

Several fuel gas compositions were used during the course of the study. The high-Btu fuel gas, simulating reformed natural gas, was a mixture of 80% H_2 and 20% CO_2 humidified at 56°C to yield an equilibrium composition of 60.0% H_2, 7.4% CO_2, 10% CO, and 22.6% H_2O at 650°C. Two different premixed gases were used to simulate a low-Btu product from an air-blown coal gasifier. The first low-Btu gas corresponded to an equilibrium composition at 650°C of 19.9% H_2, 11.4% CO_2, 9.1% H_2O, 12.8% CO, balance N_2. This mixture was used in cell EPRI-7 through the first low-Btu phase of cell EPRI-10. The low-Btu inlet gas mixture used in all later work had an equilibrium composition at 650°C of 21.1% H_2, 9.2% CO_2, 17.8% CO, 5.6% H_2O, balance N_2. A low-hydrogen content mixture was used to simulate outlet conditions for 75% fuel utilization -- 4.0% H_2, 39.9% CO_2, 4.7% CO, 17.6% H_2O, balance N_2 at equilibrium. The standard oxidant composition of 70% air-30% CO_2 was humidified at room temperature (29.1% CO_2, 14.3% O_2, 3.0% H_2O, 53.6% N_2).

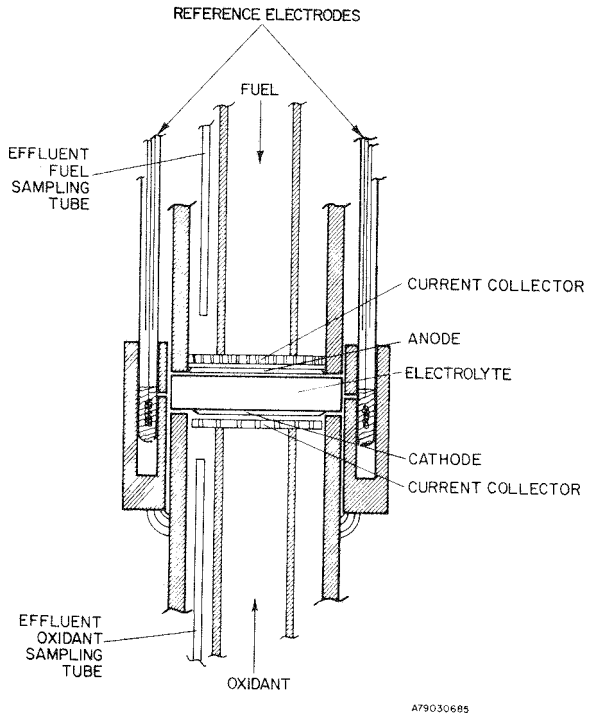

Figure 2-1. Cell With Reference Assembly

Baseline Cell Performance With Clean Feed Gases

To establish baseline performance in the absence of sulfur-containing impurities, seven cells were operated with clean fuel and oxidant gases. The performance baseline for a typical cell (EPRI-3) with high-Btu fuel and standard oxidant is shown in Figure 2-2. Results of six baseline cells with high-Btu fuel indicated the following performance bands at 100 mA/cm^2: a cell potential of 980-1000 mV, anode polarization of 30-35 mV, and cathode polarization of 45-60 mV. Overall cell resistance (including the 0.05 ohm resistance for each of the two stainless steel current collector leads) was 0.27 - 0.28 ohms. Typical anode and cathode resistances were 0.12 and 0.15 ohms, respectively. Typical anode, cathode, and cell polarization curves after 1000 hours of operation (from cell EPRI-3) are shown in Figure 2-3.

As cell testing with sulfur contaminants proceeded during the course of these investigations, more emphasis was placed on low-Btu fuel gases because of the more severe sulfur interactions in these lower hydrogen fuels. Baseline stability performance with clean low-Btu fuel and clean oxidant with S-O-A components was established in cell EPRI-15. Lifetime anode, cathode, and cell performance curves are

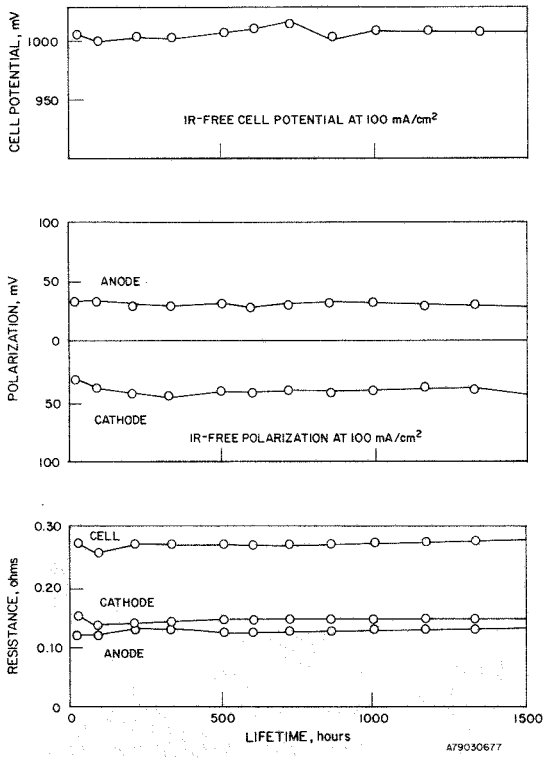

Figure 2-2. Performance of Cell EPRI-3 at 650°C With High-Btu Fuel

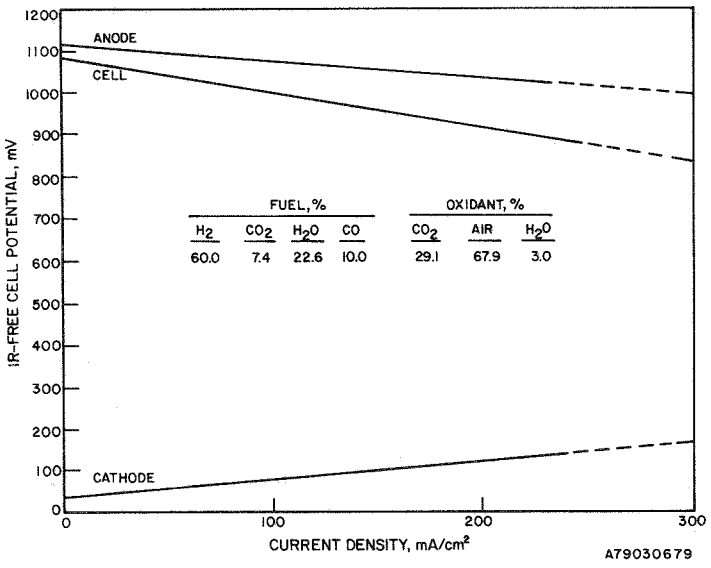

Figure 2-3. IR-Free Polarization vs. Current Density for Cell EPRI-3 After 1000 Hours of Cell Operation at 650°C. Conversions: 7.5% H_2, 15.0% CO_2 at 200 mA/cm^2

shown in Figure 2-4. After a break-in period of 200 hours, the IR-free cell potential at 100 mA/cm^2 showed some fluctuations in the range 950-960 mV. The fluctuations were minor and appeared to be largely a result of changes in the anode open-circuit voltage (OCV). The cause of these minor variations could not be determined. Despite these fluctuations, however, good anode and cathode performance and stability over 1500 hours of operation were demonstrated in this test.

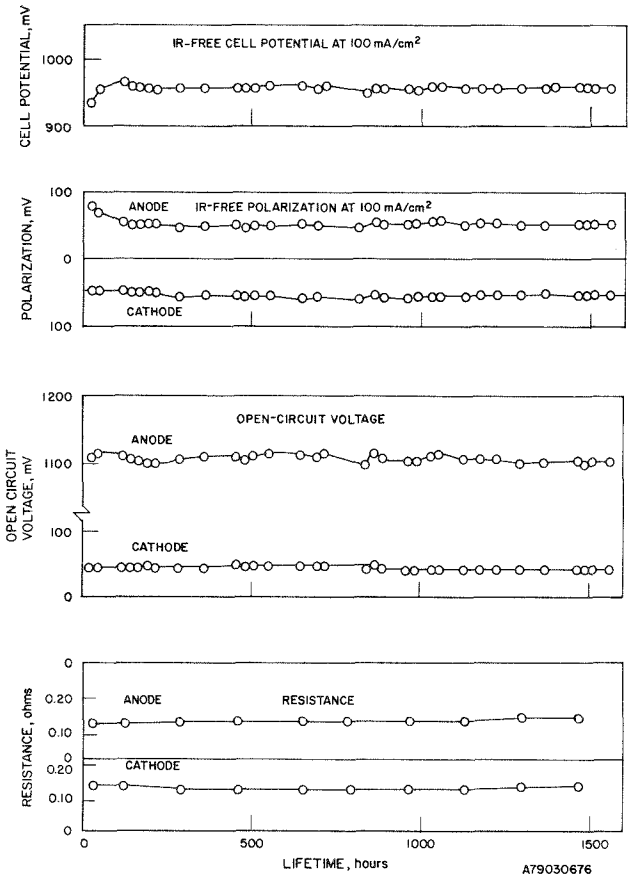

Figure 2-4. Performance of Cell EPRI-15 With Low-Btu Fuel at 650°C

Cell Performance With Oxidant Containing SO_2

Cell EPRI-7, assembled with S-O-A components, was the first test in which sulfur was introduced as SO_2 in the oxidant gas. The cell was operated 484 hours with

sulfur-free oxidant to allow it to stabilize and to confirm that typical baseline performance was being obtained. After 484 hours of operation, we began using an oxidant containing 35 - 43 ppm of SO_2 (other conditions kept constant) to identify its impact on the cell performance using reformed natural gas (60% H_2) fuel. Upon stabilization of the cell performance, a sulfur mass balance between the oxidant inlet and the oxidant and fuel outlets was determined by gas chromatography. After 380 hours of cell operation with the SO_2-containing oxidant, the fuel was changed to a simulated low-Btu air-blown coal gasification product (19.9% H_2, 11.4% CO_2, 9.1% H_2O, 12.8% CO, balance N_2 at equilibrium) to observe the effects on cell performance. The cell was terminated after 1104 total hours of operation to examine its components.

The performance of EPRI-7 under the different oxidant and fuel conditions is shown in Figure 2-5. The SO_2 in the oxidant, in general, decreased the cell performance because of lower OCV and higher electrode polarization, particularly at the anode. The largest polarization effects, as expected, were observed when low-Btu fuel was used. From Figure 2-5, cell performance deterioration is directly related to losses in open-circuit potential and to polarization increase at the anode. Cell IR resistance was found to be fairly constant throughout the course of these experiments.

The losses of cell performance by oxidant-containing SO_2 are summarized in Table 2-2. With reformed natural gas fuel, a net loss in cell open-circuit potential of 27 mV resulted from +44 mV at the anode and -17 mV at the cathode. Some shift in the measured electrode potentials may have resulted from sulfur contamination of the reference electrode. A net loss of 40 mV in the cell polarization at 100 mA/cm^2 was attributed to anode polarization, which increased from 30 to 70 mV upon introduction of SO_2 into the oxidant. The use of low-Btu fuel resulted in even greater losses of cell OCV and in polarization increases.

Gas chromatographic (GC)* analysis of the sulfur species of the oxidant inlet and fuel and oxidant outlets were performed to determine the behavior of sulfur species in the cell and for correlation with observed performance losses. These GC results are shown in Figure 2-6.

---

* Varian Model 3700 Gas Chromatograph with Poropak column and flame photometric detector was used.

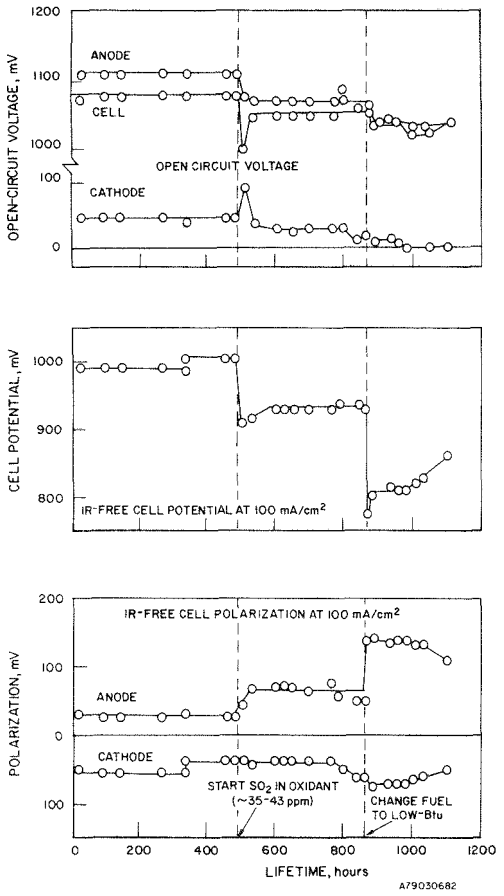

Figure 2-5. Performance of Cell EPRI-7 With and Without SO_2 in the Oxidant

Time zero (484 hours of the cell's lifetime) corresponds to the initial introduction of the SO_2-contaminated oxidant. After 380 hours of operation (864 hours of the cell's lifetime) in the sulfur-containing environment with reformed natural gas fuel, lean-hydrogen fuel was started. As seen in the figure, during operation with reformed natural gas fuel for approximately 20 hours, the electrolyte absorbed the total amount of SO_2 fed. After 20 hours, the amount of sulfur species (mainly H_2S and COS) coming out in the fuel outlet increased rapidly, and after 50 hours practically all of the SO_2 fed into the cathode came out as sulfur species in the fuel outlet. At this time (50 hours), 32.5 ppm SO_2 were being fed into the cathode, of which 28.5 ppm came out as sulfur species in the fuel outlet and 2 ppm SO_2 came out in the oxidant outlet. As seen in the figure, after 50 hours of operation in the sulfur environment, any small variation in the level of SO_2 fed caused only proportional changes in the level of sulfur species coming out in the fuel and no changes in the amount of unabsorbed SO_2.

Table 2-2

LOSSES OF PERFORMANCE CAUSED BY SO_2 IN THE OXIDANT USING REFORMED NATURAL GAS AND LOW-Btu FUEL

	EPRI-7				
	Reformed Natural Gas			Low-Btu Fuel	
	Clean	35-43 ppm SO_2	Losses Caused By Sulfur	35-43 ppm SO_2 in Ox	Total Losses
	mV				
Open-Circuit Voltage					
Anode	-1107	-1063	44	-1032	75
Cathode	-35	-18	-17	-8	-27
Cell	-1072	-1045	27	-1024	48
Polarization (IR-free at 100 mA/cm^2)					
Anode	30	70	40	140	110
Cathode	37	37	0	70	33
Cell	67	107	40	210	143
Potential (IR-free at 100 mA/cm^2)					
Anode	-1077	- 993	84	- 892	185
Cathode	-72	-55	-17	-78	6
Cell	-1005	- 938	67	- 814	191

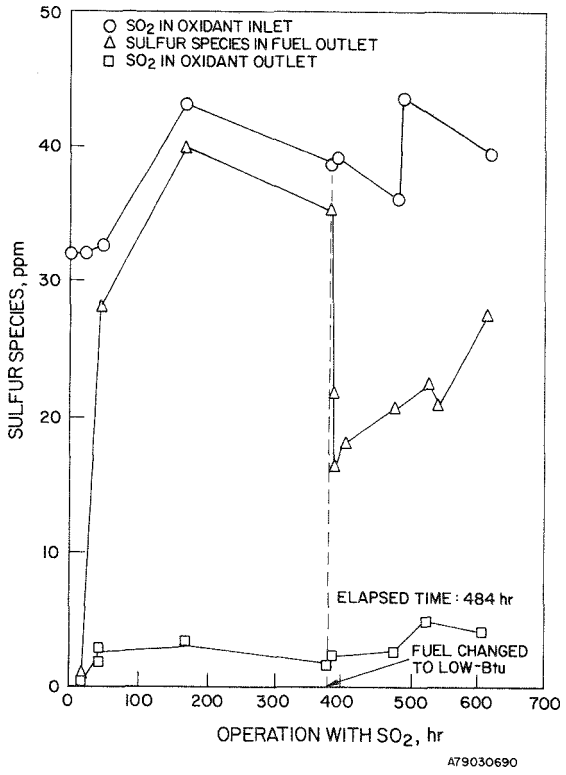

Figure 2-6. Results of Gas Chromotographic Analysis From the Oxidant Inlet and Outlet and Fuel Outlet of Cell EPRI-7

When the fuel was changed to lean hydrogen, a rapid decrease in the ppm of sulfur species coming out in the fuel outlet was observed. Out of 39 ppm of SO_2 fed, 16 ppm came out as sulfur species in the fuel outlet and 2.5 ppm of SO_2 as unabsorbed SO_2 in the oxidant outlet. The concentration of sulfur species exiting in the fuel stream then increased with time and was approaching a new steady-state mass balance situation when the test was terminated at 1104 hours. The difference between inlet and outlet sulfur levels represented accumulation in the cell due to sulfidation of the anode and stainless steel components and formation of sulfur species in the electrolyte tile.

These GC results confirmed thermodynamic calculations that indicated that SO_2 would be removed from the oxidant by conversion of carbonate to sulfate species. (See Task 4.) The sulfur analysis also indicated the transport of sulfur species through the electrolyte tile to the anode region where reduction of alkali sulfate

and/or sulfide to H_2S and COS occurred. A detailed thermodynamic analysis of the alkali carbonate/sulfate/sulfide equilibria under both cathode and anode conditions will be presented under Task 4.

Cell EPRI-8 was also assembled with S-O-A components and stabilized on clean high-Btu fuel and clean oxidant, as shown in the lifetime performance plot of Figure 2-7.

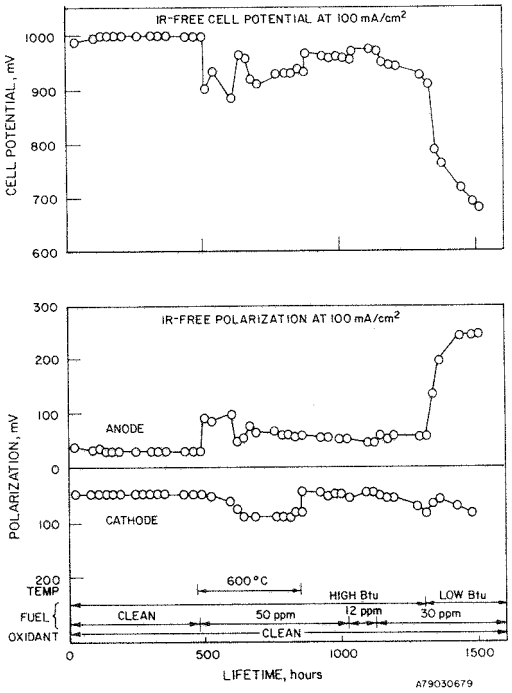

Figure 2-7. Performance of Cell EPRI-8 With and Without SO_2 in the Oxidant (High- and Low-Btu Fuels)

After 480 hours of operation with clean oxidant and reformed natural gas fuel, the cell performance was comparable to the baseline data established in cells EPRI-3 through EPRI-6 (1000 mV cell potential and 30 and 50 mV anode and cathode polarization, respectively, at 100 mA/cm^2). Flow of 50 ppm SO_2 oxidant began at 480 hours. However, the cell performance results indicated after 480 hours in this figure were affected not only by the SO_2 contaminant, but also by an undetected decrease in cell temperature from 650°C to approximately 600°C. This occurred because the potentiometer used to monitor the cell temperature was malfunctioning; the problem was

corrected at 864 hours of operation while using a different potentiometer. Cell performance remained relatively stable at 650°C during 864 to 1024 hours, during which time the following observations were made:

a. At 100 mA/cm^2 and using reformed natural gas fuel, the cell potential decreased from 1000 to 960 mV when using an oxidant containing 50 ppm SO_2.

b. The anode polarization at 100 mA/cm^2 increased from 30 to 55 mV, while the polarization of the cathode did not change.

c. The anode OCV decreased from 1110 to approximately 1095 mV while the cathode OCV did not change.

The observed short-term net loss of 40 mV in the anode potential at 100 mA/cm^2 caused by sulfur compounds in EPRI-8 compared reasonably well with the 67 mV observed in EPRI-7 under similar conditions.

At 1032 hours of operation and while using high-Btu fuel, the SO_2 concentration in the oxidant was decreased from 50 to 12 ppm. This change resulted in an increase in cell potential at 100 mA/cm^2 from 960 to 975 mV. The cell potential remained fairly stable during this 90-hour period of operation with 12 ppm SO_2-containing oxidant. At 1135 hours, the oxidant containing 50 ppm SO_2 was reintroduced into the cell, still using high-Btu fuel. The cell potential at 100 mA/cm^2 declined to approximately 950 mV in a step-like fashion as a result of the higher SO_2 level and continued to decline to 930 mV during the next 165 hours. After 1328 hours of cell operation, the anode gas was changed from high-Btu to low-Btu while maintaining the 50 ppm SO_2 level in the oxidant. These operating conditions resulted in a severe and continuing loss of cell potential, which had declined to 680 mV at 100 mA/cm^2 by the time the cell was terminated at 1515 hours. As shown in Figure 2-7, this severe decline in performance was associated with a significant increase in anode polarization -- from approximately 60 to 250 mV during the 187 hours of continuous operation on clean low-Btu fuel and oxidant with 50 ppm SO_2.

GC analyses of the fuel and oxidant gas streams again indicated the "scrubbing" of SO_2 from the oxidant gas at the cathode and transport of sulfur species through the tile to the anode. Removal of sulfur from the tile was indicated by the presence of H_2S, COS, and traces of SO_2 in the anode effluent stream. As in EPRI-7, a reasonably good mass balance was obtained between the amount of sulfur entering the cathode as SO_2 and the total amount of sulfur leaving the cell in the fuel stream.

During operation of EPRI-8, experiments were performed to study the effect of cell current density on the concentration of sulfur species in the fuel outlet. As shown by the results on Figure 2-8, the concentration of H_2S and total sulfur were dependent on current density, suggesting a Faradaic transport mechanism of sulfur through the tile from cathode to anode.

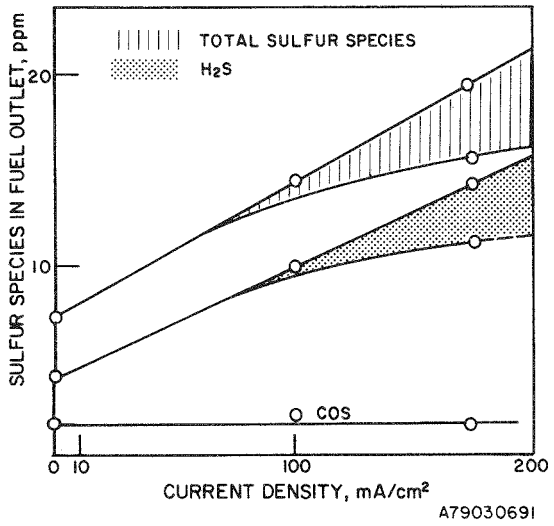

Figure 2-8. Changes in Concentration of Sulfur Species in the Effluent Fuel With Current Density in Cell EPRI-8

Cell EPRI-9, again with S-O-A components, was operated under the fuel and oxidant conditions shown in Figure 2-9. The cell was stabilized with high-Btu fuel and clean oxidant for 390 hours, at which time the anode gas was changed to a low-Btu inlet fuel composition. This change of fuel resulted in an IR-free cell potential loss of approximately 50 mV at 100 mA/cm² (from 1000 mV for high-Btu to 950 mV for low-Btu fuel). At 510 hours, while operating with clean oxidant, the fuel gas was changed to the composition corresponding to low-Btu outlet conditions.* An

* 4.0% H_2, 17.6% H_2O, 4.7% CO, 39.9% CO_2, balance N_2.

additional cell potential loss of about 140 mV resulted from this leaner fuel. At about 552 hours, and with this low-Btu outlet fuel gas, oxidant containing nominally 50 ppm SO_2 was introduced to cell EPRI-9. As shown in Figure 2-9, cell potential rapidly decreased to 570 mV at a current density of 100 mA/cm^2. Again, the severe performance loss was attributable to increased anode polarization. The cell was operated under these conditions for only a brief period of time before switching back to low-Btu inlet fuel composition. The cell recovered to a potential of 880 mV at 100 mA/cm^2 within 24 hours after switching to the richer fuel mixture, but fluctuated between 865 and 895 mV during the following 340 hours of operation with low-Btu fuel and 50 ppm SO_2-containing oxidant. During this period of "steady" operation, cell EPRI-9 was operated at a constant cell potential that yielded a current density of 126-142 mA/cm^2. This mode of operation was changed during the time period of 960 to 1070 hours, when the cell was operated at several constant current density levels rather than at constant potential. The time periods and corresponding current densities were 100 mA/cm^2 during 960-984 hours, 50 mA/cm^2 during 984-1032 hours, and back to 100 mA/cm^2 during 1032-1064 hours. The cell was operated at a constant potential (700 mV anode to cathode, uncorrected for IR effects) from 1064 hours through the remainder of the test. As shown in Figure 2-9, cell performance declined as the operating current density was decreased. Previous GC analyses of cell EPRI-8 indicated that the sulfur concentration in the fuel effluent decreased as the current density was decreased in that test. These observations indicate that the transport of sulfur through the tile and its subsequent removal at the anode as H_2S, COS, and SO_2 species are intimately coupled with the electrochemistry of the system. In addition, it is likely that the lower performance observed during operation at lower current densities is related to accumulation of sulfur species in the tile. Because of the dynamic situation involved during cell operation, an adequate description of sulfur interactions requires a knowledge of both the thermodynamics and kinetics of the controlling mechanisms in the cathode, tile, and anode.

The performance of EPRI-9 showed a continual decline after 1064 hours during constant potential operation. The cell potential at 100 mA/cm^2 had decreased to 680 mV when the test was terminated after 1320 hours of total operation. The performance losses observed near the end of the EPRI-8 and EPRI-9 tests indicate that state-of-the-art components will not endure long-time operation with clean low-Btu fuels and oxidant containing 50 ppm SO_2.

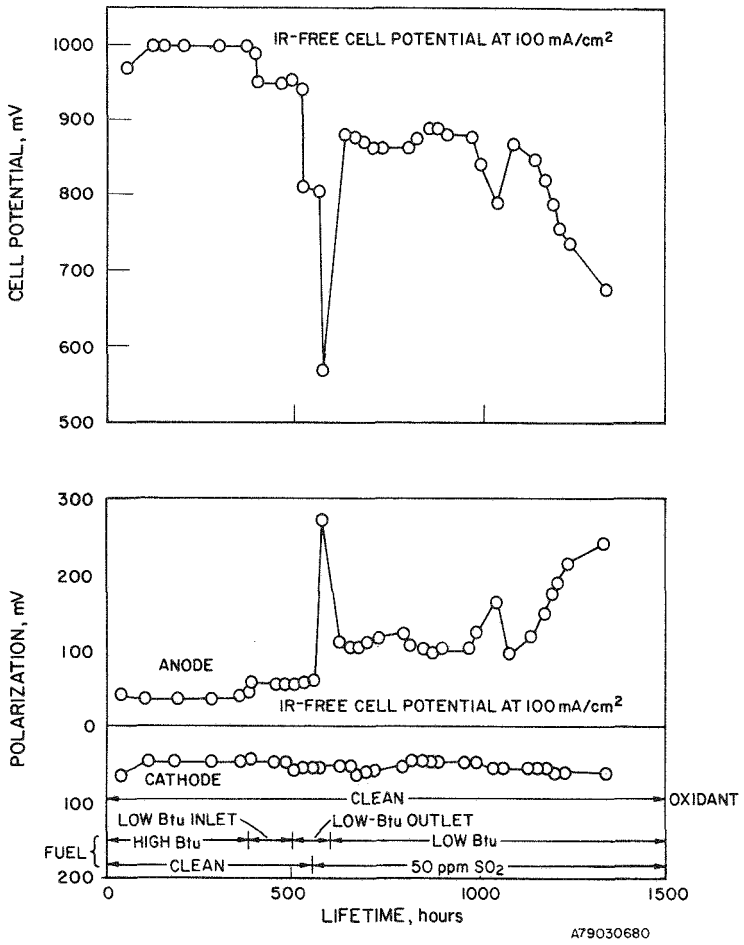

Figure 2-9. Performance of Cell EPRI-9 With and Without SO_2 in the Oxidant (High-Btu, Low-Btu Inlet, and Low-Btu Outlet Fuels)

The losses in cell potential observed in all three tests, EPRI-7, 8, and 9, with SO_2-containing oxidant were largely attributable to increased polarization at the stabilized nickel anode, although some open-circuit potential losses were also observed. No significant losses occurred at the cathode. Figure 2-10 shows anode and cathode polarization curves obtained under several different fuel and oxidant conditions. Anode losses in the presence of sulfur were seen to become increasingly severe as the fuel gas was changed from high-Btu to low-Btu inlet to low-Btu outlet composition. As will be discussed in a later section (Examination of Cell Components), metallographic analysis of the nickel-based anodes from cells EPRI-7, 8, and 9, which operated with both clean high- and low-Btu fuels and oxidant containing

approximately 50 ppm SO_2, revealed significant coarsening of the porous structure at the anode/tile interface. X-ray diffraction analyses showed that the nickel had been partially sulfided to Ni_3S_2, leading to formation of liquid Ni/Ni_3S_2 eutectic at 650°C.* To identify cell performance losses not associated with bulk sulfide formation, a series of cell tests aimed at eliminating this irreversible anode restructuring effect were initiated. A cell (EPRI-11) with stabilized nickel anode was operated with a lower level of sulfur species (approximately 10 ppm SO_2 in oxidant) in an attempt to stay below the threshold H_2S/H_2 ratio for bulk Ni_3S_2 formation at the anode.

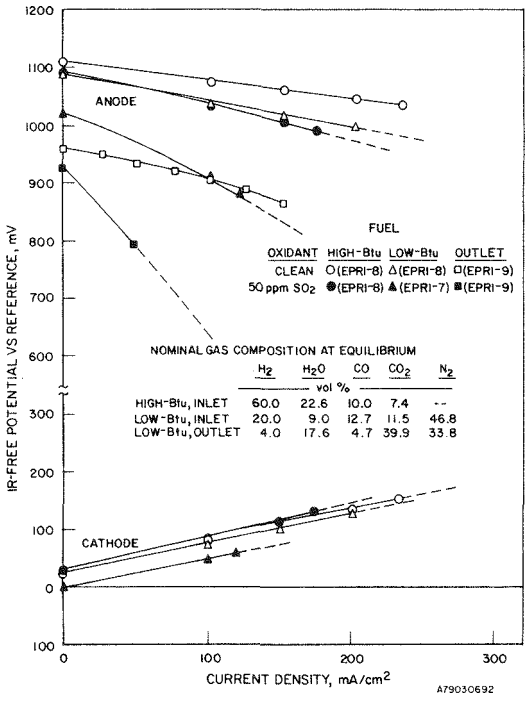

Figure 2-10. Anode and Cathode Polarizations Observed Under Different Fuel and Oxidant Conditions (Stabilized Ni Anode, NiO Cathode)

* The Ni/Ni_3S_2 eutectic temperature is 645°C.

Another cell (EPRI-10) with a stabilized cobalt anode was operated with an oxidant containing approximately 50 ppm SO_2 to compare performance losses and anode/sulfur chemical interactions with those observed with nickel. These tests emphasized performance with low-Btu fuels. The possible advantages associated with use of cobalt in sulfur-containing environments are a) the threshold H_2S/H_2 ratio for bulk cobalt sulfide formation at 650°C is nearly three times greater than that for nickel sulfide formation and b) even if it does occur, sulfidation of cobalt should not result in formation of a liquid phase at the 650°C cell operating temperature.

Cell EPRI-10 was assembled with a Co-20% Cr anode, state-of-the-art tile, and NiO cathode. The performance data for this cell using clean high- and low-Btu fuels and 70% air/30% CO_2 oxidant with 0 and 50 ppm SO_2 are summarized in Figure 2-11. Previous cells, with stabilized nickel anodes, produced stable performance when operated with clean oxidant (no SO_2) and clean fuels. As seen in Figure 2-11, cell EPRI-10 did not show such a stable performance during the operation with clean reactant gases (up to 456 hours of cell lifetime). The slow decay in performance observed in cell EPRI-10 during this period likely resulted from structural changes in the anode or inadequate pore-size matching between anode, tile, and cathode. However, the cell performance results with SO_2-containing oxidant are very encouraging in that the cobalt electrode did not experience catastrophic decay as did the stabilized-nickel anodes in cells EPRI-8 and EPRI-9 under comparable conditions.

Cell EPRI-10 operated the first 168 hours with high-Btu fuel and clean oxidant. During this period a decay of 10 mV occurred in the cell potential (IR-free at 100 mA/cm^2) because of increased anode polarization. After 168 hours of operation, the fuel was switched to low-Btu; this caused a drop of 60 mV (from 980 to 920 mV) in the cell potential at 100 mA/cm^2 because of 25 mV higher anode polarization and 35 mV lower anode rest potential. Between 168 hours and 456 hours, the cell operated with the low-Btu fuel and clean oxidant; during this period the cell potential dropped to 870 mV (from 920 mV) because of 50 mV higher anode polarization. After 456 hours, while the cell was operating with low-Btu fuel, an oxidant containing 50 ppm SO_2 was introduced. The introduction of the SO_2 in the cathode caused an increase of 65 mV (to 170 mV) in the anode polarization after 24 hours and 85 mV (to 190 mV) after 76 hours. To determine the reversibility of these performance losses, the reactant gases were switched to high-Btu fuel and clean oxidant. This switch brought about a dramatic decrease in the anode polarization from 190 mV with the SO_2-containing oxidant and the low-Btu fuel to 50 mV with high-Btu fuel and clean oxidant. Because of the much lower anode polarization, the cell potential increased to 970 mV (from 790 mV with low-Btu fuel and SO_2 oxidant). The significant

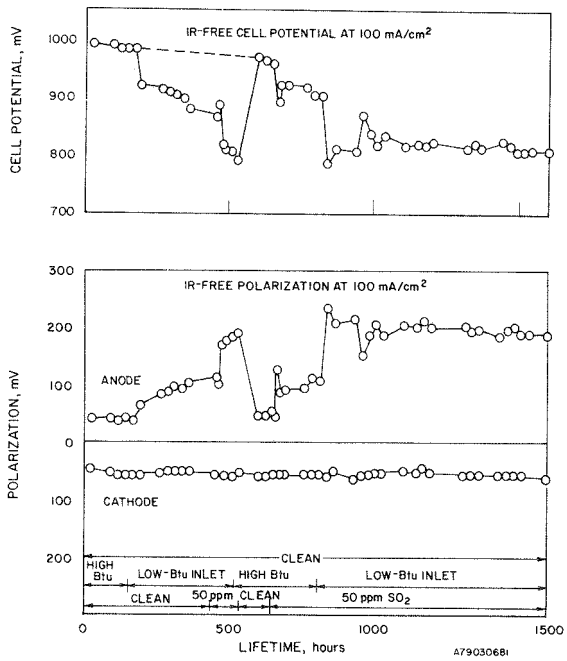

Figure 2-11. Performance of Cell EPRI-10 With and Without SO_2 in the Oxidant (High- and Low-Btu Fuels, Stabilized Cobalt Anode)

recovery of potential upon removal of SO_2 suggested that no permanent degradation of the cobalt anode had occurred. When the cell reached 648 hours of operation, while flowing high-Btu fuel, the oxidant containing 50 ppm of SO_2 was again introduced. The anode polarization increased to 90 mV (from 50 mV) after 24 hours and to 110 mV after 168 hours. At this point (816 hours cell lifetime), the fuel was switched back to low-Btu and again the anode polarization went up to 190 mV and the cell potential to approximately 810 mV. From 816 hours to 1800 hours the cell operated with the low-Btu fuel and the SO_2-containing oxidant without further performance decay. The cell was terminated after 1800 hours.

Because the cell exhibited some anode instability during operation with clean reactant gases, and because we have not generated adequate baseline data with clean low-Btu fuels using stabilized cobalt anodes, it is difficult to precisely establish the total anode polarization loss caused by sulfur compounds. However, attributing the increase in anode polarization observed within 24 to 48 hours after switching to SO_2-containing oxidant to the action of sulfur compounds, anode potential losses of approximately 40 mV occurred with high-Btu fuel and 65 mV with low-Btu fuel (at 100 mA/cm^2). Although such performance losses are significant, the results from EPRI-10 are encouraging in that the stabilized cobalt anode operated for 1152 hours

with approximately 50 ppm SO_2 in the oxidant without the catastrophic performance decay that was observed with nickel anodes in cells EPRI-8 and EPRI-9.

Cell EPRI-11 was operated with state-of-the-art components (stabilized Ni anode and NiO cathode). As shown in Figure 2-12, the performance of EPRI-11 at 650°C with high-Btu fuel and "clean" standard oxidant was comparable to the baseline performance established earlier for cells EPRI-3 and EPRI-6 (that is, approximately 1000 mV cell potential at 100 mA/cm^2). After approximately 150 hours of operation on high-Btu fuel, the cell was switched to low-Btu fuel, still with clean oxidant. The baseline performance with low-Btu fuel and clean oxidant was approximately 980 mV cell potential at 100 mA/cm^2. At 528 hours, oxidant containing approximately 10 ppm SO_2 was fed to the cell. The cell potential at 100 mA/cm^2 gradually declined to approximately 925-930 mV during the period 528-768 hours. Consistent with previous observations when sulfur was introduced into the cell as SO_2 at the cathode, loss in EPRI-11 cell potential was caused by an increase in anode polarization -- from approximately 55 to 110 mV at 100 mA/cm^2.

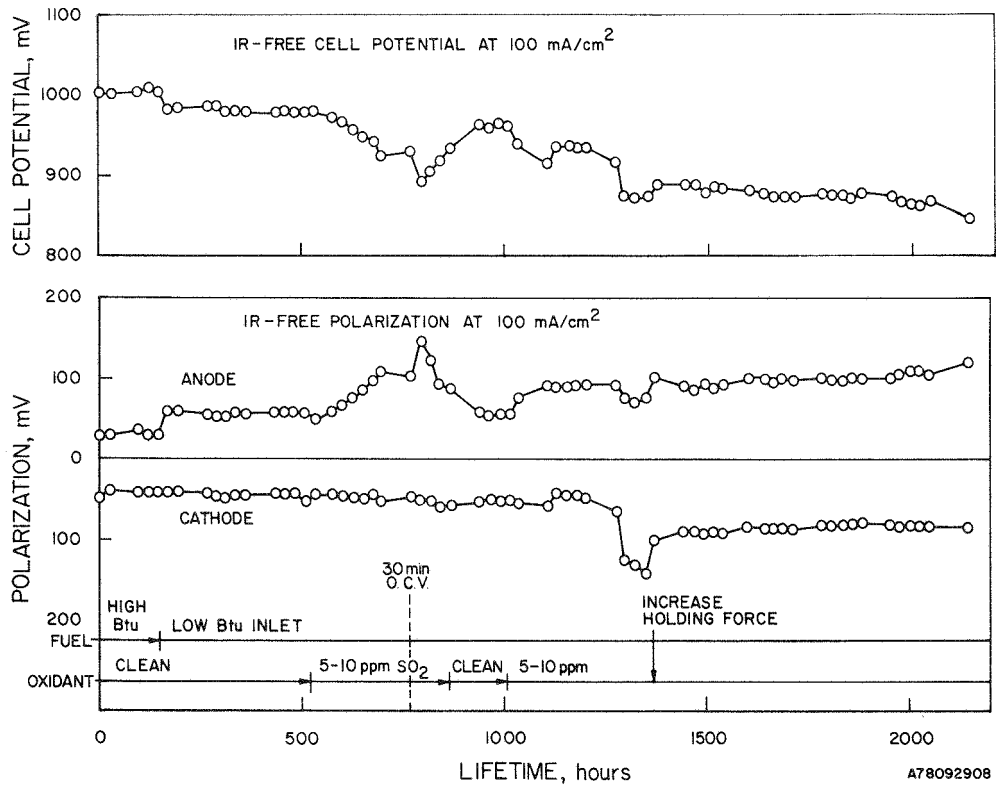

Figure 2-12. Performance of Cell EPRI-11 With and Without SO_2 in the Oxidant (Stabilized Nickel Anode)

At 768 hours of operation, EPRI-11 was held at open-circuit potential for 30 minutes to determine the effect of such a condition on subsequent cell performance. Performance was observed to be significantly lower the following day (a further cell potential loss of approximately 40 mV at 100 mA/cm^2) because of a significant increase in anode polarization. This loss in performance associated with open-circuit operation was recovered during the next 96 hours of steady operation at 700 mV anode-to-cathode potential. Based on results obtained earlier on cells EPRI-8 and EPRI-9, the losses caused by holding at open circuit for a short time were possibly related to a build-up of sulfur species in the tile at open-circuit potential, followed by a relatively large "step" release of sulfur into the anode when the cell was again put under load.

The SO_2-contaminated oxidant was replaced by clean gas at 864 hours, and the cell potential showed further recovery, back to approximately 960 mV at 100 mA/cm^2 after 144 hours on clean oxidant. This result indicated approximately 20 mV net loss in cell potential not recovered after switching back to clean gases.

Oxidant containing approximately 5-10 ppm SO_2 was reintroduced tc EPRI-11 at 1008 hours, and the cell was operated under these conditions after that time. Although the cell did not experience catastrophic decay, its performance has been somewhat erratic during the period 1008-1600 hours. (See Figure 2-12). During 1272-1344 hours, an abnormally large increase in the cathode polarization was observed. Approximately half of the 95 mV increase in cathode polarization was eliminated when the cathode holding force was adjusted at 1368 hours. Although further attempts at decreasing the polarization by holding force adjustments proved unsuccessful, it is believed that this increase in cathode polarization is related to contact resistance or carbonate distribution effects, rather than interaction of SO_2 with the NiO cathode.

After approximately 2200 total hours of operation, the cell potential of EPRI-11 at 100 mA/cm^2 had decreased from 975 to 850 mV as a result of the 10 ppm SO_2 in the oxidant gas. Of the 125 mV loss in cell potential during operation with SO_2, approximately 65 mV was due to higher anode polarization. Most of the 20 mV anode open-circuit potential loss was observed when the water vapor content of the fuel

was increased from 5.6 to 10% to avoid carbon deposition.* The 40-mV higher cathode polarization, as discussed earlier, was likely related to a carbonate distribution effect rather than to interaction of the SO_2 with the NiO cathode. When the cell was terminated after 2616 hours of operation, the IR-free cell potential at 100 mA/cm^2 had decreased to approximately 825 mV.

Cell Performance With Fuel Containing H_2S + COS

Another state-of-the-art type cell (EPRI-13) was operated to assess the effect of low levels of H_2S (approximately 10 ppm) in low-Btu fuel on cell performance and endurance. The lifetime performance plot for this cell is shown in Figure 2-13. It was operated on clean low-Btu fuel and standard oxidant for 696 hours to establish a stable performance level before low-Btu fuel containing 10 ppm sulfur as H_2S + COS was introduced. During the first 480 hours of operation with the sulfur-containing fuel, the cell potential at 100 mA/cm^2 decreased approximately 75 mV because of increased anode polarization. The presence of sulfur species did not result in a significant change in either anode or cathode open-circuit potentials. The perturbation in cell performance shown in this figure at 1050-1100 hours was associated with adjusting the cell holding force to eliminate the sharp increase in cathode polarization that was observed during that period of time. (Holding force adjustments needed to be made in other sulfur-affected cells, suggesting component deformation effects associated with contaminant interactions). After this force adjustment was made to EPRI-13, the cell potential continued to decrease with time because of increasing anode polarization. At the time the cell was terminated at 1344 hours, the 650 hours of exposure to 10 ppm H_2S + COS resulted in a 150 mV loss in cell potential at 100 mA/cm^2.

The performance of stabilized cobalt anode materials in the presence of sulfur was studied at IGT under Department of Energy (DOE) sponsorship** during FY 1978. The results obtained from cell DOE-16 are included here because of their relevance to the EPRI studies. This cell consisted of a Co-10% Cr anode, NiO cathode, and a

---

* Cell EPRI-14, which was being stabilized under sulfur-free low-Btu conditions, had to be terminated after 480 hours of operation because carbon deposition from the fuel had completely plugged the fuel inlet tube at a cooler portion (approximately 400°C) of the tube. The humidity level in subsequent cells was increased to approximately 10% in an effort, which proved successful, to avoid further carbon deposition problems.

** DOE Contract EC-78-C-03-1735 "Fuel Cell Research on Second-Generation Molten-Carbonate Systems."

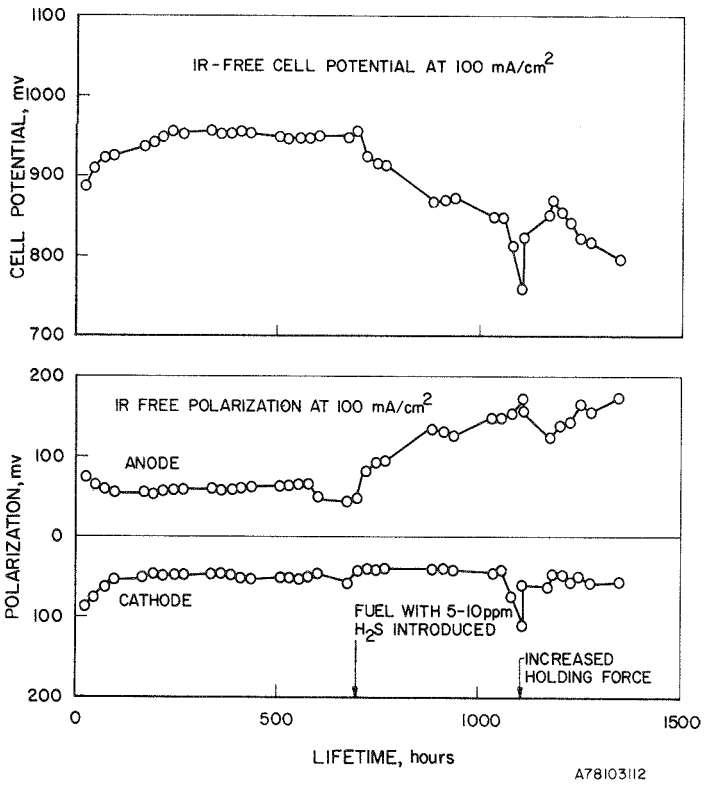

Figure 2-13. Performance of Cell EPRI-13 With and Without H_2S in Low-Btu Fuel (Stabilized Nickel Anode)

tile containing 55 wt % carbonate prepared by the aqueous slurry process. The lifetime performance plot for cell DOE-16 at a current density of 160 mA/cm^2 is presented in Figure 2-14. Low-Btu fuel containing 10 ppm H_2S + COS was introduced into the cell after it had first been stabilized on clean high- and low-Btu fuels. The cell lost approximately 50 mV cell potential at 160 mA/cm^2 during the first 70 hours exposure to sulfur species, and approximately 15 mV during the next 140 hours. It recovered approximately 40 mV when clean low-Btu fuel was reintroduced. Most of this recovery occurred within 24 hours of the switch back to clean fuel, with essentially no additional recovery during the next 100 hours. Reintroduction of the low-Btu fuel with 10 ppm sulfur resulted in a loss of 50-60 mV, and the cell showed fairly stable performance at this level (760 mV at 160 mA/cm^2, uncorrected for cell IR losses) after more than 900 hours total cell operation. The performance losses were associated mainly with increased anode polarization, although the anode IR loss appeared to be increasing gradually (from 32 mV at 265 hours to 60 mV at 930 hours). GC analyses indicated a good mass balance between sulfur species

entering (8-10 ppm H_2S + COS) and leaving (8-10 ppm H_2S + COS) the cell in the fuel stream. No sulfur species were detected in the oxidant effluent. Thus, contrary to the earlier observations of SO_2 removal from the oxidant by the electrolyte, little or no H_2S or COS were removed from the fuel gas at the anode.

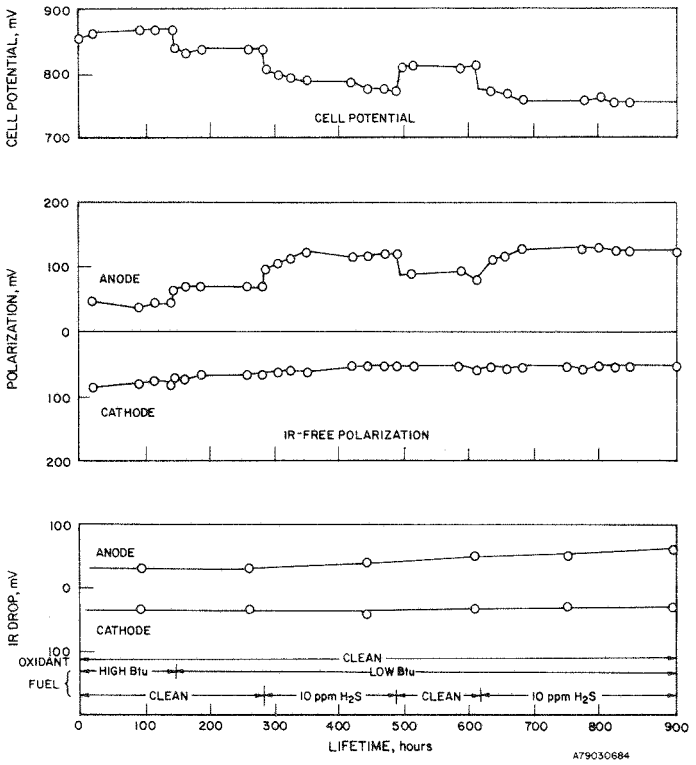

Figure 2-14. Performance of Cell DOE-16 in Low-Btu Fuel With and Without 10 ppm H_2S + COS (Co-10% Cr Anode, 160 mA/cm^2)

Anode, cathode, and cell polarization curves for cell DOE-16 after it was first stabilized on sulfur-contaminated fuel are shown in Figure 2-15. As for the stabilized nickel anode in the presence of H_2S + COS in low-Btu fuel, the sulfur species did not cause a shift in open-circuit potential, but did result in increased polarization at the anode.

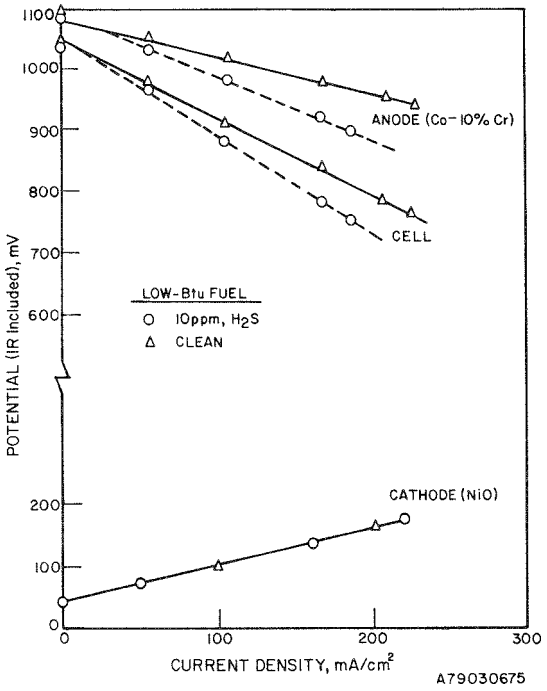

Figure 2-15. Effect of Sulfur Species in Fuel on Anode and Cathode Polarizations (Cell DOE-16)

EXAMINATION OF CELL COMPONENTS

Selected components of cells exposed to clean and sulfur-contaminated feed gases were examined to evaluate the nature and extent of interactions between sulfur and materials in the molten carbonate fuel cell. Such interactions will have an important impact on both cell performance and long-term endurance of the fuel cell system. A knowledge of these interactions is also needed to establish the mechanism(s) responsible for the observed cell performance losses.

Effect of Sulfur on Anode Stability and Current Collector Corrosion

An unusual amount of corrosion was observed on the anode and anode current collector upon disassembly of cell EPRI-7. (See Figure 2-16.) The anode itself was discolored and some cracks and "blisters" were observed on the gas side of this electrode. When the current collector was separated from the couple, approximately equal amounts of the anode remained attached to both the tile and current collector. The two fractured anode surfaces (parallel to the tile/anode interface) were examined by

X-ray diffractometry and a minor phase identified as Ni_3S_2 was observed, along with the major Ni lines. A significant sulfur peak was also observed when a fractured surface was analyzed by energy-dispersive X-ray analysis during scanning electron microscopy.

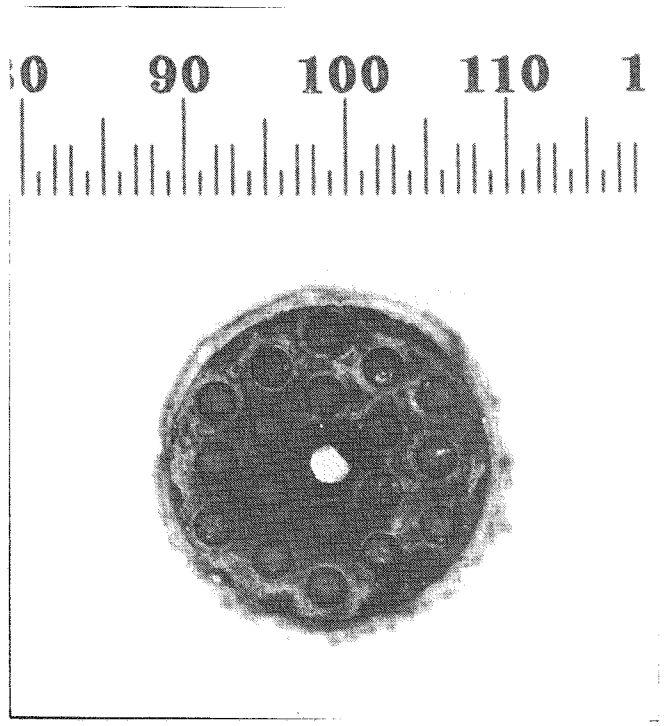

Figure 2-16. Appearance of Anode and Tile After Termination of Cell EPRI-7

A prepared cross section of the EPRI-7 anode was then examined by optical microscopy, to compare its microstructure with that of the anode from sulfur-free cell EPRI-3. A microstructural comparison is shown in Figure 2-17. The presence of sulfur has caused a very significant structural change in the EPRI-7 anode, as evidenced by the large islands of second-phase material on the tile side of the anode

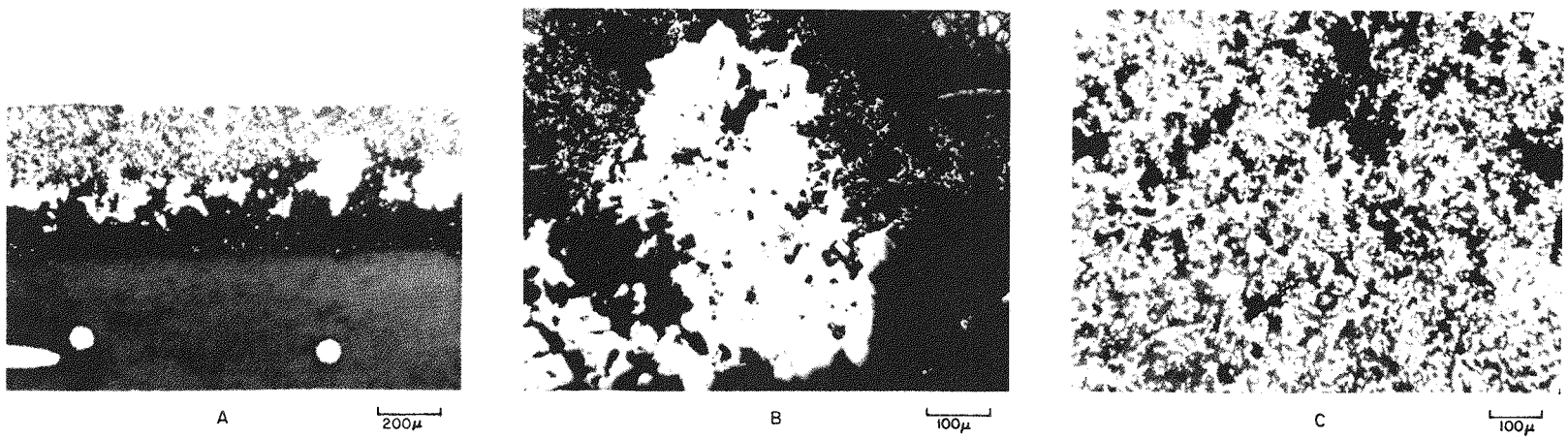

Figure 2-17. Structural Changes in Nickel-Based Anode of Cell EPRI-7 (50 ppm SO_2 in Oxidant)

(Figure 2-17a). One of these islands is shown at higher magnification in Figure 2-17b. These islands appear to have been solidified from a molten state, as would be expected for the Ni_3S_2/Ni eutectic, which melts at 645°C. The micrograph of Figure 2-17c corresponds to the typical structure of the stabilized nickel anode of EPRI-3, which operated for 1562 hours in a sulfur-free environment. Partial sulfidation of the nickel anode and the resulting destruction of its porous microstructure appear to be the major reason for the severe performance losses observed in EPRI-7 with low-Btu fuel and SO_2-contaminated oxidant. The formation of large agglomerates not only resulted in a loss of active surface area, but also disturbed the distribution of carbonate electrolyte between tile and anode due to the significant change in anode pore structure.

To compare the corrosion behavior of Type 316 stainless steel current collectors under cell conditions with 50 ppm SO_2 in the oxidant with that under sulfur-free conditions, the anode and cathode current collectors of cells EPRI-3 (sulfur free) and EPRI-7 (SO_2-containing oxidant) were prepared for metallographic examination. Photomicrographs of the anode and cathode current collectors are shown in Figures 2-18 and 2-19, respectively, for these two cells. The thickness of oxide scales observed at the gas/current collector and electrode/current collector interfaces are presented in Table 2-3.

Table 2-3

THICKNESS OF OXIDE SCALES ON TYPE 316 SS CURRENT COLLECTOR MATERIALS AT 650°C

Cell No.	Anode			Cathode		
	Gas Side	Electrode Side	Total	Gas Side	Electrode Side	Total
	μ			μ		
EPRI-3*	5	30	35	5	10	15
EPRI-7**	28	30	58	10	10	20

* Cell operated 1562 hours under sulfur-free gases with reformed natural gas fuel.

** Cell operated 1104 hours total, 620 hours with a 50 ppm SO_2 oxidant flowing (low-Btu fuel was used for 240 hours, high-Btu for 380 hours).

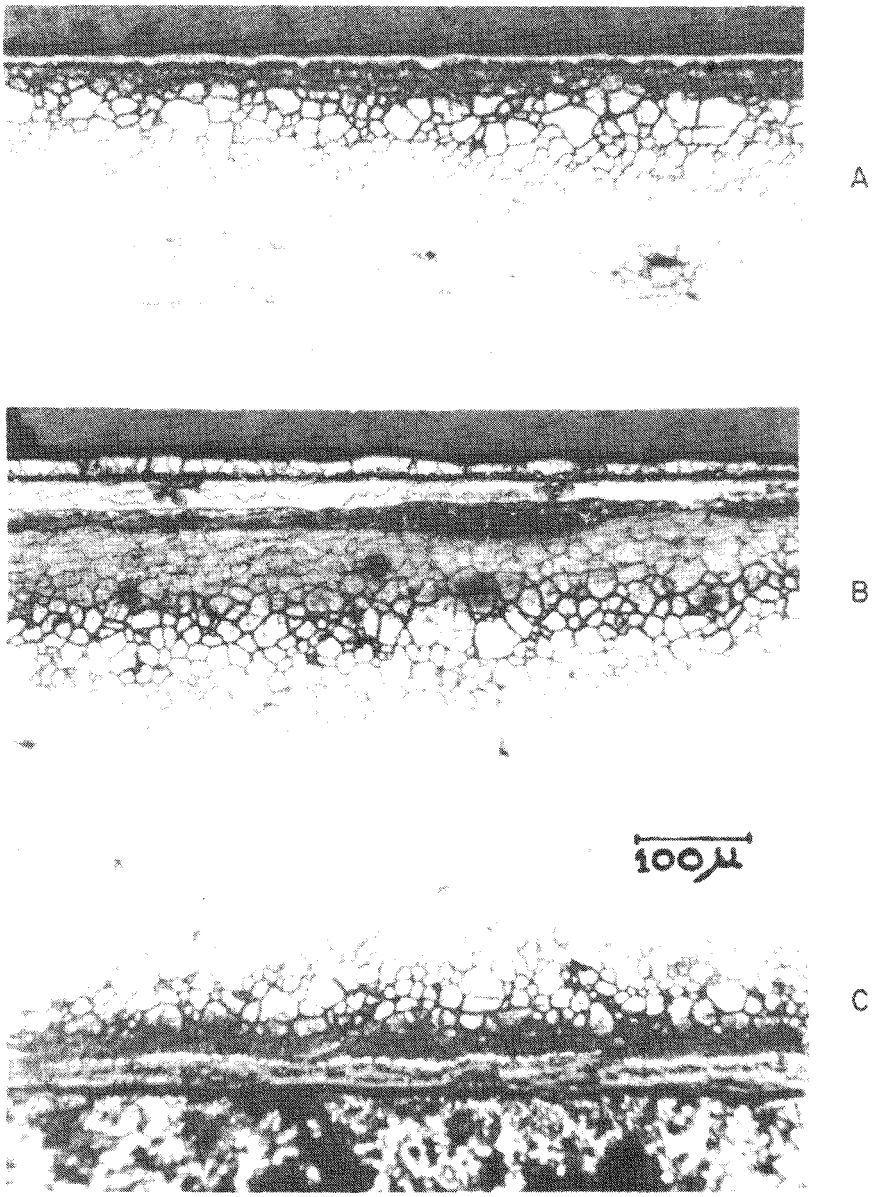

Figure 2-18. Corrosion of Type 316 SS Anode Current Collectors (A, Fuel Side of EPRI-3 With Sulfur-Free Gases; B, Fuel Side of EPRI-7 With Sulfur-Containing Gases; C, Electrode Side of EPRI-7 With Sulfur-Containing Gases; Etchant: $FeCl_3/HCl/H_2O$)

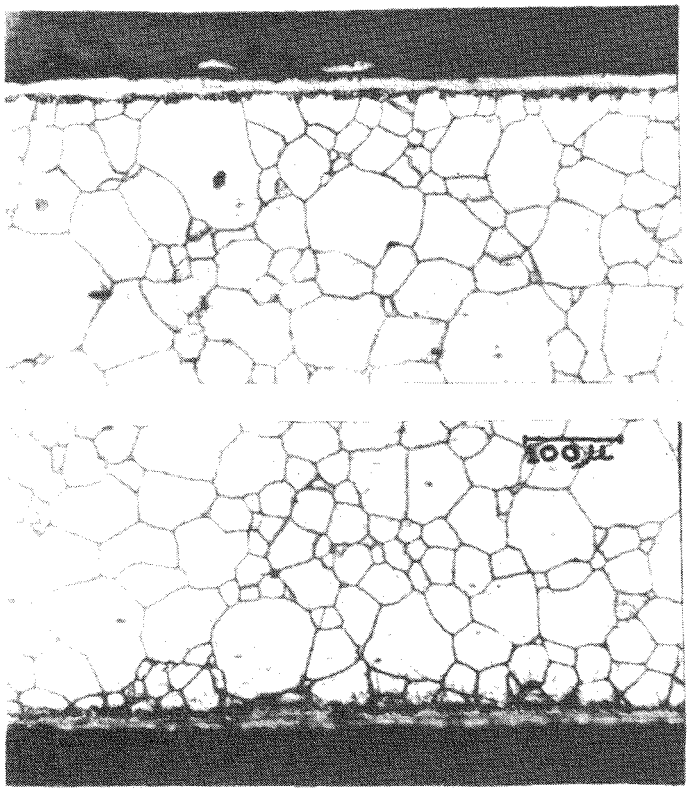

Figure 2-19. Corrosion of Type 316 SS Cathode Current Collector From Cell EPRI-3 (A, Typical of the Oxidant Side; B, Typical of the Electrode Side; Etchant: $FeCl_3/HCl/H_2O$)

As shown in the photomicrographs of Figures 2-18a and 2-18b and in Table 2-3, much greater corrosion was observed on the fuel side of the anode current collector in cell EPRI-7 than in EPRI-3, which was exposed only to "clean" gases. Approximately 5μ of oxidation was observed in the sulfur-free versus approximately 28μ in the sulfur-affected cell. The oxidation on the electrode side of the anode current collector was similar (approximately 30μ) in both cell tests.

In addition to the oxide layers on the anode current collectors, what appears to be a subscale zone of highly carburized stainless steel was very evident in EPRI-7. As shown in Figure 2-18b, the innermost region of this affected zone consists of intergranular carbide precipitation much greater than observed in the heat-sensitized base material. The heavily carburized region on the fuel side of the EPRI-7 anode current collector was approximately 100μ in depth.

Typical areas of corrosion observed in the cathode current collector of cell EPRI-3 are shown in Figure 2-19. The corrosion observed in cell EPRI-7, exposed to sulfur-containing gases, was very similar. The corrosion on the gas side appeared to be slightly higher in the sulfur-affected cell EPRI-7, but the amount of corrosion was low in both cases. A total of 15-20μ of corrosion was observed for both sides of the cathode current collectors. By contrast, the anode current collector shows approximately 35 and 58μ oxide under sulfur-free and SO_2-containing oxidant conditions, respectively. Another observable difference was that the oxide layer of the cathode current collectors was compact without cracks while that of the anode current collectors contained cracks or fissures and some porosity. This indicates that the oxide scale may provide only a limited degree of protection against further corrosion of the anode current collector, especially in the presence of sulfur.

In general, these initial results seem to indicate that, similar to the electrochemical performance of the cell, the SO_2 entering the cathode affects primarily the anode side. Increased corrosion of the anode current collector results from the transport of sulfur species through the tile to the anode side of the cell.

The stabilized nickel anodes from cells EPRI-8 and EPRI-9 were also observed to have been severely deteriorated immediately upon cell disassembly. Contrary to experience with cells operated with clean fuel and oxidant gases, the anodes from both cells EPRI-8 and EPRI-9 were easily fractured by applying a very small force to the current collectors. Both anodes fractured in a plane parallel to the electrode/tile interface, with part of each anode adhering to the current collector and the remainder to the tile surface. An unusual amount of anode discoloration was observed, and examination of the fractured surfaces at low magnification under reflected light revealed abnormally large crystallites suggesting accelerated particle growth, or sintering, of the anode structure. This latter effect was especially apparent in the EPRI-9 anode, as shown in the photographs of the two fractured anodes in Figure 2-20.

Transverse sections of the anodes from EPRI-8 and EPRI-9 were mounted in epoxy and the surfaces were ground and polished for metallographic examination. As suspected from the visual examination, both electrodes experienced significant structural changes as a result of operation with SO_2-contaminated oxidants. A typical area of the EPRI-8 anode is shown in the reflected-light optical micrographs of Figure 2-21. A high degree of sintering of the anode areas adjacent to the anode/tile interface

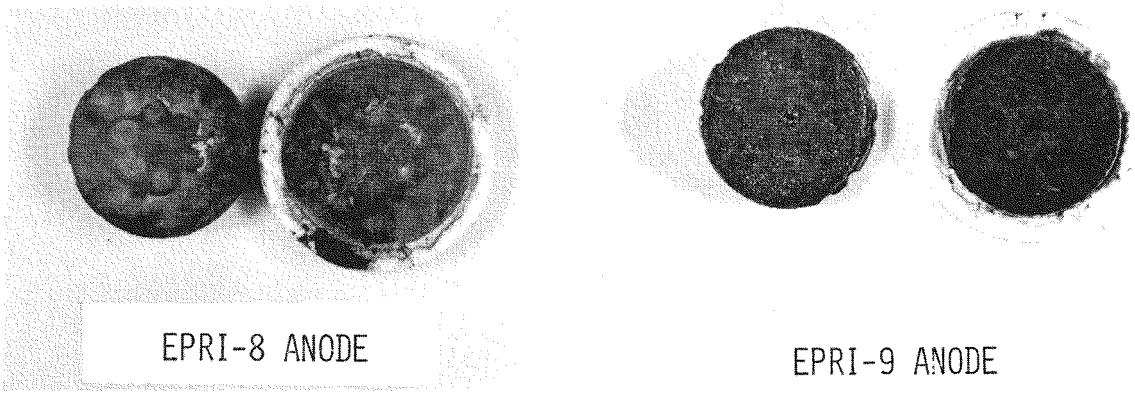

Figure 2-20. Appearance of Fractured Surfaces Through Sulfur-Affected Anodes From Cells EPRI-8 and EPRI-9

resulted in severe loss of porosity and coarsening of the anode structure in these regions. The affected areas formed a nearly continuous network of very large particles with essentially no interconnected porosity, extending parallel to the anode/tile interface. This type of degradation might be expected to lead to lower cell performance through both loss of active surface area by sintering, as well as loss of effective carbonate distribution and reactant transport by disruption of the porous anode capillary network, as observed in the EPRI-7 anode. The coarsening effect was even more pronounced in the EPRI-9 anode, and it was difficult to perform adequate metallography because of pullout of large particles from the weakened anode structure.

X-ray diffraction analysis of the fractured EPRI-8 anode surface indicated that Ni_3S_2 was present as a minor phase near the anode/tile interface. Chemical analysis of the sample of EPRI-8 anode showed $S^{=}$ and $SO_4^{=}$ concentrations below the limit of detection. However, a sample of EPRI-9 anode, which showed a significantly greater degree of structural deterioration than the EPRI-8 anode, was found to contain 6400 ppm sulfur as $S^{=}$. The greater degradation and higher sulfur concentrations in the EPRI-9 anode are very likely related to the fact that this cell operated under the more severe low-Btu fuel condition (approximately 4% H_2) for a short period of time.

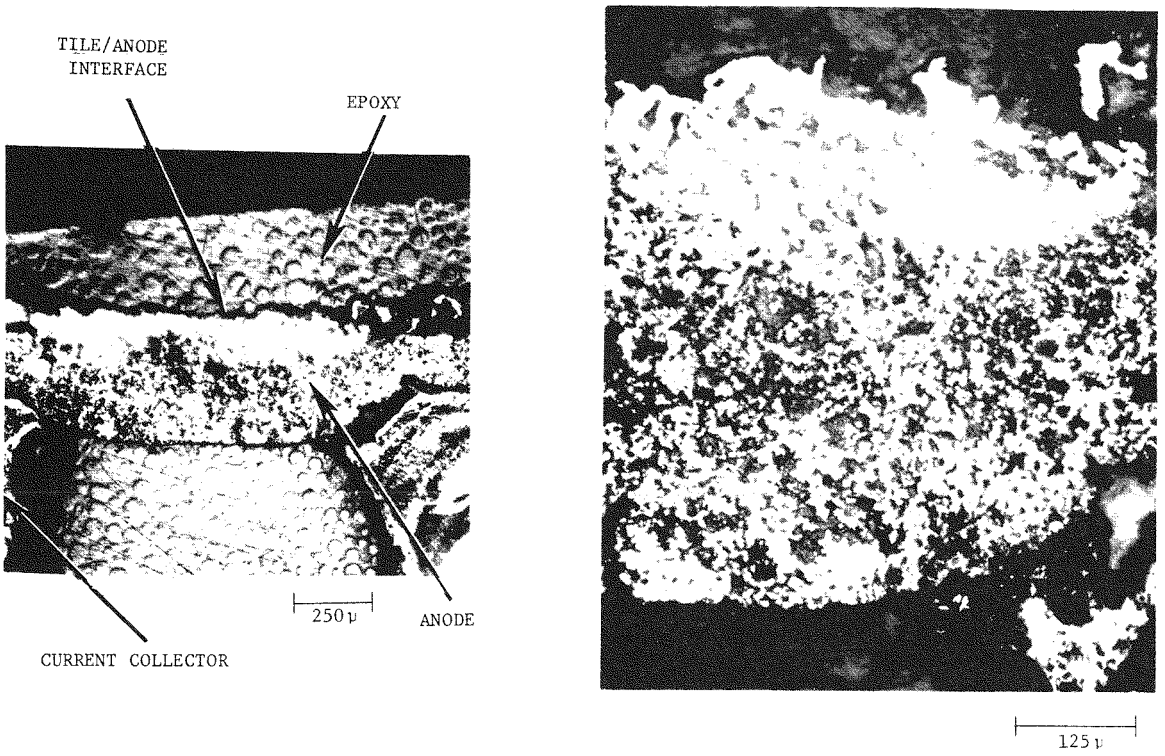

Figure 2-21. Microstructure of Sulfur-Affected Stabilized Nickel Anode From Cell EPRI-8

The formation of Ni_3S_2 and subsequent anode sintering appears to be initiated at the anode/tile interface, with the reaction front progressing through the anode structure toward the current collector. Nickel sulfidation in the absence of electrical potentials would not be expected to occur in low-Btu fuel gas at 650°C below bulk H_2S levels of approximately 385 ppm, whereas in-cell anode sulfidation has been observed with much lower (less than 50 ppm) total sulfur concentrations in the effluent fuel gas. It is apparent that predictions of sufficient conditions for anode sulfidation need to account for electrochemical sulfidation effects as well as local deviations from the average bulk concentration of sulfur species in the anode. The latter consideration is very important when sulfur from the oxidant stream is being transported to the anode through the tile. The thermodynamic condition controlling anode sulfidation behavior will be that existing at the anode/

tile interface. This interfacial thermodynamic state will depend strongly on the relative rates of sulfur transport out of the tile and of fuel gas flow across the anode, as well as local mixing effects.

The anode and anode current collector from cell EPRI-13 were also examined metallographically to determine structural changes caused by sulfur impurities introduced directly in the fuel stream. This cell had operated for approximately 650 hours with low-Btu fuel containing 10 ppm sulfur as H_2S and COS, after 700 hours of stable operation with clean low-Btu fuel. The anode was found to have experienced very severe densification, especially under the solid portions of the current collector plate. As observed from the micrograph of the polished cross section of Figure 2-22, the anode thickness under the current collector decreased from 0.030 to 0.017 in, with a corresponding increase in density and decrease in surface area and interconnected porosity. More structural details of the restructured anode and corroded current collector can be seen in the higher magnification view of Figure 2-23. For comparative purposes, the anode from cell EPRI-3 tested under sulfur-free conditions for 1500 hours is shown in Figure 2-24 at the same magnification. The anode densification was even more pronounced at the periphery of the current collector holes in EPRI-13, where the resulting volume increase from corrosion products on the current collector caused greater local loading of the anode. Significant anode sintering also occurred under the current collector holes, although not to the extent observed under the solid portions.

The anode current collector from EPRI-13 appears to have been attacked by a hot-corrosion mechanism in localized areas, as shown in Figure 2-22 and at higher magnification in Figure 2-23. The oxide layer formed at the anode/collector interface was non-protective in the presence of 10 ppm H_2S + COS in low-Btu fuel at some locations, promoting extensive subscale corrosion product formation. At the location shown in Figure 2-23, consumption of the current collector corresponded to approximately 0.012 in of the 0.050-in original thickness, during 1344 total hours of operation. The corrosion products at the anode/collector interface were about 0.031-in thick, for a corrosion product/reacted metal thickness ratio of 2.5. The gas-side surface of the anode current collector at the same location showed only slight corrosion, a two-zone layer approximately 0.001 - 0.002-in thick. (See Figure 2-25.)

A detailed examination of the sulfur-affected anode and badly corroded regions of the current collector by electron microprobe and other analytical techniques is in

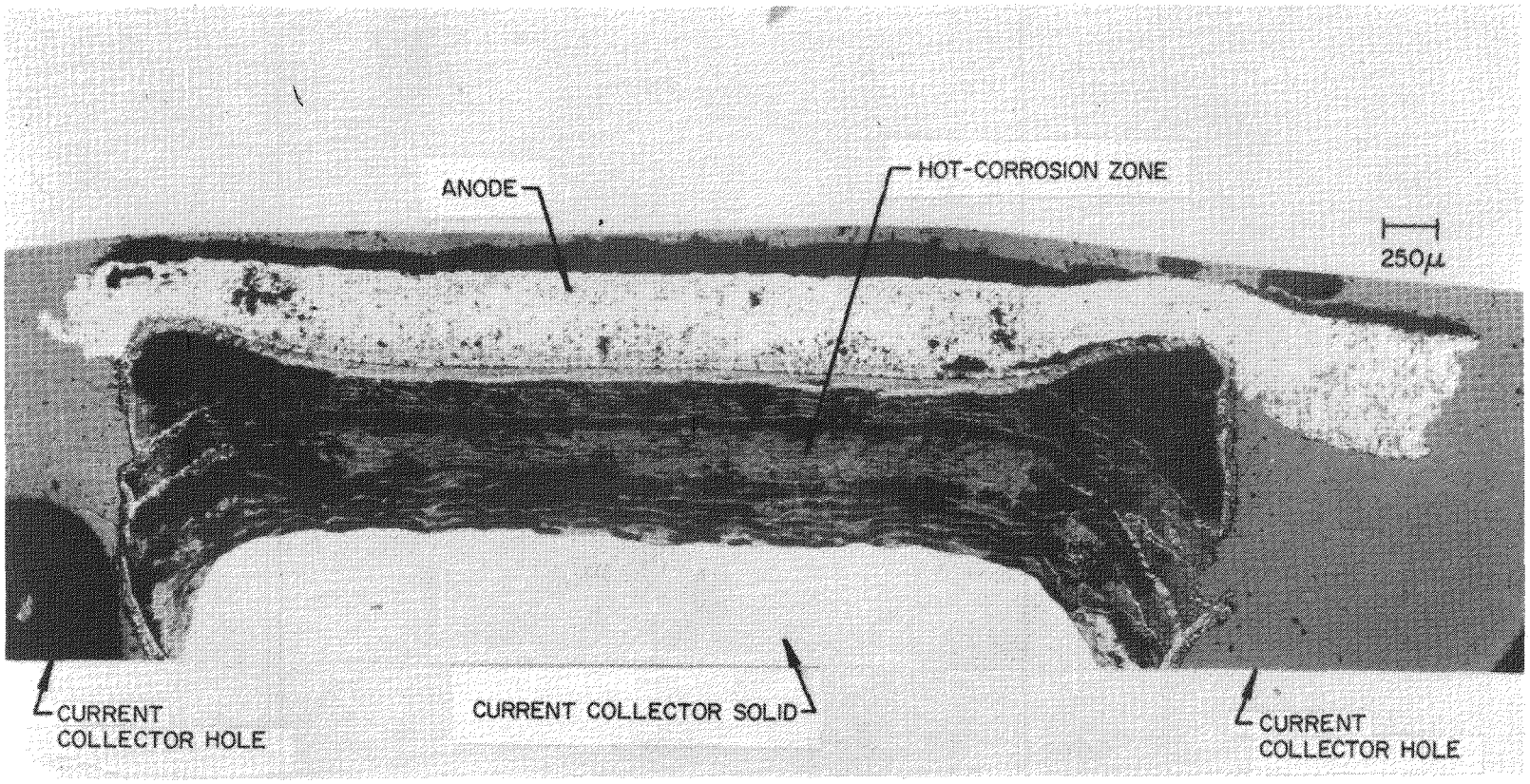

Figure 2-22. Composite Cross Section of Stabilized Nickel Anode and Anode Current Collector From Cell EPRI-13, Exposed to 10 ppm H_2S (As Polished)

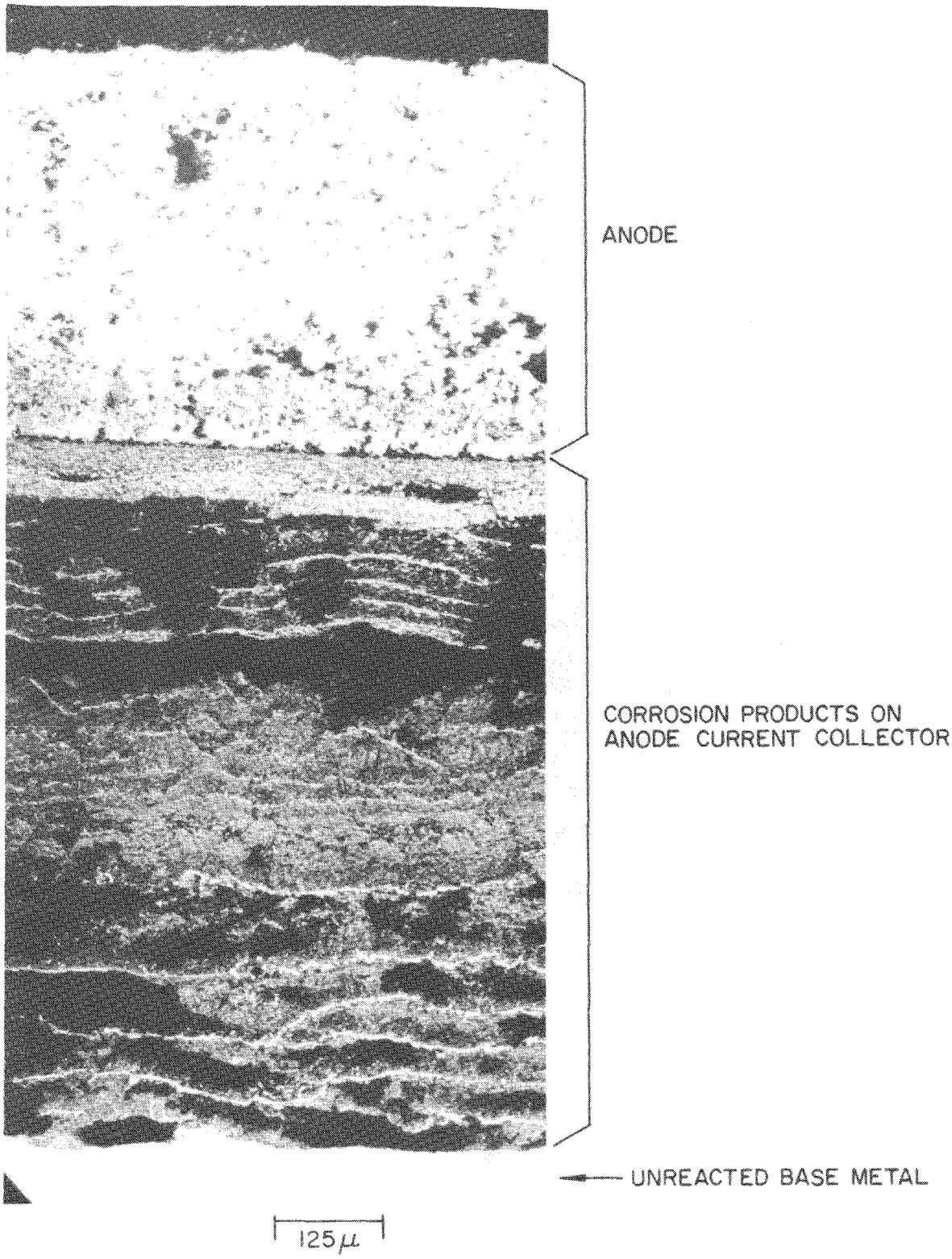

Figure 2-23. Higher Magnification View of Sulfur-Affected Anode and Current Collector From Cell EPRI-13

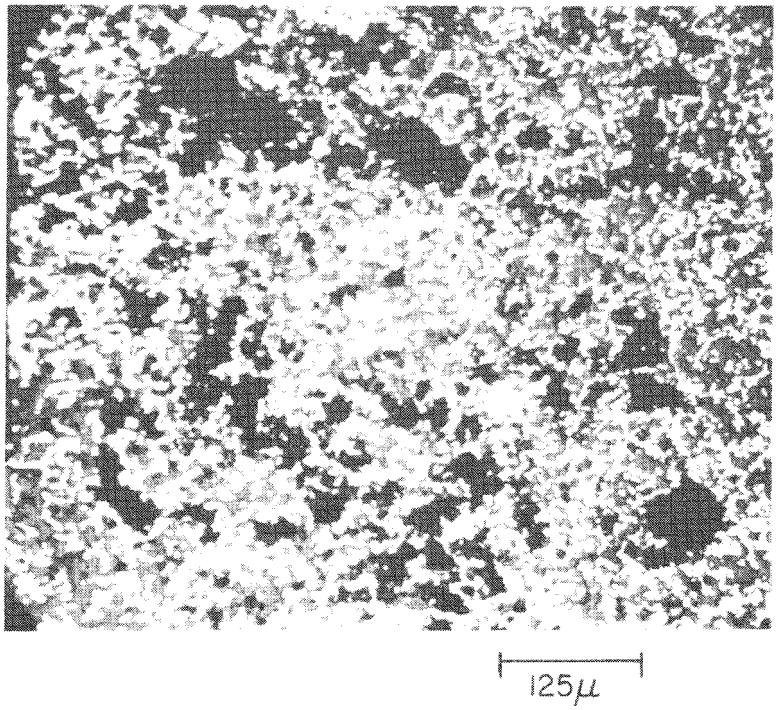

Figure 2-24. Appearance of Stabilized Nickel Anode From Cell EPRI-3 After 1500 Hours of Operation in Sulfur-Free Gases

progress in an attempt to separate the synergistic sulfur-related effects which caused the decline in performance of this cell.

Electron Microprobe Analysis of Cell EPRI-7 Components

A polished metallographic cross section of the cell EPRI-7 composite consisting of a portion of the cathode, tile, anode, and the anode current collector was subjected to electron microprobe analysis in an attempt to determine the distribution of sulfur through the cross section. A photograph of the polished cross section is shown in Figure 2-26. Twenty-four different points were examined using a 5μ electron beam. The analysis of the microprobe data for different parts of the sample are summarized in Table 2-4. Sulfur was not detected from any area by this point by point analysis except at the anode current collector.

Table 2-4

ELECTRON MICROPROBE DATA FOR POINT-BY-POINT ANALYSIS OF
CROSS SECTION OF CELL EPRI-7 COMPOSITE

Cell Component	Location	Approximate Microprobe Analysis
Cathode	Edge next to current collector	2- 4% Al, 15-20% K, 20-30% Ni
	Bulk cathode	1- 2% Al, 6-10% K, 30-50% Ni
	Edge next to tile	3- 5% Al, 15-20% K, 20-40% Ni
Tile	Near cathode	10-35% Al, 20-50% K
	Central darkened area	8-12% Al, 30-50% K, trace Cu
	Near anode	8-12% Al, 20-30% K
	Kanthal wire	4- 8% Al, 20-30% Cr, 55-70% Fe, 3- 5% K
Anode	Edge next to tile	3- 5% Al, 30-50% K, 2- 3% Ni, Trace Fe
	Edge of island structure	5-10% K, 45-65% Ni, Trace Cr
	Bulk of island structure	2- 4% K, 50-70% Ni
	Bulk anode	3-12% Al, 5-15% Al, 1- 7% Fe, 10-18% K 30-50% Ni
Anode Current Collector	Edge near anode	20-40% Cr, 8-20% Fe, 3-10% K, 2-12% Ni 1- 2% Mo, 1.5-3% S
	Bulk stainless steel	15-20% Cr, 60-70% Fe, 1- 2% K, 1- 2% Mo 8-12% Ni, 0.8% S
	Edge on gas side	4- 6% Cr, 7-12% Fe, 20-30% K, 0.5% Mo 5- 6% Ni, 1.5% S

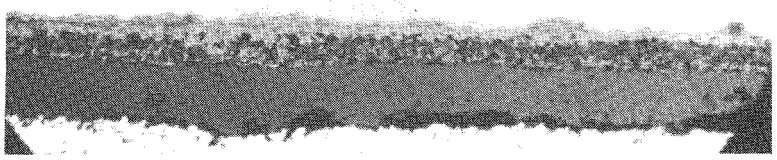

Figure 2-25. Appearance of Two-Zone Corrosion Product Layer on Gas-Side Surface of Anode Current Collector From Cell EPRI-13 (As Polished)

To eliminate potential problems associated with smearing of sulfur-containing material during metallographic preparation of the polished surface, the sample was microtomed with a diamond cutter using an oil lubricant to reveal a new surface. The new surface was examined carefully by electron microprobe under low magnification in search for sulfur-containing species. Sulfur was detected only at the tile/anode interface. A microphotograph and concentration distribution of S, Al, K, Ni, and Cr from that interface is shown in a series of photographs in Figure 2-27. Because practically each sulfur-containing area (Figure 2-27c) has a corresponding high Ni concentration (Figure 2-27d), it appears that sulfur is chemically tied up with Ni, as expected on the basis of identification of Ni_3S_2 by X-ray diffraction.

In addition to the cross-sectional sample described above, a fractured surface through the EPRI-7 anode (parallel to the tile/anode interface) was also examined for sulfur by the electron microprobe. The sulfur-containing species were observed as small particles 1 - 5μ in size. Representative micrographs and their corresponding sulfur distribution maps are presented in Figures 2-28a and 2-28b.

The concentration of sulfur species in the electrolyte tile was too low to be detectable by electron microprobe analysis (less than approximately 0.2%). This was

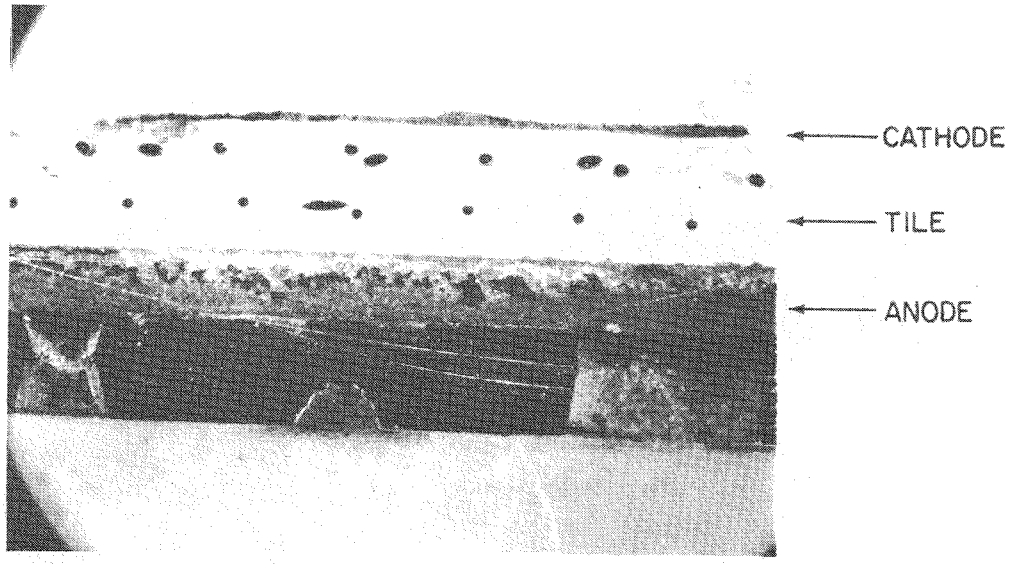

Figure 2-26. Cross Section Through Terminated Cell EPRI-7 (Note dark zone on cathode side of tile and large second-phase islands in anode.)

true even at the tile/cathode interface where SO_2 is expected to react with carbonate to form sulfate. The SO_2 concentration in the oxidant gas is low enough and the Faradaic transport of sulfate species away from the interface toward the anode is rapid enough that no bulk sulfate region forms at the cathode.

Stability of Electrolyte Tile

The chemical interactions of sulfur species with the carbonate electrolyte of terminated cells were determined by chemical analysis, and X-ray diffraction analysis was used to study the effects of sulfur on $LiAlO_2$ stability. These data are presented and discussed under Task 4.

SUMMARY OF CELL PERFORMANCE/ENDURANCE LOSSES CAUSED BY SULFUR SPECIES

Table 2-5 summarizes the anode material and test conditions for each cell tested and the observed potential losses at 100 mA/cm^2 attributed to sulfur-containing

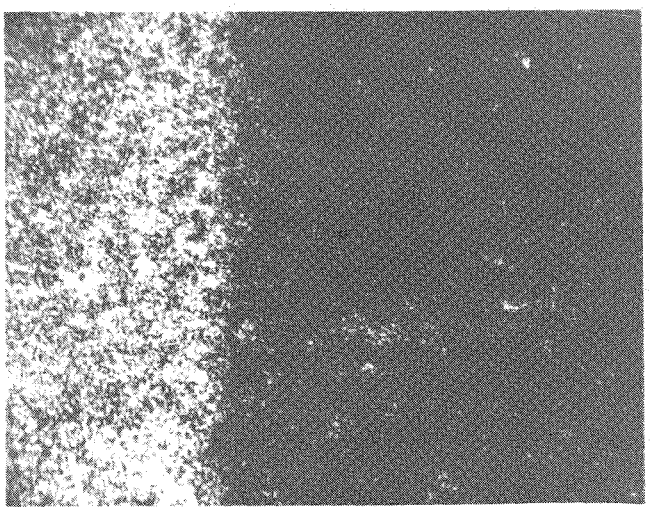

Figure 2-27a. Microphotograph of Cell EPRI-7 Tile/Anode Interface (1000X)

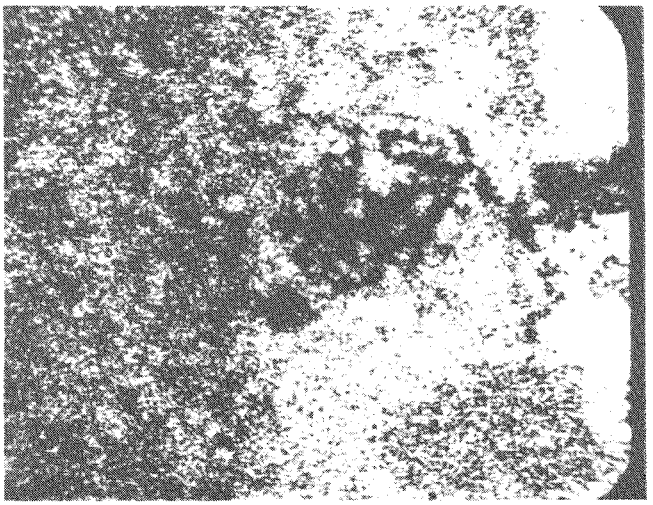

Figure 2-27b. Al Concentration Distribution for the Micrograph Shown in Part a.

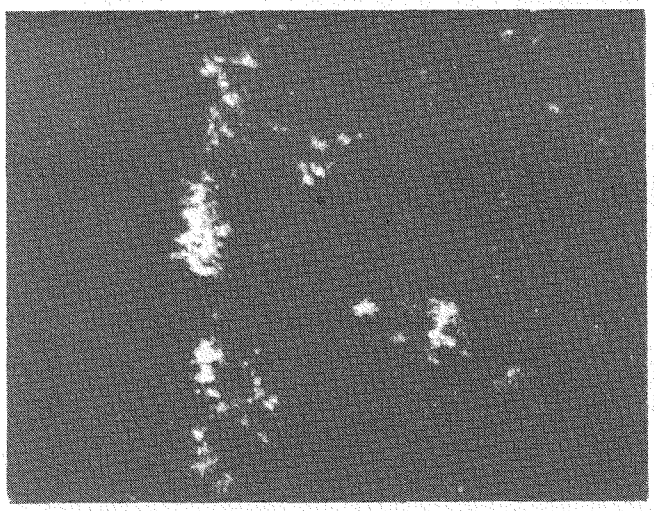

Figure 2-27c. Sulfur Distribution for the Micrograph Shown in Part a

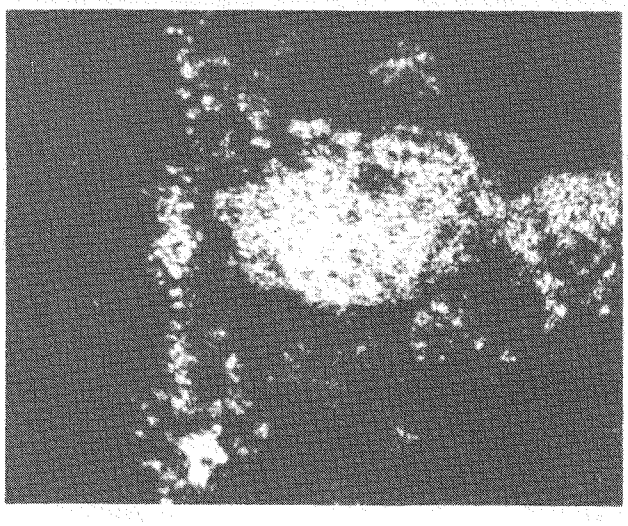

Figure 2-27d. Ni Distribution for the Micrograph Shown in Part a

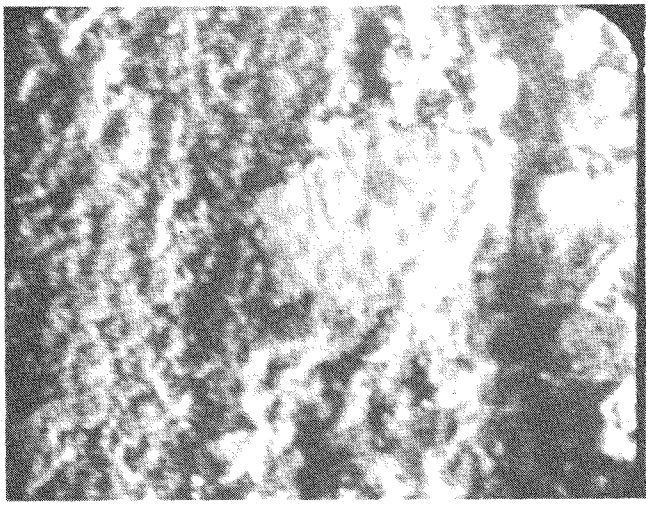

Figure 2-27e. Cr Distribution for the Micrograph Shown in Part a

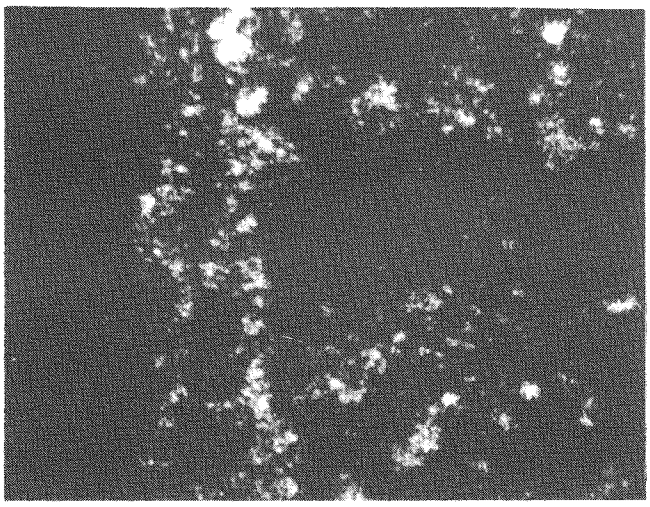

Figure 2-27f. K Distribution for the Micrograph Shown in Part a

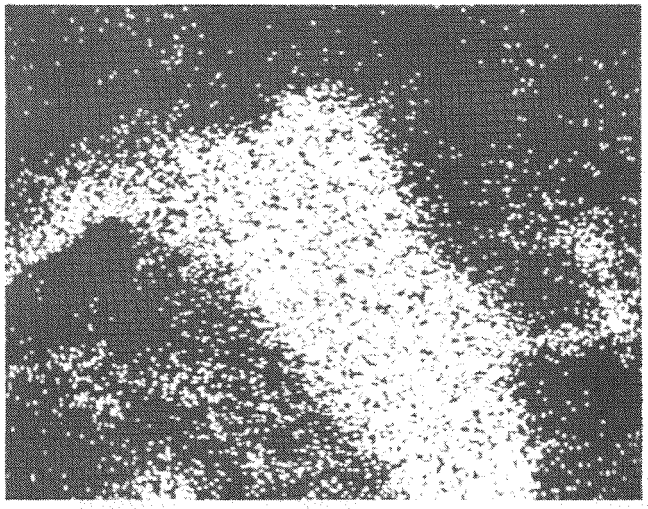

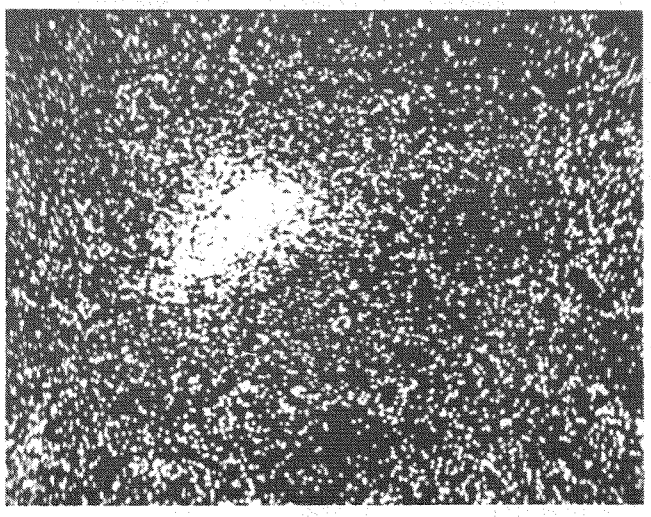

Figure 2-28. Distribution of Sulfur at Two Different Locations on Fractured Surface Through EPRI-7 Anode

contaminants. The table includes data for cell DOE-16, which was operated under the DOE program during FY 1978.

Table 2-5

SUMMARY OF CELL PERFORMANCE/ENDURANCE LOSSES
CAUSED BY SULFUR SPECIES

Cell	Anode*	Fuel	Oxidant**	Loss/Time at 100 mA/cm²#
EPRI-7	Ni	Clean High-Btu	50 ppm SO_2	65-70 mV steady loss/360 h
		Clean Low-Btu	50 ppm SO_2	150 mV steady loss/100 h followed by recovery
EPRI-8	Ni	Clean High-Btu	50 ppm SO_2	60 mV steady loss/700 h
		Clean Low-Btu	50 ppm SO_2	230 mV decline/190 h
EPRI-9	Ni	Clean Low-Btu (Outlet)	50 ppm SO_2	215 mV (short-term)
		Clean Low-Btu	50 ppm SO_2	Steady 70-90 mV loss/ 440 h; 270 mV decline/ 250 h
EPRI-10	Co	Clean High-Btu	50 ppm SO_2	60 mV decline/150 h
		Clean Low-Btu	50 ppm SO_2	Steady 70-85 mV loss/ 780 h
EPRI-11	Ni	Clean Low-Btu	10 ppm SO_2	95 mV decline/1070 h
EPRI-13	Ni	Low-Btu + 10 ppm H_2S	Clean	150 mV decline/600 h
DOE-16	Co	Low-Btu + 10 ppm H_2S	Clean	30 mV/first 70 h 10 mV/next 150 h 20 mV recovery with clean fuel

* All anode materials stabilized to minimize sintering.

** 70% air/30% CO_2.

\# Losses relative to clean fuel/clean oxidant conditions.

The results indicate that state-of-the-art materials will not tolerate sulfur contaminants at the 10 ppm concentration level in either the fuel or oxidant gas stream. The most sensitive component in the cell appears to be the nickel-based anode, which is susceptible to formation of a Ni/Ni_3S_2 eutectic which melts at 645°C.

Formation of the liquid phase leads to accelerated anode sintering, with a loss of surface area and porosity. The effect of low levels of sulfide and sulfate species in the electrolyte on performance have not been uniquely identified because of the severity of the anode restructuring problem. (See Task 4.) However, short-term results obtained with a cobalt-based anode suggest a loss of approximately 60 mV at 160 mA/cm^2 for electrode or electrolyte poisoning effects with 10 ppm H_2S + COS in low-Btu fuel. The requirement of cleaning the fuel stream to less than 10 ppm sulfur species is clearly indicated by the current work. More cell performance data are needed to establish the maximum tolerable level of sulfur species for long-term endurance.

REFERENCES

1. H. H. Kellogg. "A Critical Review of Sulfidation Equilibria." In Transactions of the Metallurgical Society of AIME, Vol. 230, 1964, p. 1622.

2. A. Rahmel. "Kinetic Conditions for the Simultaneous Formation of Oxide and Sulfide in Reactions of Iron With Gases Containing Sulfur and Oxygen or Their Compounds." Corrosion Science 13 (2), 1973, p. 125.

Section 3

TASK 4. EVALUATE ELECTROLYTE TILE STABILITY

SUMMARY

The objective of this portion of the program was to determine the effect of sulfur-containing feed gases on the stability of the electrolyte tile -- both the $LiAlO_2$ support and the alkali carbonate electrolyte. Under the electrolyte/sulfur interaction studies, we carried out thermodynamic calculations to predict the effects of SO_2 in the oxidant and H_2S + COS in the fuel on sulfate and sulfide stabilities at different points of the electrolyte tile. Because available thermodynamic data on alkali sulfates and sulfides are limited, precise estimations of relative stabilities of these species in molten carbonate electrolytes when the fuel cell is operated with sulfur-containing gases are not possible. Therefore, the stabilities were determined experimentally both in operating cell tests and in equilibration pot tests. In general, the results obtained followed the trends predicted from available thermodynamic data. Because no literature data is available on the effect of alkali sulfur species on the stability of lithium aluminate, this information was obtained by comparing the lithium aluminate used in cells operating with clean and sulfur-containing feed gases. The most significant results of this portion of the program are —

- SO_2 is scrubbed from the cathode gases almost quantitatively to form alkali sulfates at the cathode gas/electrolyte interface. A high concentration of alkali sulfates is therefore expected at this interface. Under cell operating conditions this interface was shown to be very thin.
- Sulfur species originating at this interface are transported through the tile to the anode where they are reduced to H_2S and COS. A sharp concentration gradient of sulfur species exists between the anode and cathode.
- The concentration of sulfur species in the bulk of the tile is below 10^{-2} mole fraction. The concentration at the anode interface is even lower.
- Equilibration pot testing using a variety of fuel gases verified the cell test results.
- Although some lithium aluminate changes occurred in cell testing using sulfur-containing gases, the trends are not clear and require further, more comparative testing.

Thermodynamic Considerations

Sulfur dioxide is expected to react with molten Li_2CO_3-K_2CO_3 under the oxidizing conditions existing at the cathode by the reaction -

$$M_2CO_3 + SO_2 + 1/2\ O_2 \rightleftarrows M_2SO_4 + CO_2 \qquad (3\text{-}1)$$

where M is the alkali metal under consideration. Standard free energy of formation data are available for Eq. 3-1 [from JANAF(1)] for the sodium system (M-Na). In this case, ΔG_1° for Eq. 3-1 at 650°C is -61.0 kcal, and the equilibrium constant -

$$K_1 = \frac{[M_2SO_4]\ P_{CO_2}}{[M_2CO_3]\ P_{SO_2} P_{O_2}\ 1/2} \qquad (3\text{-}2)$$

has a value of 2.8×10^{14}. Thus, essentially complete conversion of carbonate to sulfate is expected to occur at the cathode even with a few ppm of SO_2 in the oxidant gas.

The alkali sulfates thus formed at the cathode are expected to exist as M^+ and $SO_4^=$ species, leading to the potential for electrochemical transport through the tile from cathode to anode. The M_2SO_4 species is much less stable at the anode than at the cathode, although, as will be shown, its stability relative to M_2CO_3 at the anode is very dependent on the local gas composition. At the anode, M_2SO_4 can be reconverted to M_2CO_3 by the reactions -

$$M_2SO_4 + \rightleftarrows M_2S + 4H_2O \qquad (3\text{-}3)$$

$$M_2S + CO_2 + H_2O \rightleftarrows M_2CO_3 + H_2S \qquad (3\text{-}4)$$

$$M_2SO_4 + CO_2 + 4H_2 \rightleftarrows M_2CO_3 + H_2S + 3H_2O \qquad (3\text{-}5)$$

The standard free energy of reaction and equilibrium constant for these reactions at 650°C for M = Na are calculated from the JANAF Tables to be -

$$\Delta G_3^\circ = -19.8 \text{ kcal} \qquad (3\text{-}6)$$

$$\Delta G_4^\circ = +0.6 \text{ kcal} \qquad (3\text{-}7)$$

$$\Delta G_5^\circ = -20.5 \text{ kcal} \qquad (3\text{-}8)$$

$$K_3 = \frac{[M_2S]}{[M_2SO_4]} \frac{P_{H_2O}^4}{P_{H_2}} = 5.0 \times 10^4 \quad (3\text{-}9)$$

$$K_4 = \frac{[M_2CO_3]}{[M_2S]} \frac{P_{H_2S}}{P_{CO_2} P_{H_2O}} = 1.4 \quad (3\text{-}10)$$

$$K_5 = \frac{[M_2CO_3]}{[M_2SO_4]} \frac{P_{H_2S} P^3_{H_2O}}{P_{CO_2} P_{H_2}^4} = 7.2 \times 10^4 \quad (3\text{-}11)$$

Using these estimated values, activity ratios of the various species were calculated for four different anode gas compositions representing a wide range of thermodynamic conditions. The results, presented in Table 3-1, indicate that sulfate and sulfide activities at the anode with these gases are of the order of 10^{-3} or less, using data for the sodium system.

A schematic diagram of how $SO_4^=$, $S^=$, and $CO_3^=$ activities could vary with tile thickness at one point in the cell, based on the foregoing discussion, is shown in Figure 3-1.

The sulfate/carbonate activity ratio was calculated using available data for the sodium and potassium systems. As shown in Figure 3-2, the theoretical ratio is very dependent on local anode gas composition (inlet versus outlet), and the most severe condition with respect to sulfate formation exists at the outlet at high utilizations. Potassium carbonate appears to be less stable against sulfate formation under these conditions. Experimentally determined values of $[M_2SO_4]/[M_2CO_3]$ in the Li-rich Li_2CO_3 eutectic, to be discussed in the next section, are shown in this figure for comparison. Alkali sulfate stability in this eutectic appears to be greater than that predicted on the basis of available K_2SO_4/K_2CO_3 equilibrium data, although still in the 10^{-3} to 10^{-2} range for 75% utilized low-Btu fuels.

CARBONATE-SULFATE-SULFIDE EQUILIBRATION TESTS

Because anodic performance is most seriously affected when the fuel cell is operated with sulfur-containing gases, it is important to determine the relative stabilities of sulfate, sulfide, and carbonate under anode environments. Because available

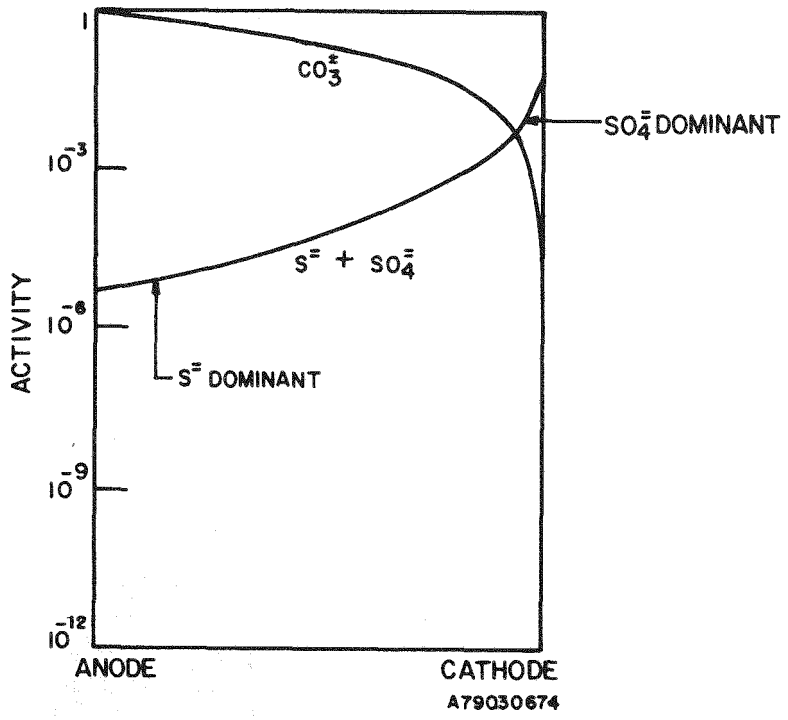

Figure 3-1. Schematic Ionic Activity Profiles in Electrolyte Tile Under Low-Btu Inlet Conditions

thermodynamic data are not sufficient to perform quantitative estimates, equilibration experiments of electrolyte melts under anode gas environments at 650°C were carried out to determine the equilibrium electrolyte composition at the anode. The anode gas composition chosen for most of the tests corresponded to a 75% utilized low-Btu fuel gas with a nominal composition of 4% H_2, 17.6% H_2O, 4.7% CO, 39.9% CO_2, and 33.8% N_2 and containing 50 ppm H_2S. It was chosen as representing the "worst case" because sulfate formation is expected to be most favorable at high utilizations at the anode outlet. (See Table 3-1.)

The experimental setup is illustrated in Figure 3-3. It consisted of a vertically supported quartz tube with a fitted top cover. Below the cover was a hook from which a sample containing Au-Pd crucible could be suspended. The cover was also fitted with a gas inlet tube and a thermocouple well. The gas inlet tube could be adjusted so that the gas mixture could be either blown over the melt surface or bubbled through the melt. The gas exited at the bottom of the tube. Hydrogen sulfide could be trapped from the effluent gas as sulfide to monitor the sulfur material balance of the system. Unless otherwise specified, the gas flow rate was

Table 3-1

RESULTS OF THERMODYNAMIC ANALYSIS OF CARBONATE/SULFIDE/SULFATE EQUILIBRIA UNDER VARYING ANODE GAS CONDITIONS AT 650°C

	Gas	Composition (mol fraction)						Activity Ratios for M=Na		
		H_2	H_2O	CO	CO_2	N_2	H_2S	$\frac{[M_2SO_4]}{[M_2CO_3]}$	$\frac{[M_2S]}{[M_2CO_3]}$	$\frac{[M_2S]}{[M_2SO_4]}$
1.	Reformed Methane Inlet	0.60	0.23	0.09	0.08	--	5×10^{-5}	8.2×10^{-10}	2.0×10^{-3}	2.3×10^{6}
2.	Low-Btu Inlet	0.211	0.056	0.178	0.092	0.463	5×10^{-5}	6.7×10^{-9}	7.0×10^{-3}	1.0×10^{6}
3.	Low-Btu Outlet, 75% Util.	0.040	0.176	0.047	0.399	0.338	5×10^{-5}	3.7×10^{-6}	5.1×10^{-4}	1.3×10^{2}
4.	Low-Btu Outlet, 90% Util.	0.015	0.190	0.018	0.455	0.322	5×10^{-5}	2.1×10^{-4}	4.1×10^{-4}	1.9

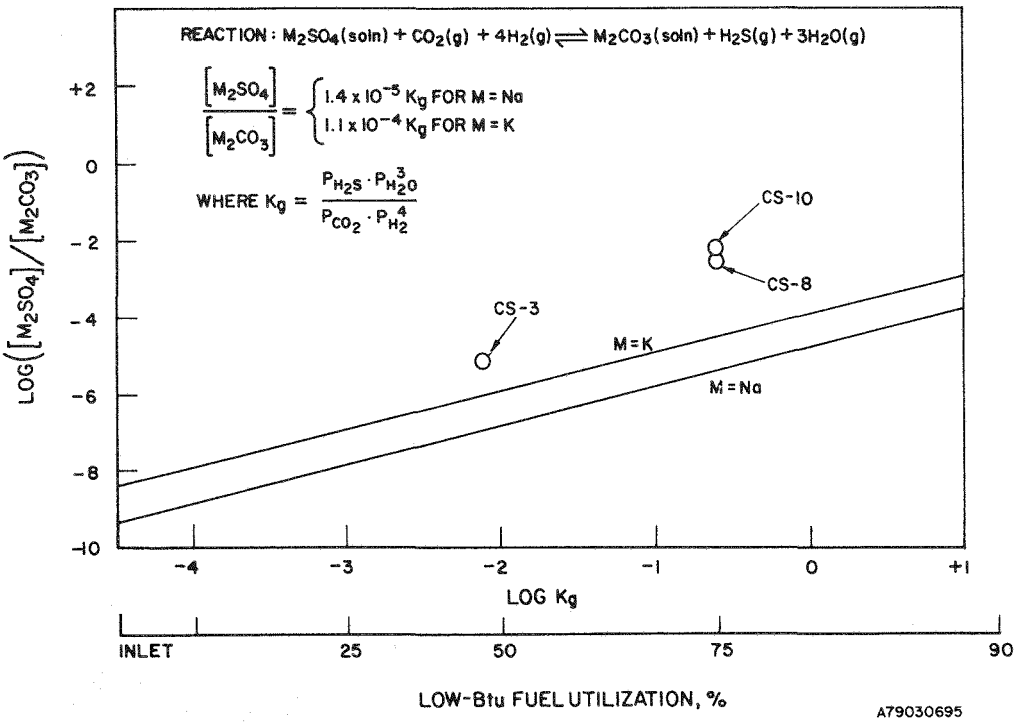

Figure 3-2. Variation of $[M_2SO_4]/[M_2CO_3]$ Activity Ratio With Thermodynamic Conditions at the Anode

maintained at 125 cc/min dry gas basis, and the test temperature was 650°C in all cases. The alkali composition of the melt was always maintained at a Li/K molar ratio of 62:38, equal to that of the Li-rich carbonate eutectic. Because of the slow approach to chemical equilibrium, particularly in sulfate-content melts, the composition of the $S^{=}/SO_4^{=}/CO_3^{=}$ anionic constituents was varied in many of the experiments while holding the gas composition constant. Relative changes in composition in this ternary system then indicated the ultimate equilibrium composition being approached under the 75% utilized fuel-outlet condition.

A series of preliminary experiments (Runs CS-1 through CS-4) were performed to check the apparatus and provide initial samples to the analytical laboratory for chemical analysis. These runs were generally performed under thermodynamic conditions representing low fuel utilizations where sulfate was expected to become relatively more stable. All subsequent runs (starting with CS-5) were performed in the 75% utilized fuel mixture containing 50 ppm H_2S. The best conditions and initial and final melt compositions for these runs are summarized in Table 3-2. Each test will be briefly described in the following sections.

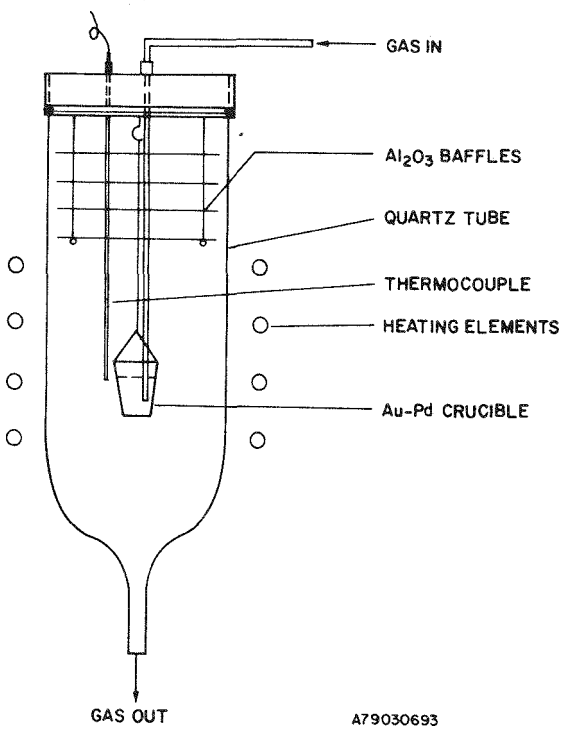

Figure 3-3. The Equilibration Test Apparatus

Runs CS-5-1 and CS-5-2

The starting sample was a 5-g mixture of 62 mol % Li_2SO_4 + 38 mol % K_2SO_4 that was molten at 650°C. The alumina inlet gas tube was immersed in the melt to bubble the gas through the melt for better gas/melt contact. As shown in Table 3-2, after 88 hours of test, the melt (CS-5-1) was found by chemical analysis to be still essentially sulfate. Then, the CS-5-1 melt was re-exposed to the same gas stream for an additional 88 hours. An increased carbonate content and some sulfide traces were detected by chemical analysis from the tested sample (designated CS-5-2). The melt, however, remained essentially sulfate (96.81%).

Atomics International (AI) reported that the rate of reduction of sulfate to sulfide according to Eq. 3-3 was controlled by mass transport of hydrogen through the melt(2). Thus, the overall sulfate-to-carbonate conversion reaction, Eq. 3-5, may also be kinetically limited by Eq. 3-3. This appeared to be the case in our experiments because the fuel gas used was only 4% H_2.

Table 3-2

CHEMICAL ANALYSES OF TEST MELTS EXPOSED TO 75% UTILIZED LOW-BTU FUEL CONTAINING 50 ppm H_2S

Run No.	Test Period (hr at 650°C)	Composition* (mol %) Initial	Final
CS-5-1	88	100% M_2SO_4	0.8% M_2CO_3 99.2% M_2SO_4
CS-5-2	88	0.8% M_2CO_3 99.2% M_2SO_4	2.98% M_2CO_3 0.13% M_2S 96.81% M_2SO_4
CS-6-2	52	74.62% M_2SO_4 10.12% M_2S 15.26% Unidentified sulfur-free phase as M_2O	24.99% M_2CO_3 0.20% M_2S 72.21% M_2SO_4 2.61% Unidentified sulfur-free phase as M_2O
CS-7	123	100% M_2SO_4	0.36% M_2CO_3 0.98% M_2S 99.46% M_2SO_4
CS-8	120	75% M_2CO_3 24% M_2S	99.53% M_2CO_3 0.12% M_2S 0.35% M_2SO_4
CS-9	188	93.1% M_2CO_3 6.9% M_2SO_4 In 38 w/o $LiAlO_2$	96.49% M_2CO_3 0.19% M_2S 3.31% M_2SO_4
CS-10-1	1	95.12% M_2CO_3 4.88% S	99.34% M_2CO_3 0.31% M_2S 0.35% M_2SO_4
CS-10-2	146	99.34% M_2CO_3 0.31% M_2S 0.35% M_2SO_4	99.37% M_2CO_3 0.12% M_2S 0.50% M_2SO_4

* M = 0.62 Li -0.38K

Run CS-6-2

Realizing the kinetic limitations of the sulfate-to-carbonate conversion under lean H_2 gas environments, a mixture of 62 mol % Li_2SO_4 and 38 mol % K_2SO_4 was first exposed to pure H_2 gas at 650°C for 120 hours to cause a partial reduction to sulfide. Previously, the AI workers had found that the reduction of sulfate to sulfide appeared to be an autocatalytic reaction. The pre-reduced melt was then removed from the test apparatus for analytical sampling before re-exposing it to the

low-Btu fuel gas. Analysis of the H_2-reduced melt indicated that about 25.4% of the original sulfate was reduced. However, only 10.12 mol % was accounted by analysis as sulfide M_2S. The balance, which was probably also sulfide in situ, may have formed into oxide, hydroxide, or carbonate as a result of sample exposure to air during handling for analysis. After 52 hours of exposure to the low-Btu fuel outlet gas at 650°C, the sample was cooled and chemically analyzed. The analysis indicated significant conversion of alkali sulfide and sulfate and unidentified alkali phase(s) to carbonate by the low-Btu fuel outlet gas.

Run CS-7

This test was a repeat of Run CS-5. However, a $CdCL_2$-Na_2CO_3 trap solution for H_2S was installed at the gas exit port of the system. The amount of H_2S trapped in the solution during an equilibration test compared with the amount of sulfur in the fresh inlet gas stream is an indication of the amount of sulfur evolved or absorbed by the sample. Four H_2S traps were collected during Run CS-7. The total amount of H_2S evolved during the entire 125 hours of test as estimated from these trappings, however, was relatively small. Nevertheless, it was consistent with the amount of carbonate formed in the melt during the test, according to Eq. 3-5, thus confirming the slow conversion rate of sulfate to carbonate.

Run CS-8

The initial sample was approximately a 10 g mixture of 38 mol % Li_2CO_3, 38 mol % K_2CO_3 and 24 mol % Li_2S. The flow rate of the 75% utilized low-Btu fuel gas was 25 cm^3/min for the first 50 hours and 125 cm^3/min for the remainder of the test. During the test, H_2S concentration of the exit gas was monitored by periodically connecting a Kitagawa H_2S detector tube and a $CdCl_2$-Na_2CO_3 trap for H_2S to the gas exhaust line. In general, data from the Kitagawa tubes were lower than from the $CdCl_2$-Na_2Co_3 trappings and were perhaps associated with the type of tube used (low range, B type). Higher range tubes were not available at the time the test was conducted. The H_2S concentration in the effluent gas increased substantially above the 50 ppm level in the inlet gas (30 to 100X) because of sulfide reduction and sulfur removal from the melt. The test was terminated at 120 hours, after the decrease of H_2S concentration to the baseline level indicated approach to the carbonate/sulfate/sulfide equilibrium point. Chemical analysis of the terminated sample corresponded to a composition of 99.53 mol % M_2CO_3, 0.35 mol % M_2SO_4, and 0.12 mol % M_2S. Thus, significant conversion of sulfide to carbonate, rather than to sulfate, occurred during Run CS-8 at 650°C. It should be noted that the equivalent amount of H_2S removed from Run CS-8 as indicated by chemical analysis was greater than

that estimated from the Kitagawa tube and trap analysis. This apparent discrepancy was due to the relative instability of Li_2S in the initial mixture during handling and upon exposure to air. However, any such Li_2S instability would not have influenced the subsequent conversion of the remaining sulfide to carbonate during the test.

Run CS-9

The initial melt was a mixture of 10 grams of electrolyte (consisting of 40 wt % $LiAlO_2$ and 60 wt % 62 Li/38 K carbonate eutectic) and 600 mg of 62 Li/38 K sulfate for an overall melt composition of 93.1 mol % carbonate and 6.9 mol % sulfate. The purpose of incorporating $LiAlO_2$ in the mixture was to create a porous structure for higher melt surface area exposed to the gas atmosphere, thus increasing the kinetics of the sulfate-to-carbonate conversion process. The gas flow was maintained at 25 cm^3/min except from the 68th to the 100th hour of the test period, when the gas flow was increased to 125 cc/min. By analysis of the H_2S trapped in $CdCl_2$-Na_2CO_3 solution at the exit port of the system, it appeared that H_2S evolved from the sample at a constant rate throughout the test, regardless of the flow rate at an average of 0.393 mg/hr. This rate is about two times higher than that measured from Run CS-7, in which the melt sample did not contain a $LiAlO_2$ support. The total amounts of H_2S evolved by the sample during the entire test, as estimated from the traps and from the chemical analysis of the tested melt considering Eq. 3-3 and Eq. 3-4, were consistent with each other.

Runs CS-10-1 and CS-10-2

Because sulfate-to-carbonate conversion was slow even with the use of $LiAlO_2$ support matrix, Run CS-10-1 was performed by starting with 10 g of carbonate (Li/K) ratio of 62:38) to which 100 mg sulfur was added. Upon reaction, enough sulfur was expected to form the equilibrium sulfate and sulfide composition in the melt with some excess to be gasified as H_2S or COS. The flow rate was maintained at 25 cm^3/min during the entire test. An H_2S trap at the gas exit port was provided to monitor the sulfur material balance over the system. The test was interrupted immediately after 650°C was reached during the first heating. The system was cooled down, exposed to air, and a sample (CS-10-1) was obtained for analysis to determine the progress in melt composition. The remaining sample was allowed to equilibrate with the fuel gas for a total of 146 hours until the amount of H_2S trapped from the effluent gas was equal to the baseline level. The final sample was designated CS-10-2. From the sulfur material balance, the sulfur level in the effluent gas,

and the odor of the sample, it appeared that CS-10-1 still contained unreacted sulfur. Nevertheless, its $SO_4^=$ composition remained essentially unchanged during the subsequent 146 hours of exposure to the fuel gas at 650°C. In the CS-10 test series, the total H_2S trapped from the effluent gas corrected by the amount of H_2S in the inlet gas was fairly consistent with the chemical analysis of the sample. The compositions of these CS-10 melts were also similar to the final CS-8 melt, which was a conversion product from a sulfide-carbonate mixture. (See Table 3-2.)

The conversion paths for the various tests, presented in a ternary phase diagram of the $SO_4^=$, $S^=$, $CO_3^=$ systems are shown in Figure 3-4. It can be seen that all tested melts, regardless of their starting composition, tend to approach the carbonate-rich region. The equilibrium electrolyte composition under the stated test conditions appears to be close to that of the final CS-8, CS-10-1, and CS-10 melts, whose average was 99.41% carbonate, 0.4% sulfate, and 0.18% sulfide. This composition corresponds to a sulfate-to-carbonate molar ratio of 4×10^{-3}.

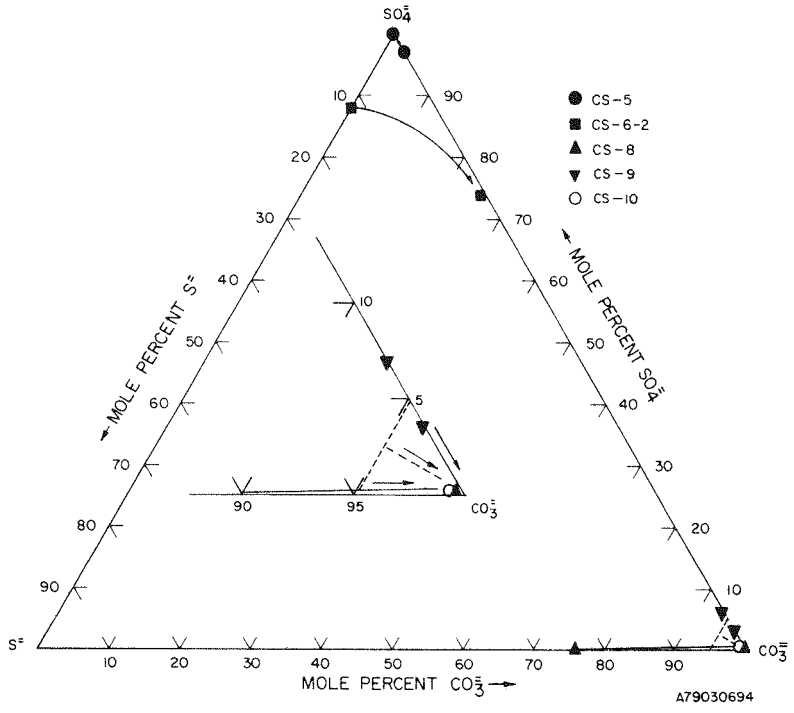

Figure 3-4. Conversion Paths for Various Test Melts Exposed to 75% Utilized Low-Btu Fuel Containing 50 ppm H_2S

CHEMICAL ANALYSIS OF ELECTROLYTE TILES EXPOSED TO SULFUR-CONTAINING GASES

The chemical stability of the 62 mol % Li_2CO_3/38 mol % K_2CO_3 electrolyte observed in the equilibration tests just described is consistent with chemical analysis of tiles from 3-cm^2 cells operated with sulfur-containing gases. The tiles from cells operated with SO_2-contaminated oxidant or H_2S-contaminated fuel were dissolved and analyzed for sulfide and sulfate levels. The results appear in Table 3-3, on the basis of mole fraction of each sulfur species in the carbonate electrolyte.

Table 3-3

SULFUR ANALYSES OF TILES FROM CELLS EPRI-7 AND EPRI-8

	Cell EPRI-7	Cell EPRI-8	Cell EPRI-10	Cell EPRI-13
	mole fraction			
S as $S^{=}$	1×10^{-2}	$<9 \times 10^{-5}$	3.8×10^{-3}	5.6×10^{-3}
S as $SO_4^{=}$	$<1.5 \times 10^{-3}$	4×10^{-5}	3.2×10^{-3}	3.6×10^{-3}

The sulfide content of the EPRI-7 tile, listed as 1×10^{-2} mole fraction, appeared to include a significant amount of nickel sulfide from the anode, so this result should be discounted. Thus, in general, the sulfur contents of cell-tested electrolytes were found to be very low (approximately 10^{-3} mole fraction), as calculated from available thermodynamic data and consistent with out-of-cell equilibration studies.

$LiAlO_2$ STABILITY

Tiles from selected cells were analyzed to determine the effect of sulfur on $LiAlO_2$ stability. The $LiAlO_2$ particles were characterized by B.E.T. surface area, X-ray diffraction, and chemical analyses after removal of the carbonate phase by dissolution in an acetic acid/acetic acid anhydride solution. The results from cells operated on sulfur-containing gases, as well as on clean gases, are compared in Table 3-4 with the initial characteristics of the $LiAlO_2$ before cell testing.

Table 3-4

CHANGES IN $LiAlO_2$ PROPERTIES DURING CELL OPERATION

Cell No.	Total Cell Life (hr)	Fuel Gas	Oxidant Gas	Surface Area (m^2/g)	$\alpha/\beta/\gamma$ $LiAlO_2$ (%)
Initial Powder	--	--	--	13.0	0:75:25
EPRI-3	1500	Clean High-Btu	Clean	11.1	0:78:22
EPRI-9	1064	Clean High-Btu Clean Low-Btu	Clean 50 ppm SO_2	9.5	24:55:21
EPRI-11	2616	Clean Low-Btu	5-10 ppm SO_2	12.8	33:47:20
EPRI-13	1344	5-10 ppm H_2S in Low-Btu	Clean	9.0	17:53:30
EPRI-15	1560	Clean Low-Btu	Clean	9.1	26:54:20

The $LiAlO_2$ exhibited reasonably good stability under sulfur-free conditions with high-Btu fuel (EPRI-3), with a 15% decrease in surface area but essentially no change in $\alpha/\beta/\gamma$ phase composition. However, significant transformations of β to α phase were observed in other cells that operated with low-Btu fuel for a significant period of time, including cell EPRI-15, which was not exposed to any sulfur species. Thus, the significant β to α transformation does not appear to be uniquely related to the presence of sulfur, but rather mainly associated with the gas environment established by low-Btu fuel compositions. Although the $LiAlO_2$ from cell EPRI-11 was an exception, $LiAlO_2$ from cells operated on low-Btu fuel showed significantly greater losses in surface area (27 - 31%) than $LiAlO_2$ exposed to high-Btu fuel.

More data are needed to confirm these observations of $LiAlO_2$ instabilities in low-Btu gases and to establish means of improving the long-term stability in this type of fuel. Long-term data in both clean and contaminated low-Btu gases are needed to determine the effects of sulfur on the chemical and physical stabilities of $LiAlO_2$.

REFERENCES

1. National Bureau of Standards. JANAF Thermochemical Tables. Washington, D.C.: Government Printing Office, 1971. NSRDS-NBS 37.

2. Development of a Molten Carbonate Process for Removal of SO_2 from Power Plant Stack Gases, Summary Report, June 1, 1967 to February 28, 1968. Atomics International Contract No. PH86-67-128 with the U.S. Public Health Service, Dept. of Health, Education and Welfare.

Section 4

TASK 5. EVALUATE CELL PERFORMANCE AT 5 AND 10-ATM PRESSURE

SUMMARY

Under this task, cell testing was conducted at pressures of 1, 5, and 10 atm with anode feeds simulating the product gases from -

- Naphtha steam-reforming (high-Btu)
- O_2-blown coal gasification (intermediate-Btu)
- Air-blown coal gasification (low-Btu).

The equilibrium fuel inlet-gas compositions, at 1, 5, 10-atm pressure, considering water-gas shift, methanation, and carbon deposition reactions were thermodynamically evaluated for the above three product gases, and anode inlet and outlet gas compositions were calculated as functions of hydrogen utilization and operating pressure. From this thermodynamic evaluation, it was concluded that, at pressures above 1 atm for a second-generation fuel cell system to operate at high total fuel utilization -- that is, at high fuel conversion efficiency -- the energy content in CH_4 and CO must be utilized. Direct electrochemical oxidation of these species at a typical state-of-the-art cell operating temperature (approximately 650°C) occurs at very slow rates. Thus, high fuel conversion efficiencies can only be obtained if CO and CH_4 are utilized chemically in the cell to produce H_2 via the reactions -

$$CH_4 + H_2O \rightarrow CO + 3H_2 \quad \text{(Steam reforming)} \qquad (4\text{-}1)$$

$$CO + H_2O \rightarrow CO_2 + H_2 \quad \text{(Water-gas shifting)} \qquad (4\text{-}2)$$

Both reactions are thermodynamically favored under cell operating conditions. The kinetics of the water-gas shift reaction are rapid under cell operating conditions, so H_2 will form from CO and H_2O. However, under the same conditions and in the presence of molten carbonate fuel cell anode catalysts, the kinetics of the methane steam-reforming reaction are very slow, so the thermodynamic equilibrium will not

be attained. Approaches to improve methane utilization in the cell were thermodynamically evaluated. Anode recycling slightly improves methane utilization, hence, efficiency, but apparently it will be necessary to -

- Optimize fuel cell operating pressure to establish the trade-off between cell performance improvement, a function of log p, and fuel conversion efficiency in the cell, which will be related to methane utilization.
- Improve the internal CH_4 reforming capabilities of molten carbonate fuel cells by either increasing the surface area of present anodes, by inclusion of dopants in the anode structure, or by providing an active catalytic surface on the anode housing, especially by the outlet where the fuel composition is rich in H_2O and lean in H_2, a condition favoring CH_4 reforming.

A total of 12 bench-scale (4 X 4 in) molten carbonate fuel cells were assembled and operated during the course of this program. We were not able to obtain reliable data because these cells deteriorated early in life as a result of increasing IR losses, gas crossover, gas leakage through the wet seals, heavy corrosion, and considerable carbonate losses. These were related to the electrolyte retention capabilities of the $LiAlO_2$ in the electrolyte batch we used, which deteriorated as a result of aging and hydration, and to difficulties in maintaining proper ΔP across the tile and the wet seals with existing equipment. Valuable and significant experience relative to electrolyte storage and pressure operation was gained during this testing.

EVALUATION OF FUEL GAS INLET COMPOSITION

Fuel gas for a fuel cell power plant is supplied by a fuel processor, which probably is a coal gasifier or a hydrocarbon reformer. The operating conditions (temperature, pressure, and residence time) of the existing fuel processors are quite different from those of second-generation molten carbonate fuel cells. If the fuel processor is operated under conditions favoring product gas compositions richer in H_2 and CO and lower in CH_4 than the equilibrium compositions at cell operating temperature (1200°F) and pressure, such gas will attain the thermodynamic equilibrium corresponding to cell conditions during cooldown or soon after introduction into the anode. This equilibrium will be attained because of the "fast" rates of the carbon deposition, methanation, and shift reactions, as listed below, under cell temperature and projected pressure operating ranges.

$$2CO \rightleftarrows C\downarrow + CO_2 \qquad (4\text{-}3)$$

$$CO + 3H_2 \rightleftarrows CH_4 + H_2O \qquad (4\text{-}4)$$

$$CO + H_2O \rightleftarrows CO_2 + H_2 \qquad (4\text{-}5)$$

The equilibrium fuel gas compositions for reformed naphtha and air-blown gasifier products as a function of pressure were calculated and are shown in Figures 4-1 and 4-2. Figure 4-2 presents the actual low-Btu gasifier product gas composition in thermodynamic equilibrium at 1200°F. As shown, carbon deposition will occur, probably at the heat exchanger where the gasifier product gas is cooled from the reactor outlet temperature (1700°F) to cell inlet temperature (1100° to 1200°F). Carbon formation increases with increasing pressure. To avoid carbon deposition during cooldown of the gasifier output, the CO_2 content and/or steam content needs to be increased. Increasing the CO_2 content will slow down carbon formation, but at the cost of valuable H_2 (Eq. 4-3, shifting to the left). Increasing H_2O will control carbon formation and also CH_4 formation while increasing H_2 content. We calculated the volume of water that needs to be added to avoid carbon deposition during cooldown, as a function of pressure. Results are presented in Figure 4-3. As we have stated, the addition of water to the gasifier product stream will not only control carbon deposition but will also enhance its H_2 content and reduce its CH_4 formation.

FUEL FLOW RATES AND ANODE OUTLET GAS COMPOSITIONS — HYDROGEN UTILIZATION

An existing computer program was modified to determine the anode inlet flow rates and outlet gas compositions as functions of the fuel-pretreatment process (inlet composition), system pressure, and hydrogen utilization.

Throughout this report, two different hydrogen utilizations* are used: electrochemical and total. Electrochemical hydrogen utilization is defined as the volume of hydrogen the cell consumes electrochemically with respect to the hydrogen content of the fuel inlet gas equilibrated at 650°C. Total hydrogen utilization is defined as the volume of hydrogen the cell consumes electrochemically plus the hydrogen

---

* $U_{Electrochemical} = \dfrac{I(amp) \times 7.5 \dfrac{ml\ H_2}{min\text{-}amp}}{ml\ H_2\ in\ at\ equil.}$; $U_{Total} = \left[\dfrac{H_2\ in - H_2\ out}{H_2\ in}\right]_{equil.}$

consumed or made by the water-gas shift and reforming reaction with respect to the hydrogen content of the fuel inlet gas equilibrated at 650°C. Total hydrogen utilization will be lower than the electrochemical hydrogen utilization if the water-gas shift and reforming reactions generate H_2; it will be higher if the reverse water-gas shift and methanation reactions occur. In this report, when we refer to H_2 utilization, we mean total H_2 utilization, because the effects of the water-gas shift and reforming reactions must be considered to determine the overall fuel-cell efficiency.

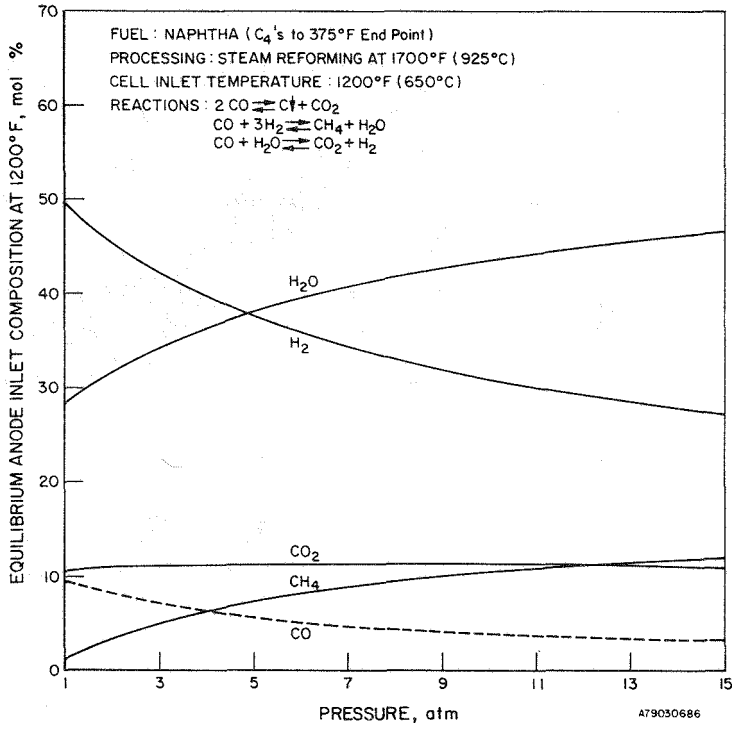

Figure 4-1. Effects of Pressure on the Anode Inlet Composition

UTILIZATION OF ENERGY CONTENT IN CH_4

Increasing the operating pressure of molten carbonate fuel cells results in performance improvements (Nernst gains) due to the increase in the partial pressures of the

reactants. Higher operating pressure should also produce increases in gas solubilities and mass transport rates, and, hence, additional improvements in cell performance.

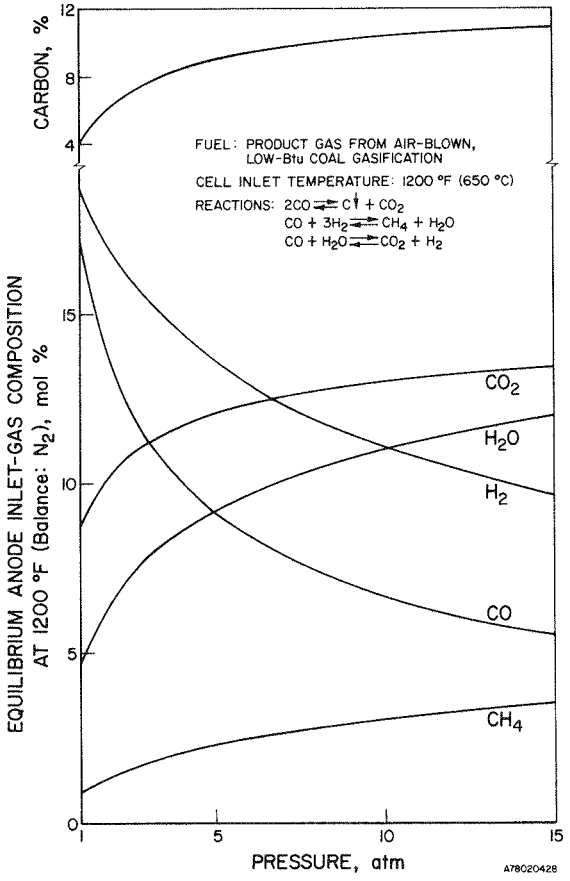

Figure 4-2. Effect of Pressure on the Equilibrium Anode Inlet Composition (Temp:1200°F, Fuel: Air-Blown, Low-Btu Coal Gasification Product Gas)

Cell performance improvement after pressurization is shown in Figure 4-4 for a high-Btu fuel gas in a bench-scale (4 X 4 in) cell(1). These cells tested under pressure were first operated for 100 to 150 hours at 1 atm on simulated reformed methane fuel and standard oxidant (70% air/30% CO_2) to establish baseline performance. During the next 50 to 60 hours, performance and utilization data at 1 atm were monitored as a function of fuel and oxidant gas compositions. Then the cell

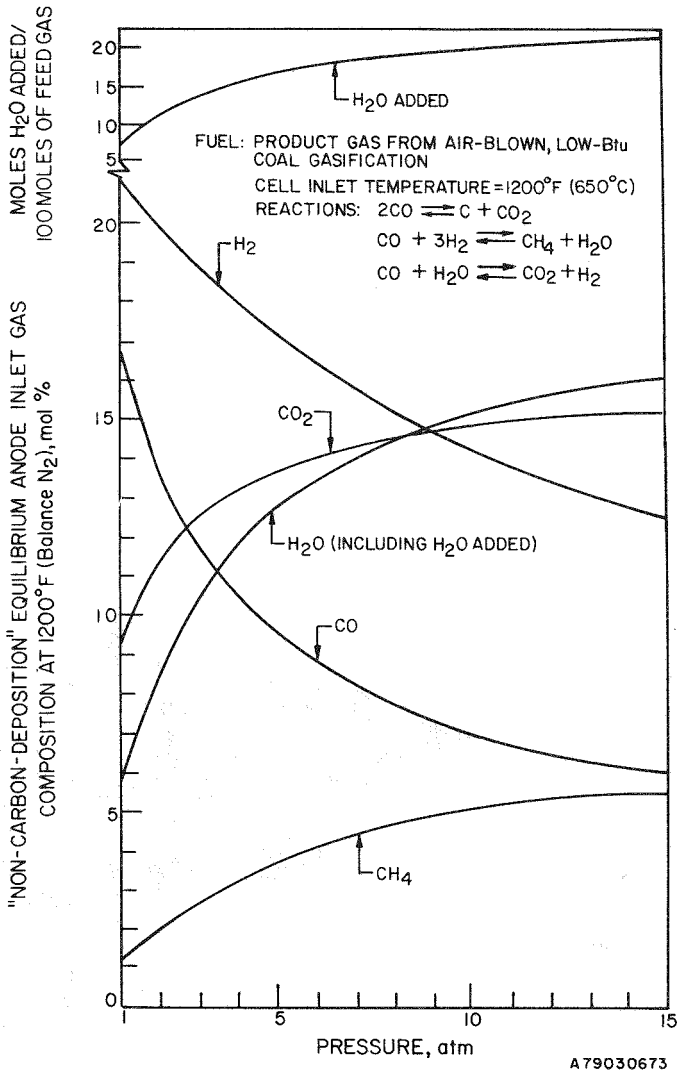

Figure 4-3. Effect of Pressure on the "Non-Carbon-Deposition" Equilibrium Anode Inlet Composition (Temp: 1200°F, Fuel: Air-Blown, Low-Btu Coal Gasification Product Gas)

operating pressure was increased to 5 atm, and then to 10 atm, at an approximate rate of 0.5 atm/hr. Increasing the operating pressure by a factor of five, from 1 to 5 atm, resulted in a Nernst gain of 40 mV, as reflected by an increase in OCV from 1072 to 1112 mV. Doubling the operating pressure from 5 to 10 atm resulted in a Nernst gain of 8 mV, as reflected by an increase in the OCV from 1112 to 1120 mV. This total increase agreed with our theoretical prediction of a 46-mV Nernst gain when the operating pressure is increased from 1 to 10 atm. The Nernst gains are

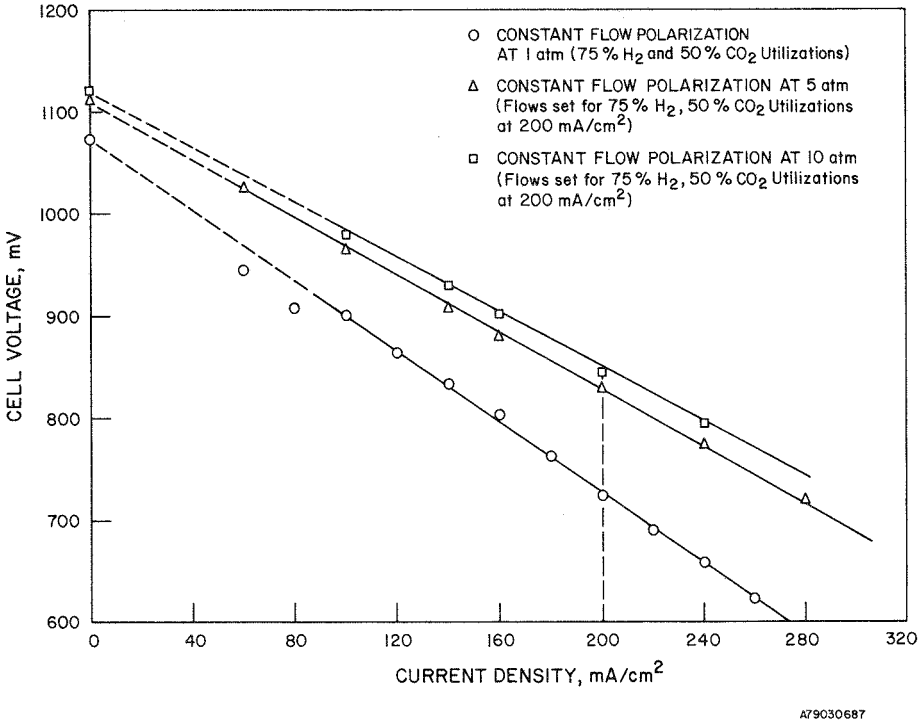

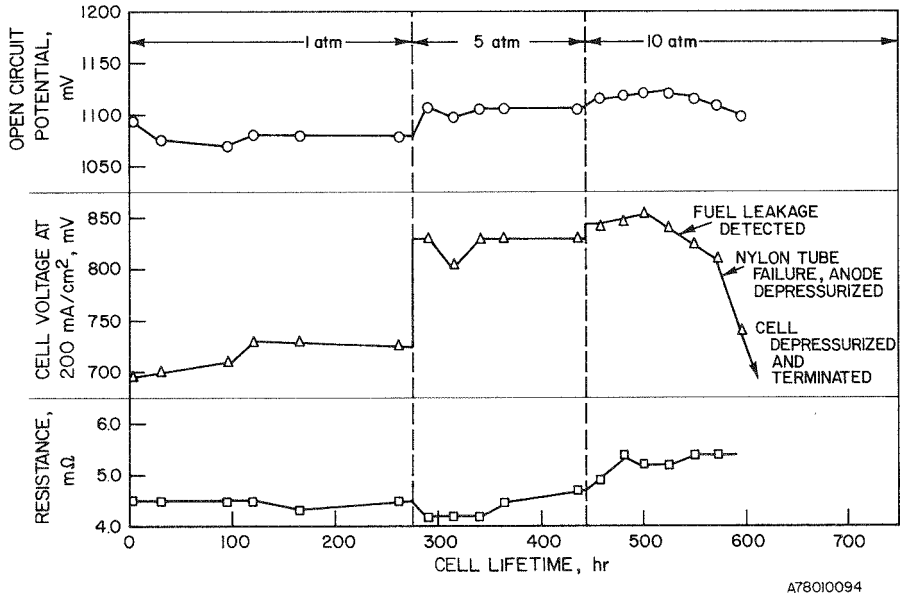

Figure 4-4. Benefits Associated With Operation of Molten Carbonate Fuel Cells at Pressures Above 1 atm

proportional to ℓn P; that is, the major part of the Nernst gain is obtained between 1 and 5 atm. The performance gain obtained under load conditions is much larger than the predicted Nernst gain. At 200 mA/cm^2 and at 75% H_2 and 50% CO_2 utilization, cell voltage increased by 105 mV when the pressure was increased from 1 to 5 atm, and it increased by an additional 15 mV when the pressure was raised from 5 to 10 atm. When a bench-scale cell was operated on the simulated product gas from an air-blown low-Btu coal gasification process and the standard oxidant, a similar increase in the OCV was observed. Under load conditions, at 200 mA/cm^2 and at 75% H_2 and 50% CO_2 utilization, cell voltage increases ranged from 225 to 240 mV when the pressure was raised from 1 to 10 atm.

The fuel flow rates used for above pressurized cell evaluations were calculated on the basis of 75% total H_2 utilization and CH_4-free fuel gas compositions. As shown in Figures 4-1 and 4-3, H_2 concentrations decrease significantly at higher pressure because of CH_4 formation. Therefore, cells for the above pressure-effect study were operated at H_2 utilization higher than 75%. However, cell performance improvements due to increased operating pressure still greatly exceed the predicted Nernst gains; hence, it appears that the contributions from other mechanisms, such as improved gas solubilities and mass transport rates, are very significant at pressure.

Direct electrochemical oxidation of CH_4 at a typical state-of-the-art cell operating temperature (650°C) occurs at very slow rates. Thus, high fuel conversion efficiencies can only be obtained if CH_4 is utilized chemically inside the cell to produce H_2 via the reactions -

$$CH_4 + H_2O \rightarrow CO + 3H_2 \qquad (4\text{-}6)$$

$$CO + H_2O \rightarrow CO_2 + H_2 \qquad (4\text{-}7)$$

From the view of hydrogen utilization, the important role of these two reactions is shown in Figure 4-5 and 4-6. The calculations are based on the assumption that methane could be reformed inside the cell according to the thermodynamic equilibrium. To operate at 90% total H_2 utilization of a fuel feed from reformed naphtha at 1 atm, 20% of the H_2 consumed electrochemically needs to be supplied internally from CO and CH_4. However, with a fuel feed from reformed naphtha at 5 and 10 atm and at 90% total H_2 utilization, 60 and 132%, respectively, of the H_2 consumed electrochemically needs to be supplied internally from CO and CH_4. As shown in Figure 4-6, with the product from an air-blown coal gasifier, the volume of H_2 that needs to

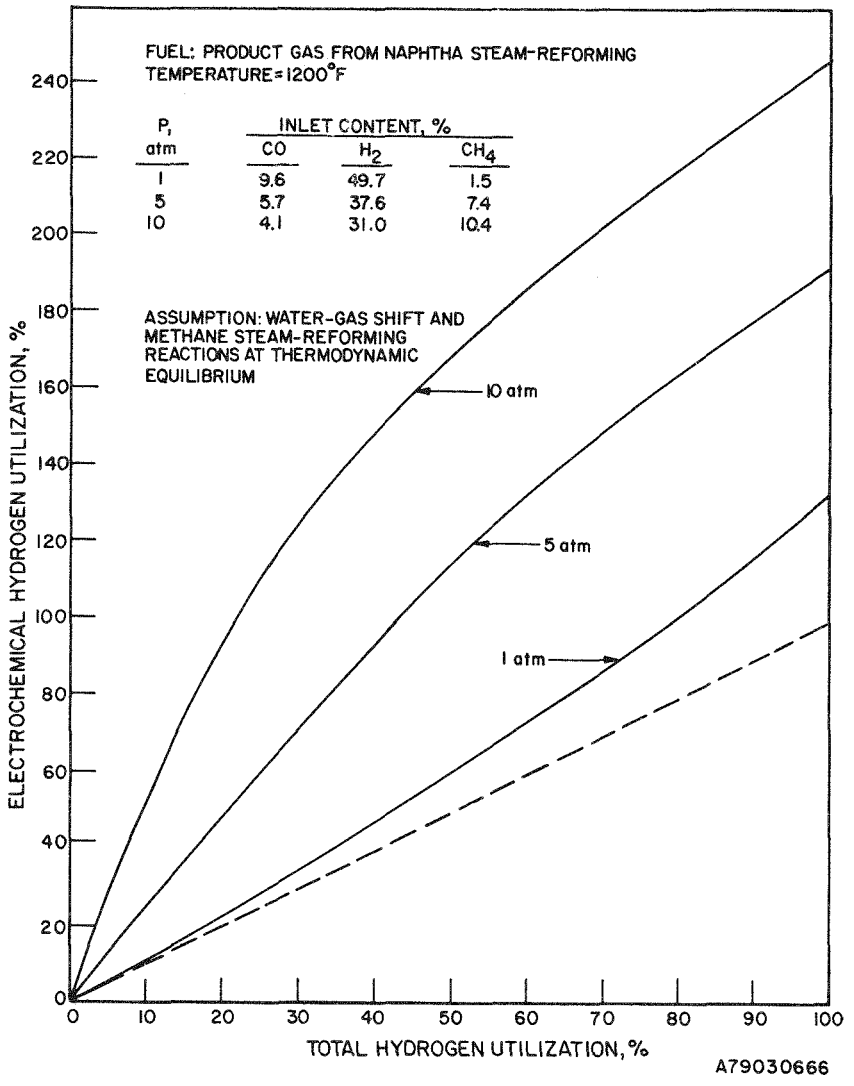

Figure 4-5. Electrochemical vs. Total Hydrogen Utilization for Product Gas From Naphtha Steam-Reforming

be internally supplied from CO and CH_4 is greater than with a reformed naphtha fuel. From the view of fuel heating value, the importance of the above two reactions is reflected in Figure 4-7. At 1-atm system pressure, the CH_4 content of the fuel is low (approximately 1%), and, if not internally reformed, its impact on total system efficiency is not significant. However, at 10-atm system pressure, where the fuel inlet CH_4 content is much higher, the impact on fuel cell system efficiency is significant. The maximum attainable (ideal) fuel heating value efficiency when operating with a reformed naphtha fuel feed at 10-atm pressure is only 50% if the energy

content of CH is not utilized. The significance of methane utilization to second-generation fuel cell systems and its impact on efficiency, mainly at pressures above 1 atm, is therefore evident.

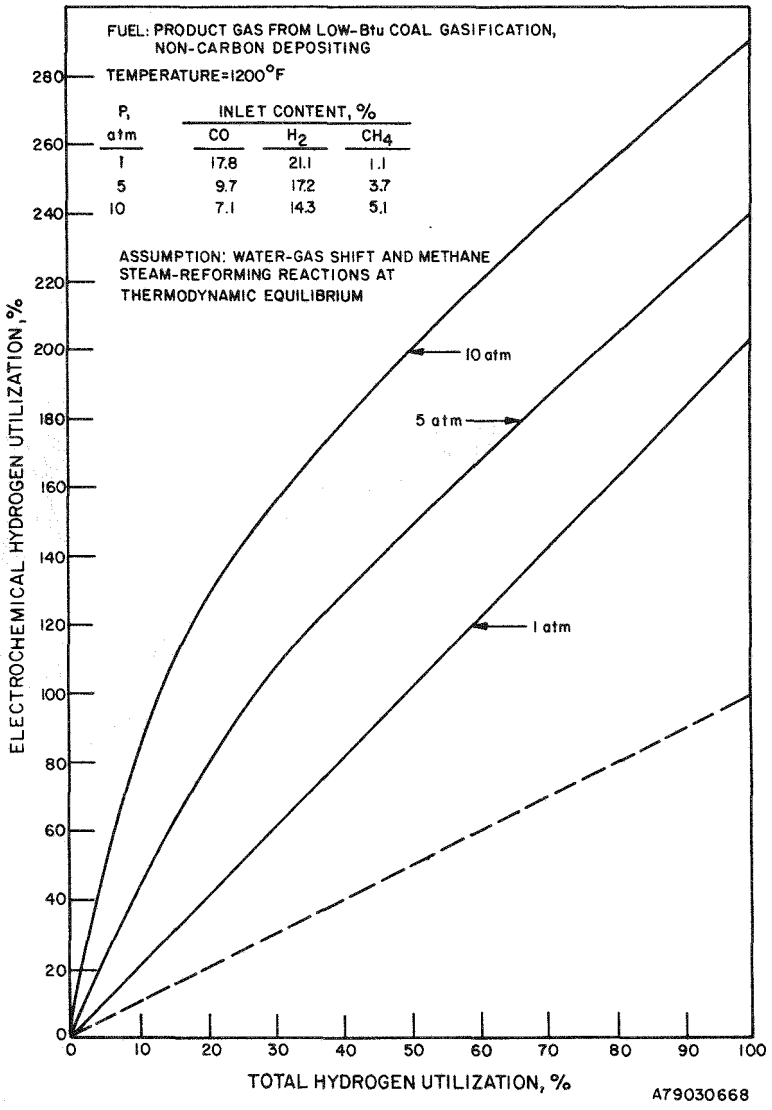

Figure 4-6. Electrochemical vs. Total Hydrogen Utilization for Product Gas From Low-Btu Coal Gasification

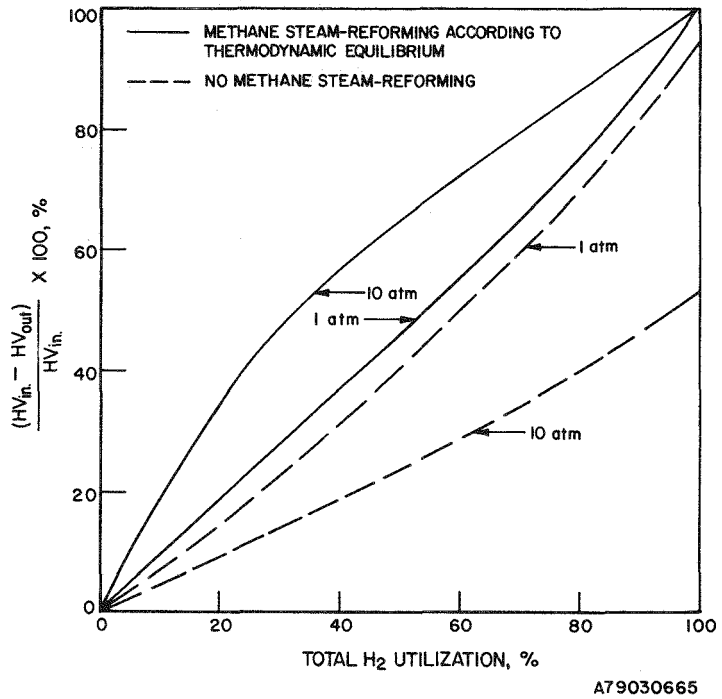

Figure 4-7. Ideal Efficiency vs. Total H_2 Utilization When CH_4 Either Being Internally Reformed or as an Inert

There is no problem in extracting the energy content of CO because at cell operating temperature and at 1 to 10-atm pressure, the shift reaction is very "fast" in attaining thermodynamic equilibrium. However, steam-reforming of CH_4 at 1200°F and 1 to 10-atm pressure in the presence of unsupported, low-surface-area nickel catalyst is very "slow" if it occurs at all. Hence, under prevailing conditions, little energy content of CH_4 can be extracted; that is, most CH_4 will flow through the anode compartment as an inert. This has been experimentally shown in bench-scale cells. (See Table 4-1; also see Reference 2.) To increase the hydrogen and fuel heating value utilizations, it became necessary to improve the internal CH_4 reforming capabilities of molten carbonate fuel cells by increasing the surface area of present anodes, by inclusion of dopants in the anode structure, or by providing an active catalytic surface on the anode housing, preferentially by the outlet where the fuel composition is rich in H_2O and lean in H_2.

Table 4-1

CH_4 FORMATION IN ATMOSPHERIC AND PRESSURIZED FUEL CELL — EXPERIMENTAL DATA (EPRI PROJECT)

Exp. No.	Life (hr)	Simulated Fuel Dry Mixture $\%H_2$	$\%CO_2$	ml/min	Humi. Temp.	mA/cm^2	psig	Anode Outlet Composition, Dry CO	H_2	CH_4	CO_2	N_2
EPRI-5												
	115	72	28	256	51.7	OCV	0	18.73	65.36	.04	15.78	.09
EQUIL.*	--			--	51.7	OCV	0	(15.2)	(65.4)	(2.1)	(17.3)	--
	115			256	51.7	160	0	6.38	5.65	--	87.36	.61
EQUIL.	--			256	51.7	160	0	(9.8)	(20.8)	(0.0)	(69.3)	--
	165			256	73.9	OCV	58.8	14.22	44.41	8.57	32.62	.18
EQUIL.*	--			256	73.9	OCV	58.8	(11.4)	(53.7)	(13.5)	(21.4)	--
	187			196	96.1	OCV	58.8	15.74	55.45	7.98	20.61	.22
EQUIL.*	--			196	96.1	OCV	58.8	(10.2)	(57.5)	(10.4)	(21.9)	--
EPRI-7												
	194			224	96.2	160	58.8	3.10	22.9	6.0	68.0	--
EQUIL.*	--			224	96.2	160	58.8	(7.3)	(15.7)	(0.1)	(77.0)	--
	194			224	96.2	OCV	58.8	8.3	63.55	10.6	17.5	.05
**	194			224	96.2	OCV	58.8	8.4	64.72	10.6	16.25	.03
	194			224	96.2	OCV	58.8	8.4	64.58	10.5	16.5	.02
	311			224	96.2	OCV	58.8	10.78	59.27	11.64	18.27	.04
EQUIL.*	--			224	96.2	OCV	58.8	(10.2)	(57.5)	(10.4)	(21.9)	--

* Numbers in parentheses are thermodynamic equilibrium compositions, considering methanation/reforming and shift reactions.

** Three consecutive samplings at 10 min/sample rate.

RECYCLE OF THE ANODE EFFLUENT

The anode effluent has a high level of heat content if the CH_4 content is not used, (that is, if CH_4 is inert in the cell). If this heat content is utilized by recycling some effluent back to the anode inlet as shown in Figure 4-8, the fuel heating value efficiency will increase, as indicated in Figure 4-9. As the recycle ratio is increased, the heating value efficiency increases, especially at lower hydrogen utilizations. When the heating value efficiency is improved, the fresh fuel requirement should decrease. This is indicated in Figure 4-9. However, as fresh fuel is saved from recycling anode effluent, total feed into the cell is increased significantly (Figure 4-10), especially at lower H_2 utilizations. Therefore, a compromise among recycle ratio, hydrogen utilization, and total feed into cell needs to be established. If the recycle ratio and total H_2 utilization are set at 50% and 40%, respectively, the fresh fuel savings and the heating value efficiency improvements tabulated in Table 4-2 are possible. The fuel heating value effiency is increased from 18 to 70% when CH_4 is reformed inside the cell and the anode effluent is recycled at 50%.

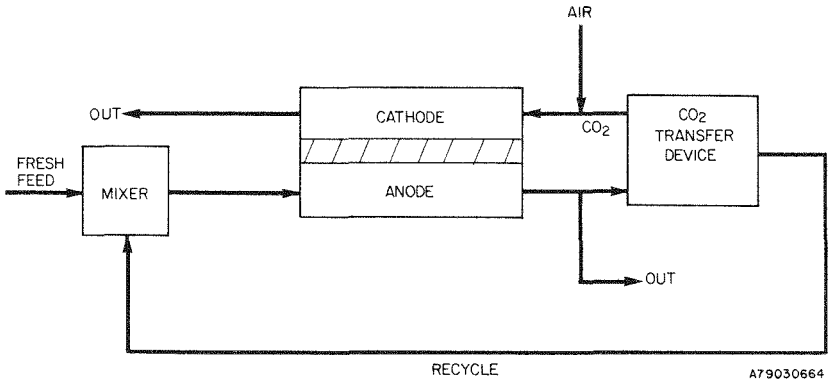

Figure 4-8. Recycling Fuel to Increase Fuel Utilization

CELL TESTING

The objective of this part of Task 5 was to operate bench-scale cells (4 X 4-in) using high- and low-Btu fuels (clean and with H_2S) and a 70% air + 30% CO_2 oxidant (clean and with SO_2) at 1, 5 and 10-atm pressure to generate both life and performance (at 3 combinations of conversion) data.

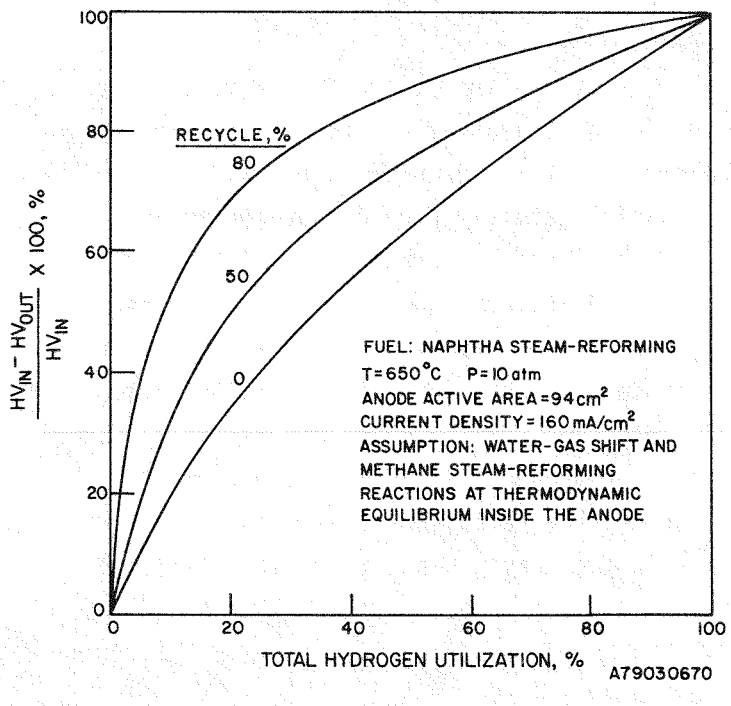

Figure 4-9. "Ideal" Efficiency vs. H_2 Utilization With Percent Recycle as a Parameter

Two stations for testing 4 X 4-in cells under pressure were modified by replacing the existing rotameters with mass flowmeters (to improve the accuracy of the inlet flow measurements) and by altering the tubing arrangement downstream from the anode and upstream from the pressure control valve (to avoid water condensation, which causes flow pulsation).

A total of 12 bench-scale cells were assembled and operated during the course of this program. The first cell (EPRI-1L) was operated for 600 hours. It was operated at 1 atm on a fuel simulating the product gas from naphtha steam-reforming and the standard oxidant (70% air + 30% CO_2). During the first 200 hours of operation, its output increased from 650 to 725 mV at 200 mA/cm^2 (75% H_2/50% CO_2 utilizations), as shown in Figure 4-11. The performance exceeded the prerequisite (700 mV at 160 mA/cm^2) of this program for further parametric testing. During this 200-hour period, gas crossover (through the tile) from the cathode to the anode, at a ΔP of 0.4-in H_2O, as indicated by the presence of nitrogen in the anode effluent, was insignificant (0.01% N_2). At this time, loss of tile integrity was indicated by a sudden increase in nitrogen crossover to about 1% and continual increasing to 4.5%

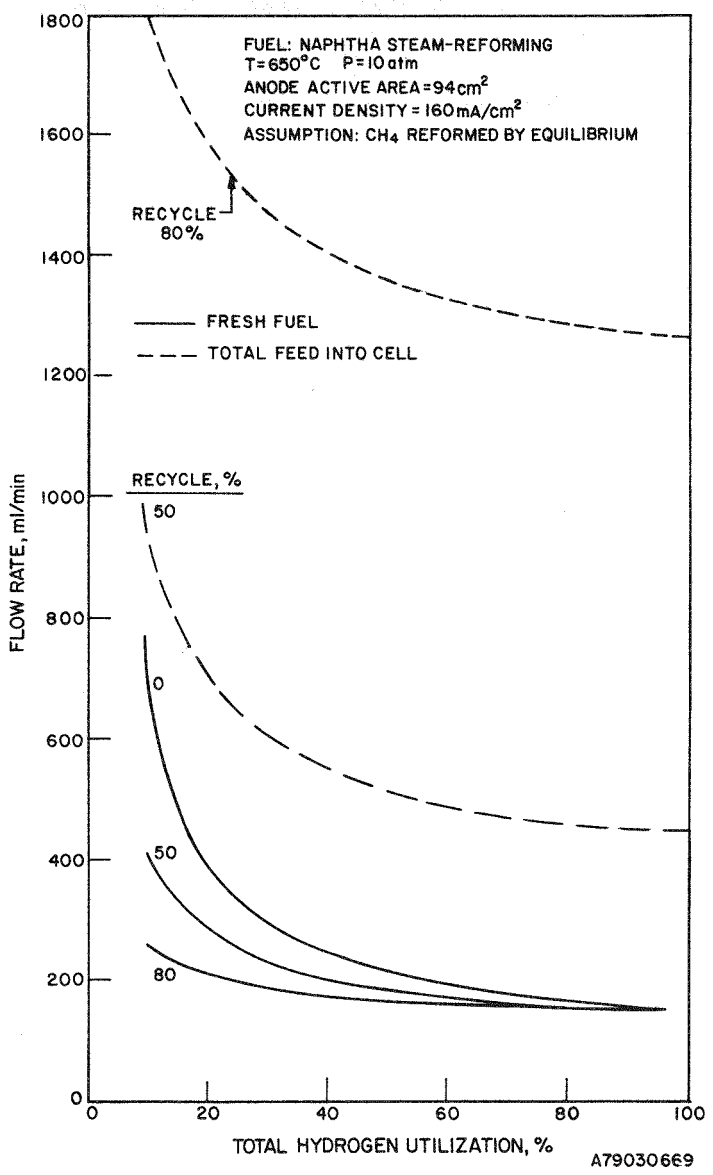

Figure 4-10. Effect of Recycling Anode Effluent on Fuel Flowrate Requirements

of the anode effluent during the next 100 hours. As a result, cell resistance slowly increased while cell performance decreased, as shown in Figure 4-11, due to oxidation of the anodic components.

This cell was terminated after 600 hours of operation. A second cell, EPRI-2L, was also terminated early in life because of low performance. For the next four cells, we still were not able to obtain reliable data because these cells deteriorated

Table 4-2

FRESH FUEL SAVINGS WHEN CH_4 IS REFORMED INSIDE THE ANODE*

CH_4 Reforming	Recycle (%)	Fresh Fuel (ml/min)	Total Feed (ml/min)	HV Efficiency (%)
No	0	1037	1037	18
No	50	500	1400	28
Thermodynamic Equilibrium	0	245	245	56
Thermodynamic Equilibrium	50	200	550	70

* Fuel: Naphtha Steam-Reforming
T = 650°C, P = 10 atm, I = 160 mA/cm^2
A = 94 cm^2
Total H_2 Utilization = 40%

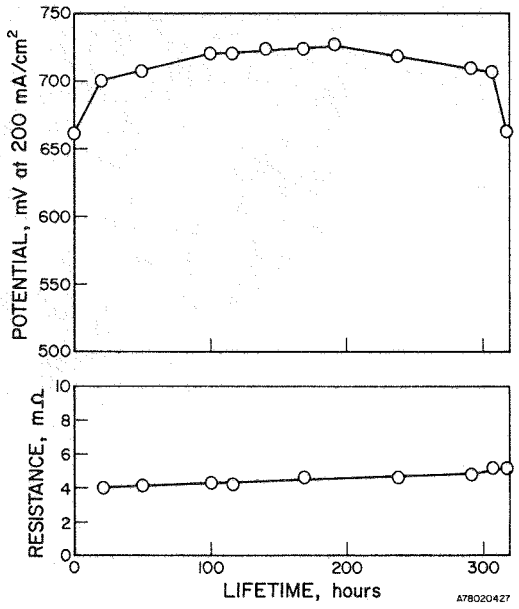

Figure 4-11. Lifegraph of Cell EPRI-1L (94-cm^2 Active Electrode Area)

early in life as a result of increasing IR losses and gas crossover, heavy corrosion of the anode wet-seal, and considerable carbonate losses. These problems were found to be related to the electrolyte retention capabilities of the $LiAlO_2$ in the electrolyte batch we used. Because of long storage (15 mo), the $LiAlO_2$ of this batch hydrated and its characteristics changed. Reprocessing of the batch* resulted in dehydration, but also significantly decreased the $LiAlO_2$ surface area and its carbonate retention capabilities. A cell assembled with the reprocessed electrolyte showed good performance during the first 100-200 hours, but deteriorated soon thereafter. Upon disassembly, we found considerable carbonate creepage and serious corrosion of the anode wet seal. These findings are significant in that they show the need for good retention capabilities and the limitations and problems associated with long-term storage of $LiAlO_2$.

A "fresh" electrolyte batch was then prepared, using the state-of-the-art multistep firing process. We assembled and operated two cells with the freshly prepared electrolyte batch. Both cells failed early in life as a result of high carbonate losses. Based on these results and on thermal expansion experiments conducted, which showed that tiles from this batch "slump" during the second cycle, we concluded that this electrolyte did not possess the required characteristics. Such electrolyte batch-to-batch nonreproducibility has plagued us in the past and was the primary reason why we recommended that alternative preparation techniques be investigated in the concurrent DOE-sponsored effort. At the time these EPRI tests were underway, the alternative (aqueous slurry techniques) processes were showing a great deal of promise although the processing conditions were not fully developed. Three cells (EPRI-10, 11, and 12) were assembled with electrolyte tiles prepared by the DOE process. The first cell failed after pressurization and the other two cells did not reach the prerequisite performance (700 mV at 160 mA/cm^2) during the stabilization period. Since these tests, additional slurry work has been done and we feel confident that the process is superior to the state-of-the-art processes used in the EPRI program. At the present time, DOE testing is showing good performance and stability.

From the experience of operating fuel cells at pressure, we have identified the following problems, which result in an unusually high cell failure rate.

---

* 40 hours at 400°C in CO_2.

- Main Problems

  --Undue transient differential pressures: Increasing or decreasing total system pressure causes differential pressures between the anode, cathode, and vessel that are higher than those tolerable by the cell assembly.

  --Undue steady-state differential pressures: At steady-state operation (constant system pressure) differential pressures often develop between the anode, cathode, and vessel that are higher than those tolerable by the cell assembly.

  --Condensation in the anode and cathode effluent lines inhibits the proper functioning of the controlling valves.

  --Constant C_V controlling valves, which do not allow flow rate changes above or below those of the valve range, limit utilization studies.

- Minor Problems

  --There is high-pressure vessel leakage through the flange along the bolt diameter, a result of corrosion and vessel seal area due to usage and thermal cycling.

  --Fluctuations in the air delivery pressure to the vessels cause constant adjusting responses of the controlling valves.

  --The system has dead volume.

We feel that the operation of molten carbonate fuel cells at pressure can be achieved when the above problems are resolved.

CONCLUSIONS

Operation of molten carbonate fuel cells at pressure is very attractive because the performance improvements exceed the Nernst gains (proportional to ℓn P). On the other hand, pressurization also presents some problems to the cell operations.

1. Carbon deposition increased.
2. Methane formation increased, resulting in a lower CO and H_2 partial pressure and overall fuel heating value efficiency. (See Table 4-1).
3. Reactant leakage increased because of insufficient electrolyte tile bubble pressure and wet-seal efficiency at higher pressure differential from pressure fluctuations.

Also, to provide sufficient bubble pressure and wet-seal efficiency, the importance of proper electrolyte storage and handling to prevent aging and hydration is increased for pressurized fuel cells. For pressure operation, the methane

utilization becomes very important; the fuel heating value efficiency is very low if methane is not utilized. We believe that by providing a reforming catalytic surface and recycling anode effluent, the heating value of methane can be utilized.

REFERENCES

1. Institute of Gas Technology. "Fuel Cell Research on Second-Generation Molten-Carbonate Systems, Vol. 1." Final Report under ANL Contract No. 31-109-38-3552, Chicago, Il., September 1977, p. 82.

2. Ibid., p. 87.

Appendix A

DETAILED CALCULATIONS FOR DETERMINING
SO_2 CONCENTRATIONS IN OXIDANT GASES

I. STEAM REFORMED NAPHTHA

Inlet Equilibrium Composition:

52.7% H_2

10.4% CO_2

26.2% H_2O

10.7% CO

Anode Outlet Composition at 75% H_2 Utilization:

9% H_2

41.2% CO_2

4.2% CO

45.6% H_2O

Assume that 200 ppm H_2S (0.02%) is also present in the outlet.

Dry Inlet Flow Rate at 75% Utilization = 263 cc/min

Water Added (this equilibrates to 26.2% water) = 18.19%

Wet Inlet Flow Rate (at humidifier temperature) = 310.8 cc/min

CO_2 produced (at 19A) = 19 A X 7.5 $\frac{cc}{min - A}$ = 142.5 cc/min

Therefore, Total Anode Outlet Flow Rate = 310.8 + 142.5 cc/min

= 453.3 cc/min

H_2S Flow Rate = $\frac{0.02}{100}$ X 453.3 = 0.0907 cc/min

H_2S reacts with O_2 as follows:

$$H_2S + O_2 \rightarrow SO_2 + H_2. \qquad \text{(A-1)}$$

Case A: 75% H_2 Utilization, 25% O_2 Utilization

Dry Oxidant Flow Rate (at 19A) Based on Burner Design = 1725 cc/min

Water Content = 5%

Therefore, Wet Flow Rate = 1811.3 cc/min

SO_2 Flow Rate = 0.0907 cc/min

Therefore Total Oxidant Flow Rate = 1811.3907 cc/min

SO_2 Content in Oxidant $= \frac{0.0907}{1811.3907} \times 100$

$= 0.005\%$

$= \underline{50 \text{ ppm}}$

Case B: 75% H_2 Utilization, 50% O_2 Utilization

Dry Oxidant Flow Rate = 1029 cc/min

Water Content = 5%

Wet Flow Rate = 1080.5 cc/min

SO_2 Flow Rate = .0907 cc/min

Therefore, Total Oxidant Flow Rate = 1080.5907 cc/min

SO_2 Content in Oxidant $= \frac{0.0907}{1080.5907} \times 100$

$= 0.0084\%$

$= \underline{84 \text{ ppm}}$

Case C: 75% H_2 Utilization, 75% O_2 Utilization

Dry Oxidant Flow Rate = 797 cc/min

Water Content = 5%

Wet Flow Rate = 836.9 cc/min

SO_2 Flow Rate = .0907 cc/min

Therefore, Total Oxidant Flow Rate = 836.9907 cc/min

SO_2 Content in Oxidant $= \frac{0.0907}{836.9907} \times 100$

$= .0108\%$

$= \underline{108 \text{ ppm}}$

II. LOW-Btu COAL GASIFICATION (Air Blown)

Inlet Equilibrium Composition:

18.6% H_2

11.4% CO_2

7.8% H_2O

14% CO

48.2% N_2

Anode Outlet Composition at 75% H_2 Utilization:

3.7% H_2

35.7% CO_2

3.8% CO

17.7% H_2O

Assume that 200 ppm H_2S (0.02%) is also present.

Dry Inlet Flow Rate	= 538 cc/min
Water Added (this equilibrates to 7.8% H_2O)	= 12.7%
Wet Inlet Flow Rate (at humidifier temperature)	= 606.3 cc/min
CO_2 Produced at 19 A = 19 A X 7.5 $\frac{cc}{min - A}$	= 142.5 cc/min
Total Anode Flow Rate	= 606.3 + 142.5
	= 748.8 cc/min
H_2S Flow Rate = $\frac{0.02}{100}$ X 748.8	= 0.15 cc/min

Case A: 75% H_2 Utilization, 25% O_2 Utilization

Dry Oxidant Flow Rate (at 19 A)	= 1809 cc/min
Water Content	= 5%
Wet Flow Rate	= 1899.5 cc/min
SO_2 Flow Rate	= 0.15 cc/min

Total Flow Rate = 1899.65 cc/min

SO_2 Content in Oxidant $= \frac{0.15}{1899.65} \times 100$

$= .0079\%$

$= \underline{79 \text{ ppm}}$

Case B: 75% H_2 Utilization, 50% O_2 Utilization

Dry Oxidant Flow Rate (at 19 A) = 1113 cc/min

Water Content = 5%

Wet Flow Rate = 1168.7 cc/min

SO_2 Flow Rate = 0.15 cc/min

Therefore, Total Oxidant Flow Rate = 1168.85 cc/min

SO_2 Content in Oxidant $= \frac{0.15}{1168.85} \times 100$

$= .0128\%$

$= \underline{128 \text{ ppm}}$

Case C: 75% H_2 Utilization, 75% O_2 Utilization

Dry Oxidant Flow Rate = 881 cc/min

Water Content = 5%

Wet Flow Rate = 925.1 cc/min

SO_2 Flow Rate = 0.15 cc/min

Total Oxidant Flow Rate = 925.25 cc/min

SO_2 Content in Oxidant $= \frac{0.15}{925.25} \times 100$

$= 0.0162\%$

$= \underline{162 \text{ ppm}}$